A NEW METHODOLOGY FOR THE DESIGN AND TUNING OF ROBUST PID CONTROLLERS IN ELECTRIC DRIVES

A Dissertation
Submitted to the Graduate Faculty
of the
North Dakota State University
of Agriculture and Applied Science

By

Chaudhry Arshad Mehmood

In Partial Fulfillment
for the Degree of
DOCTOR OF PHILOSOPHY

Major Department:
Electrical and Computer Engineering

August 2014

Fargo, North Dakota

North Dakota State University
Graduate School

Title

A NEW METHODOLOGY FOR THE DESIGN AND TUNING OF ROBUST PID CONTROLLERS IN ELECTRIC DRIVES

By

Chaudhry Arshad Mehmood

The Supervisory Committee certifies that this *disquisition* complies with North Dakota State Universitys regulations and meets the accepted standards for the degree of

DOCTOR OF PHILOSOPHY

SUPERVISORY COMMITTEE:

Dr. Rajesh Kavasseri

Chair

Dr. Ivan T. Lima Jr.

Dr. Nikita Barabanov

Dr. Sumathy Krishnan

Approved:

20 August 2014
Date

Dr. Scott C. Smith
Department Chair

ABSTRACT

AC induction motor-drive systems are the backbone for numerous industrial applications, such as aerospace, medical equipment, and nuclear power plants. The control performance of electric drives is sensitive to several uncontrollable disturbances from changes in ambient conditions in the form of machine parameter variations such as: magnetizing inductance (L_m), and rotor resistance (R_r). Such variations may trigger instability because of mismatch between the reference and desired conditions. The most common techniques to solve the issue are: **(a)** gain adaptation that requires instrumentation to monitor system, **(b)** nonlinear control methods, such as sliding mode, feedback linearization, and **(c)** robust control method, such as H_∞, and μ-analysis to account for motor uncertainties. Despite the prevalence of PID controllers, a systematic method to tune their parameters to ensure robustness remains an open problem.

In this dissertation, a systematic method to tune PI controllers while factoring uncertainties is developed. Two major design methods are proposed: **(a)** based on Kharitonov's theorem and **(b)** based on fractional order controllers. In **(a)**, the control design problem for AC drives can be cast into as a set of interval polynomials that can be analyzed via Kharitonov's theorem. Also proposed a method to solve the resulting polynomials, which then yield the controller coefficients. In **(b)**, we show how fractional order controllers (FrOC)-a generalization of PID that consider fractional values for the integral and derivative coefficients can be designed to achieve our main objectives. A unique advantage of such controllers is the so-called iso-damping property (constant phase) and robustness. The performance of controllers is assessed by comparing them with two well established techniques: traditional method based on gain/phase margin requirements, and symmetric optimum techniques an industrially popular technique that requires constant gain over a desired bandwidth.

While both these techniques use reduced order models, the proposed methods are advantageous because they can handle the full model of the machine. The simulation results suggest that the proposed controllers remain robust against the chosen uncertainties while both traditionally designed controllers succumb to instability. The work paves a novel way for the design and tuning of robust PID controllers in electric drives.

ACKNOWLEDGMENTS

I am very grateful to take this opportunity to thank Dr. Rajesh R. Kavasseri, Dr. Ivan T. Lima, Jr., Dr. Nikita Barabanov, and Dr. Sumathy Krishnan for serving on my graduate committee. Dr. Rajesh Kavasseri is my Ph.D. advisor in power electronics. I cannot thank him enough for the guidance, encouragement and wisdom he gave me during my graduate studies. He has shown me the joys of teaching, rewards of research and importance of life, and for this I thank him.

I would like to thank Dr. Ivan T. Lima Jr., and Dr. Nikita Barabanov for serving on my graduate committee. I have always enjoyed discussing many aspects of engineering and mathematics with these two gentlemen and look forward to future discussions.

I would especially like to thank Dr. Sumathy Krishnan for serving on my graduate committee. I appreciate the comments and help you have provided as well as the willingness to serve on my committee.

Finally, I would like to thank my family for their support and understanding that I had to leave my home country to pursue this work.

DEDICATION

To my MOM the BaiBai, my inspiration, my Father, who approved of my being inquisitive, my wife, daughters, sons, brothers, sisters, nephews, nieces, and to all my friends for their endless love, support and encouragement throughout my career.

TABLE OF CONTENTS

LIST OF TABLES

LIST OF FIGURES

LIST OF SYMBOLS

a ..... Phase-a

b ..... Phase-b

c ..... Phase-c

ω ..... Speed in radians/sec

i_a ..... Current a-phase

i_b ..... Current b-phase

i_c ..... Current c-phase

i_{sd} ..... Stator d-axis current

i_{sq} ..... Stator q-axis current

v_a ..... Voltage a-phase

v_b ..... Voltage b-phase

v_c ..... Voltage c-Phase

v_a^{ref} ..... Reference a-phase voltage

v_b^{ref} ..... Reference b-Phase voltage

v_c^{ref} ..... Reference c-Phase voltage

v_{ds} ..... Stator d-axis voltage

v_{qs} ..... Stator q-axis voltage

ω_s ..... Synchronous speed (rad/sec)

λ_{qs} ..... Stator q-axis flux linkages

λ_{ds} ..... Stator d-axis flux linkages

i_{sd}^{ref} ..... Stator d-axis reference current

i_{sq}^{ref} ..... Stator q-axis reference current

ω^{ref} ..... Reference speed in radians/sec

θ_{mech} ..... Position of rotor

R_s ..... Stator resistance

R_r ..... Rotor resistance

L_s ..... Stator inductance

L_r ..... Rotor inductance

L_m ..... Magnetizing inductance

J_eq ..... Equivalent inertia

p ..... Number of poles

FrOC ..... Fractional order control

PI ..... Proportional integral

PID ..... Proportional integral and derivative

K_P ..... Proportional gain

K_I ..... Integral gain

AC ..... Alternating current

KT ..... Kharitonov theorem

SO ..... Symmetric optimum

RC ..... Robust control

In ..... Intelligent control

IT ..... Inverter type

PC ..... Parameter compensation

CCS ..... Comparison of control schemes

ST ..... Sensor type

M ..... Multiple

IFOC ..... Indirect field oriented control

IM ..... Induction motor

SRM ..... Switch reluctance motor

Ad ..... Adaptive control

PI ..... Proportional integral

IC ..... Inverter comparison

CS ..... Control scheme

MT ..... Motor type

Reli ..... Reliability

OL ..... Open loop

DTC ..... Direct torque control

PM ..... Permanent magnet

PWM ..... Pulse width modulation

V/f ..... Voltage hertz

E/f ..... Back EMF hertz

SRS ..... Slip recovery scheme

S ..... Speed

P ..... Position

T ..... Torque

CHAPTER 1. INTRODUCTION

High performance drive refers to an electric drive with ability to offer precise control, rapid dynamic and a good steady state response. High performance drives are indispensable in safety critical applications due to their precision of control. Since the inception of AC machines, several techniques have evolved to control speed, torque, and position of machines. The basic control inputs are the voltage and frequency of the applied voltage/current to the motor. Since, the grid supply voltage and frequency are fixed, power electronic converters are used as an interface between the grid supply and the electric motor. It is well-known that variable speed drive offers significant energy savings in industrial applications.

Numerous control strategies employing inverter provide decent steady state but poor dynamic response. The dynamic response signifies that the poor performance arises due to deviation of air gap flux linkages from their set values. The discrepancy in flux linkages have to be controlled by the magnitude and frequency of the stator and rotor phase currents. The oscillations in the air gap flux linkages result in fluctuations in electromagnetic torque and in speed. This is detrimental in many high performance applications, such as, robotic actuators, centrifuges, servos, metal-rolling mills, and process drives. All of the aforesaid mentioned applications require high precision, fast positioning, or speed control. Such requirements will not be met with the sluggishness of control due to the flux oscillations. Moreover, air gap flux variations result in large digression of stator currents, requiring large peak converter and inverter ratings to meet dynamics.

The control of a separately excited dc drive is simple and requires control of flux and torque separately. Likewise, the independent control of flux and torque is possible in ac drives. The stator current phasor can be resolved, along the stator flux linkages. The component along the rotor flux linkages is the field producing

current, but this requires the position of the rotor flux linkages at every instant. The requirement of phase, frequency, and magnitude control of the current and the flux phasor is achieved by inverter control. The control is achieved in field coordinates and hence known as field oriented control, also sometimes known as vector control, because it relates to the phasor control of rotor flux linkages.

The rest of the chapter discusses the parameter mismatch and its effects on drive performance. Brief motivation and contribution of the thesis are also presented later in the chapter.

1.1. Tuning of Vector Controller and Parameter Sensitivity

The tuning of the vector control requires the exact values of rotor resistance, mutual inductance, and rotor self inductance of the induction machine. The tuning task is simple if the motor parameters remain constant. The fact that the rotor resistance and magnetizing inductance changes with temperature and frequency and the leakage inductance changes with the magnitude of the stator currents complicates the tuning problem.

A mismatch between the vector controller and induction motor occurs as a result of either the motor parameters changes with operating conditions, such as temperature rise and saturation or of the wrong instrumentation of the parameters in the vector controller. The later phenomenon is controllable, but the former is dependent on the operating conditions of the motor drive and hence is uncontrollable. The mismatch produces a coupling between the flux and torque resulting in channels production in the machine. This has the following consequences:

1. Rotor flux linkages diverges from the commanded (reference) value.

2. Electromagnetic torque diverges from commanded (reference) value producing a nonlinear relation between the actual torque and its commanded value.

3. During torque transients, an oscillation is caused both in the rotor flux linkages and in torque responses, with a settling time equal to the rotor time constant. The rotor time constant is large on the order of 0.5 second or greater.

In a torque drive, above mentioned consequences **2** and **3** are most undesirable. Although, in speed controlled drive the nonlinear torque-to-torque command will not have a detrimental effect on the steady state operation, its effect is considerable during the transients. The torque excursions can be smoothened, so they may not appear as speed ripples with load and motor inertia.

Several techniques have been worked out to address the parameter sensitivity in indirect field oriented control. Most of them are parameter adaptation techniques based on the following strategies.

1. Direct monitoring of flux and torque producing stator current components.

2. Continuous measurement of instantaneous rotor and stator resistances [1], [2], [3], [4], [5], [6], [7].

These techniques are classified as direct scheme for parameter adaptation. Most of the parameter adaptation algorithms are themselves parameter dependent. This particular aspect can cause significant error in the computation of the variables used in parameter compensation techniques.

The parametric variations of the induction motor, if not properly taken care of, can cause performance degradation of electric drives tremendously [1], [2], [3], [8] and serve as the root cause in the development of robust control strategies for improved performance of electric drives. Robust control techniques have also been developed for rotor time constant [4] using model reference adaptive system (MRAS) to estimate speed and current through fuzzy logic. Robust, indirect vector control using the third order model of induction motor, to estimate electromagnetic torque is

given in [5]. The robust controller using H_∞ loop shaping cascaded with already well tuned PI controller is designed by authors in [9], which improved the performance of the controller with rotor resistance uncertainty. Robust indirect field oriented control using a slip frequency calculation in feedback loop is presented in [5], where the controller is dependent on the machine parameters. The auto disturbance rejection controllers, are employed to overcome disturbances and parameter variations [10]. The plugin robust controller for already well tuned PI controller is presented in [9].

1.2. Motivation

The challenges in designing the high performance electric drives are multi-faceted. There is stringent requirement of high precision in speed, torque, and position control of electric drives. Moreover, the controller design under parametric uncertainty for electric drives sets new challenges for the control engineers. Furthermore, the parametric inconsistency generates the mismatch between the induction motor and vector controller.

The parametric inconsistency causes the coupling between the flux and torque producing channels in the machine that generates the torque and speed oscillations. A flurry of controllers exists to reduce the effects of parametric uncertainty. The most commonly used in electric drives and motion industry is PI controller. Its application is adequate for wide control problems with modest performance requirements. Although PI is simple in structure and easy to implement, but still tuning of PI controller for particular performance metrics is an open problem. The controller tuning is always an important factor to obtain the required optimal speed, torque o position tracking. Since, it is hard to achieve the robust optimal tracking without a controller. The robust tuning of controller are required to reject the external disturbances like load torque variations and machine parametric variations.

This thesis proposed two techniques to tune the PI controller. The proposed techniques are:

1. Synthesis of PI controller using Kharitonov theorem: Kharitonov theorem is an analysis tool to verify the robust stability of the system with characteristic equation having unknown coefficients, used to synthesize the PI controller including all parametric uncertainty. Since the theorem produces four corner polynomial of controller parameters. Each polynomial is solved to obtain the controller parameters numerically.

2. Fractional Order PI controller: The fractional order PI controller that provides an extra degree of freedom to tune the controller is the order of integral. The extra degree of freedom from the use of fractional order integrator and differentiator made it possible to further improve the performance of traditional PID controllers. Unlike a conventional PI controller, there is no systematic and yet rigorous design or tuning method existing for a fractional PI controller.

The PI tuned with the proposed technique will be robust to parametric and load torque perturbations. The proposed techniques are novel techniques to design the integer order PI and fractional order PI.

1.3. Contribution of Dissertation

In the previous section we mainly highlighted the parameter uncertainty and their effects on the performance of the drive system. The dissertation proposes the robust control strategies for the indirect field oriented control of induction motor. The proposed techniques are advantageous, since full dynamics of the induction machine are considered instead of using reduced order model. Synthesis of PI controller using Kharitonov's theorem and fractional order PI controller are proposed in this thesis to design the robust controller for electric drives.

Kharitonov theorem is used to check the stability of the system with characteristic equation having unknown coefficients. The coefficients are only needed to be defined in the interval. The theorem generates the four corner polynomials and the stability of each polynomial guarantees the robust stability of the system. The thesis exploited four corner polynomials to synthesize the controller gains K_P and K_I, such that the system is stable under all perturbation.

The fractional order control uses fractional integral and not as integer order integral. The fractional order integral has the property to behave as infinite length linear filter which also exhibits the iso-damping property. The fractional order integral is implemented using Oustaloup approximation techniques, since, we can generate third order controller with the proposed technique.

1.4. Dissertation Organization

The dissertation is organized in six chapters. The general introduction about drives and parameter sensitivity is presented in the first chapter. The second chapter focuses on the literature review about drives and robust control techniques. The third chapter details the Kharitonov theorem and its applications for the synthesis of the PI controller for vector controlled induction motor. The fourth chapter proposes fractional order controller as an alternate solution to the PI controller as a robust controller.

CHAPTER 2. LITERATURE REVIEW ON DRIVES AND ROBUST CONTROL

High performance drive refers to an electric drive with ability to offer precise control, rapid dynamic and a good steady state response. High performance drives are indispensable in safety critical applications due to their precision of control. Since the inception of AC machines, several techniques have evolved to control speed, torque, and position of machines. The basic control inputs are the voltage and frequency of the applied voltage/current to the motor. Since, the grid supply voltage and frequency are fixed, power electronic converters are used as an interface between the grid supply and the electric motor. It is well-known that variable speed drive offers significant energy savings in industrial applications.

Numerous control strategies employing inverter provide decent steady state but poor dynamic response. The dynamic response signifies that the poor performance arises due to deviation of air gap flux linkages from their set values. The discrepancy in flux linkages have to be controlled by the magnitude and frequency of the stator and rotor phase currents. The oscillations in the air gap flux linkages result in fluctuations in electromagnetic torque, and if overlooked results in speed oscillations. This in detrimental in many high performance applications, such as, robotic actuators, centrifuges, servos, metal-rolling mills, and process drives. All of the aforesaid applications require high precision, fast positioning, or speed control. Such requirements will not be met with the sluggishness of control due to the flux oscillations. Moreover, air gap flux variations result in large digression of stator currents, requiring large peak converter and inverter ratings to meet dynamics.

The control of a separately excited dc drive is simple and requires control of flux and torque separately. Likewise, the independent control of flux and torque is possible in ac drives. The stator current phasor can be resolved, along the stator

flux linkages. The component along the rotor flux linkages is the field producing current, but this requires the position of the rotor flux linkages at every instant. The requirement of phase, frequency, and magnitude control of the current and the flux phasor is achieved by inverter control. The control is achieved in field coordinates and hence known as field oriented control, also sometimes known as vector control, because it relates to the phasor control of rotor flux linkages.

In this chapter, we describe the brief history of the AC drives with the machine classifications. The perturbation effects and parameter sensitivity to the temperature variations. The proposed research and motivation to establish the research techniques is discussed at the end.

2.1. Introduction

AC drive motor systems are predominantly used in different industries, like steel mills, traction drives, in electric hybrid vehicles. Variable speed AC drives became popular with the birth of vector control which uses the separate control of direct and quadrature components of stator current. The d and q components can be used to control the inverter magnitude, frequency and phase angle of output voltage. The vector control was first proposed in 1968 in Germany by K. Hasse [11], based on the concept of speed and torque control without direct measurement of flux, called indirect field oriented control. The direct field oriented control, based on the concept of direct measurement of flux was introduced by F. Blaschke in 1971 [12]. The introduction of vector control was inspired by the development of dynamic model of induction machine [13] in 1959, using the concept of Park's transformation [14]. Direct self control (DSC) [15] by Depenbrok, and direct torque control (DTC) [16] by Takahashi and Noguchi proposed control strategies where transformations are not required and are therefore scalar techniques. The DSC and DTC removed the dependency of current loops and directly controlled the torque and flux using hysteresis control.

2.2. A Brief History of the AC Drives

Electric drive is an integral part of speed control of motors, such as DC motors, induction motors, synchronous motors, permanent magnet synchronous motors, and switch reluctance motors. The drives are used for the soft starting, stopping and gentle speed variations giving the four quadrant operation. The drives are used to limit the currents for meticulous torque control. They help to run the motor beyond their rated maximum speed, which is represented in torque speed curve as a constant power region in Figure 1.

2.3. Motor Types

The AC motor used could either be induction motor or permanent magnet synchronous motor depending on the requirements. AC machines can be classified broadly as Synchronous Machines (SM) and Asynchronous Machine (ASM) also called Induction Machine(IM) and electronically commutated machine [17]. The brief classification of AC machines is shown in Figure 2.

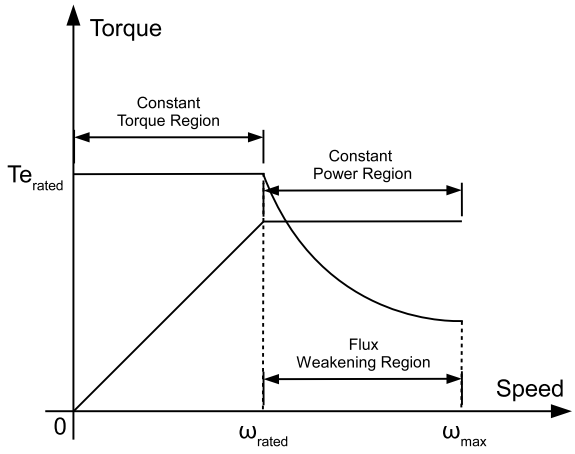

Figure 1. Torque speed curve.

2.4. Stability of Drives

The stability of the machine is important factor while working under variable loads and speeds. The drive is in state of equilibrium when load torque and developed torque becomes equal. If disturbance occurs in equilibrium position, the drive tries to bring the speed of motor back to operating speed. If the operating speed is achieved back then the machine is in stable equilibrium. If machine hits unstable equilibrium, it either comes to rest or runs at a very high speed. The steady-state stability and dynamic or transient stability points are important for AC drives.

The stability of drive at fixed speed is perturbed either by load torque variation or due to the motor increased temperature over a prolonged period of operation. The high temperature excursions generates the deviation of machine parameters from their nominal values. Most of controller schemes described in Table 1 are parameter dependent, which make them sensitive to parameter variations and disturbances.

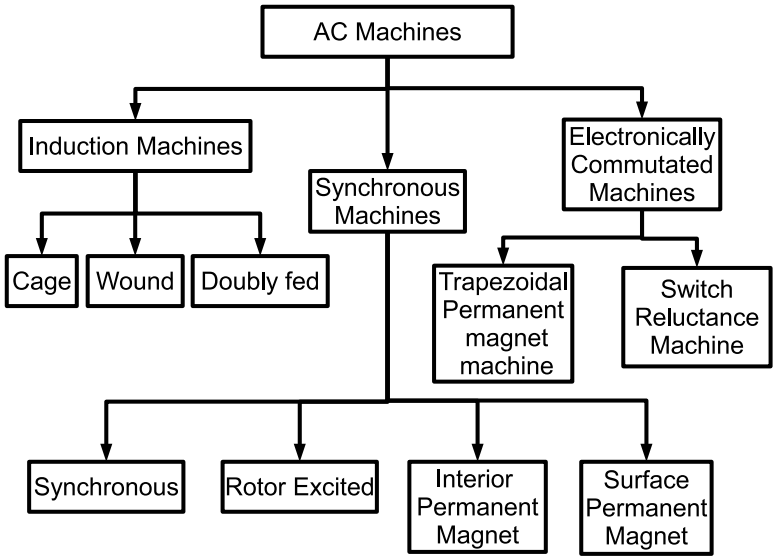

Figure 2. AC machine classifications.

Table 1. Summary of some generic state of the art surveys providing the control schemes, controller structure, reliability and motor types.

Reference	RC	Ad	In	PI	IT	IC	PC	CS	CCs	MT	ST	Reli
[18]	×	×	×	×	M	√	×	OL	√	IM	Sensored	×
[19]	×	×	×	√	M	√	×	IFOC	√	IM/DC/Sync	Sensored	×
[20]	×	×	×	×	M	√	×	×	×	IM/DC	×	×
[21]	×	×	√	×	M	√	×	Vector	×	IM/Sync	Sensored	×
[22]	√	×	×	×	PWM	×	√	DTC	×	IM	Sensorless	×
[23]	×	×	×	×	M	√	×	OL	√	IM	×	×
[24]	×	×	×	×	PWM	×	×	×	×	IM MP	×	√
[25]	√	×	×	√	PWM	×	√	Vector	√	PMSM	Sensorless	√
[26]	×	×	×	×	×	×	×	×	×	IM/PM/SRM	×	√
[27]	×	×	×	√	M	×	√	M	√	IM	Both	√
[28]	√	√	√	√	PWM	×	×	M	√	IM/PM/SRM	Both	×
[29]	×	×	×	√	M	√	√	M	√	IM/PM	Both	√
[30]	×	×	×	×	M	√	×	×	×	M	Both	×
[31]	×	×	×	×	M	√	×	×	*times*	IM	×	√
[32]	×	√	×	√	M	√	×	Multiple	√	IM	Both	√

2.5. Drive Control Schemes

The implementation of control techniques require the setup of machines and inverter under different control schemes. The different control schemes used for the AC machine can be classified either as open loop or closed loop control.

The open loop control is used when exact, precise control is not required. The speed can be varied by just varying the voltage, frequency or both simultaneously. Closed loop control is used when accurate or precise torque or speed control is required. The closed loop control schemes can be further classified into, scalar control and vector control.

2.6. Scalar Control

Scalar control methods provide an easy, cheap, and coarse control of torque and speed. They are simple to implement and do not require sophisticated instrumentation. However, performance of this control scheme degrades during transients. The degradation occurs due to inherit coupling between torque and field producing current components of motor current. The most widely used scalar control techniques are shown in Figure 3.

2.7. Field Oriented Control

The control of a separately excited dc drive is simple and requires control of flux and torque separately. Likewise, the independent control of flux and torque is possible in ac drives. The stator current phasor can be resolved, along the stator flux linkages. The component along the rotor flux linkages is the field producing current, but this requires the position of the rotor flux linkages at every instant. The requirement of phase, frequency, and magnitude control of the current and the flux phasor is achieved by inverter control. The control is achieved in field coordinates and hence known as field oriented control, also sometimes known as vector control, because it relates to the phasor control of rotor flux linkages.

The field oriented control (vector control) is a high performance control scheme for AC drives. This is the most common control scheme used in industry for high precision control of speed, torque, and position. The scheme gives better speed tracking in dynamic and steady state operations compared to scalar control. The field oriented control are is normally implemented either in direct field oriented or indirect field oriented control scheme.

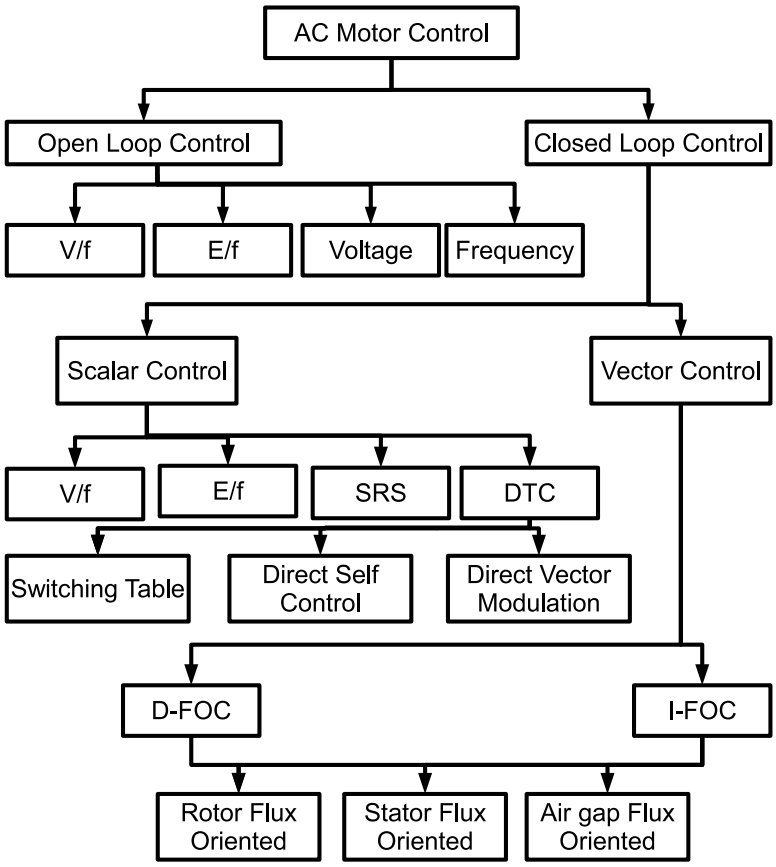

Figure 3. AC machine control schemes.

2.7.1. Direct Field Oriented Control

This method relies on direct measurement of flux and does not require flux estimation. The schemes is called 'direct' because of the haul effect sensors used to measure the flux directly. The control scheme can also be used as sensor-less drive. The sensor-less schemes requires estimation of speed through direct current measurements.

2.7.2. Indirect Field Oriented Control

This scheme does not require hall effect sensors and hence the name indirect. The tuning of the vector control requires the exact values of rotor resistance, mutual inductance, and rotor self inductance of the induction machine. The tuning task is simple if the motor parameters remain constant. The fact that the rotor resistance and magnetizing inductance changes with temperature and frequency and the leakage inductance changes with the magnitude of the stator currents complicates the tuning problem.

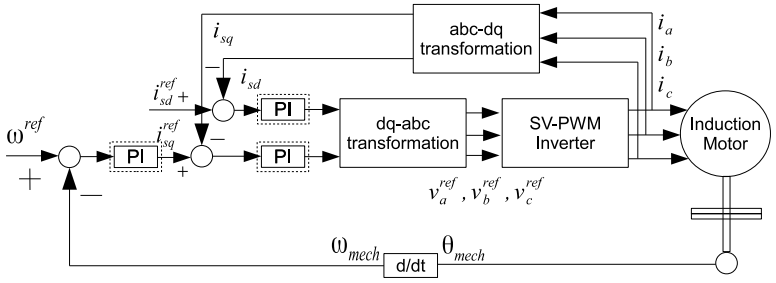

Figure 4. Indirect field oriented control.

A mismatch between the vector controller and induction motor occurs as a result of either the motor parameters changing with operating conditions, such as temperature rise, saturation, or wrong instrumentation of the parameters in the vector controller. The later phenomenon is controllable, but the former is dependent on the operating conditions of the motor drive and hence is uncontrollable.

The most affected parameters are the rotor resistance R_r, magnetizing inductance L_m and rotor self inductance (L_r) [2]. The parameter variations caused by temperature and magnetic saturation causes a mismatch of plant from controller in both steady state and transients. Several solutions for removing parameter sensitivity from field oriented control are presented in [33], [34].

2.8. Direct Torque Control

The scheme takes the advantage of controlling the stator flux and torque directly and uses the hysteresis control structure for flux and torque. This method uses feedback control of torque and stator flux, which are computed from the measured stator voltages and currents. As the method does not use a position or speed sensor to control the machine and uses its own electrical output currents and resulting terminal voltages, this is also referred as a direct self-control scheme. The method uses a stator reference model of the induction motor for its implementation, thereby avoiding the trigonometric operations in the coordinate transformations of the synchronous reference frames. This is one of the key advantages of the control scheme. The scheme depends only on stator resistance and no other parameters. The implementation of the scheme requires flux linkages and torque computations, plus generation of switching states through a feedback control of the torque and flux directly without inner currents loops. The torque and flux feedback loops contain no PI controller(or any other controller) so, tuning of PI controller is therefore not a problem. Rather it is a problem of choosing the best method to control inverter switching table. Improved estimation techniques to estimate torque and flux also enhances the performance of DTC. The main disadvantages of direct torque control are, variable switching frequency, chattering at low speed, direct control of current is absent, and high ripples in current and torque.

2.9. Flux Weakening

The flux weakening operation allows the speed of the motor go beyond the base speed usually two to three times of the rated speed. The flux weakening region is also known as the constant power operation, since power is kept constant and torque is reduces as shown in Figure 1. The field weakening region requires proper dq-current distributions for the torque capabilities [35]. The optimal strategies used for the torque maximization are either the calculations of i_{ds} and i_{qs} based on motor parameters or selection of i_{ds} and i_{qs} using flux and voltage regulators.

2.10. Issues in AC Drives

The low voltage AC drives usually ranging from 0 to 2.3 KV and have applications in home appliances and very small industries. The medium voltage AC drives ranging from $2.3 - 13.8KV$ are mostly used in industries such as, rolling, milling, oil and gas, cement, and metal industry. The medium voltage drives constitute only 3% of variable speed drives in different applications [36]. The electric drives for these applications can reduce the overall energy losses and cost. Energy efficiency is a trade-off and the most common challenges and problems that arises for drives are:

1. Switching devices problems, which includes, switching losses, maximum rated current, voltage, and switching frequency.

2. Motor side problems, such as $\frac{dv}{dt}$, puts stress on insulation of motor winding, shaft vibration and common mode voltage generated by PWM inverter.

3. Line side problems for example, power factor problem arises due to distorted currents at source, power quality which depends on converter topology, and resonance of LC filters.

Switching losses occur due to AC-DC conversion and then DC-AC conversion within semiconductor switching devices. The maximum voltage from AC mains is

lower at the terminals of AC machine. The switching also generates losses and chattering in current and voltage. The sine wave quality of output voltage is very low. The patterns of PWM signals in inverter usually give rise to common mode voltage. The common mode voltage generated between neutral point of inverter and ground acts as a source and causes problem.

2.10.1. Low Speed Operation Issues

The applications of high torque and low speed operation of the induction motor is critical to control for variable speed drive. For example, hybrid vehicles or electric vehicles have major requirement of high torque at low speed. The design of cruise control acting on brake pedals and throttle of autonomous Citrön C3 vehicle using fractional order controller is designed to setup robustness against un-modeled parameters and change in parameters [37].

The removal of speed dependent terms in estimator help to design a drive that can operate even at very low speed [38]. The sliding mode observer can remove the dependency on the speed dependent terms for parameter estimation. The model reference adaptive control (MRAC) can be used to estimate the speed and other control variables based on measured currents also gives the robustness to parameter variations and low speed operation [39].

2.10.2. Flux Weakening Operation Issues

The induction motor runs at the maximum speed (rated speed) of synchronous speed $N_s = \frac{2\pi f_s}{p}$. The synchronous speed is attained at no load condition. The maximum attainable speed depends on load torque and hence slip. The normal mode of operation with the slip greater than unity causes the speed go beyond rated speed. The induction motor above rated speed behaves like generator. The maximum speed is also dependent on f_s the supple frequency. The increase in f_s, beyond rated value reduces the stator flux linkages. The reduction in flux linkages arises due

to fixed DC bus voltage. The increase in speed beyond rated speed speed reduces flux, consequently reducing the torque. The flux weakening region is also known as constant power region since, torque producing component remains constant.

The motoring operation beyond the rated speed can be attained using the flux weakening operation mode. The flux weakening operation can be obtained using:

- Stator Flux Linkages controlled (Direct Scheme)
- Rotor Flux Linkages controlled (Indirect Scheme)

The stator flux linkages controlled is obtained by considering the stator dq-voltages. The resistive drop can be eliminated and assuming the steady state operation:

$$V_{qs} = p\lambda_{qs} + \omega_S \lambda_{ds} \tag{2.1}$$

$$V_{ds} = p\lambda_{ds} - \omega_S \lambda_{qs} \tag{2.2}$$

with

$$\begin{aligned} V_s &= \sqrt{V_{qs}^2 + V_{ds}^2} \\ V_s &= \omega_s \sqrt{\lambda_{qs}^2 + \lambda_{ds}^2} \qquad (2.3) \\ \lambda_s &= \frac{V_s}{\omega_s} \qquad (2.4) \end{aligned}$$

The direct vector control scheme assumes that λ_{ds} is aligned with the stator flux linkages phasor. The alignment of axis causes the q-axis flux linkages λ_{qs} go to zero.

$$\lambda_{qs} = 0 \tag{2.5}$$

$$\lambda_{ds} = \lambda_s \tag{2.6}$$

$$T_e = i_{qs}\lambda_s \tag{2.7}$$

The air-gap power then reduces to:

$$P_a = T_e\omega_s = V_s i_{qs} \tag{2.8}$$

The constant i_{qs} in flux weakening region therefore gives constant power. The rotor flux linkages (indirect scheme) simply can be implemented as a function of rotor speed as:

$$\lambda_r^{ref} = \frac{\omega_b}{|\omega_r|}\lambda_b, \pm\omega_b \leq \pm\omega_r \pm \omega_{r(max)} \tag{2.9}$$

The basic control scheme for flux weakening is not enough to obtain the maximum possible speed (beyond rated speed). The rotor flux is not a linear function of stator flux. The change in rotor flux linkages produces big change in stator flux linkages. The change of stator flux may demand more voltages than the rated values. The DC-link is fixed and limited, and high demand sets constraints on constant power operation. The implementation of flux weakening requires in rotor flux linkages controlled operation requires much attention [40].

2.10.3. Perturbation Effects

The perturbation in the form of load, voltages, and frequency variations produces undesired operations in steady state and dynamic response of the induction motor. The sudden load variation tends to vary the stator currents accordingly. The increase in load demands the high generated torque from the motor. The high demand of the torque require high stator currents. The supply voltage variations also sets the constraint on inverter. The inverter that can compensate the variations in frequency and voltage requires high cost. The low frequency harmonics can be eliminated by choosing appropriate switching frequency. The high frequency harmonics are attenuated using the LC-filters.

2.11. Detuning of Controller

The controller tuning requires known parameters of the induction motor. The parameters of induction motor do not remain constant over the operation of drive. The parameter variations arises due to ambient temperature of the induction motor causes the performance degradation of field oriented control scheme. The parameter variations produces the detuning effect. The variation in machine parameter arises due to the ambient temperature variations and operating conditions. The rotor time constant ($\tau_r = \frac{L_r}{R_r}$) depends on rotor resistance (R_r) and rotor inductance (L_r). The magnetizing inductance (L_m) and stator resistance (R_s) also varies with ambient temperature. The detuning of controller produces inconsistency in commanded and desired signals.

2.12. Control Methodologies

The adaptive control, Model Reference Adaptive System (MRAS), self tuning adaptive regulators are proposed in literature to overcome the performance issues of electric drives discussed in previous sections [10]. The artificial intelligent control techniques based on self-learning and self-adaptation to have a robust control, despite of perturbation are a major control methodologies used for electric drives.

The robust control techniques such as H_∞, Youla parameterization [9] gives the robustness in a certain interval of parameter variations. The new emerging control technique based on Fractional Order Controller (FrOC) is making its place in the field of robust controllers. Fractional order calculus is an area of mathematics that deals with the derivatives and integrals from non-integer order. The fractional order proportional, integral, and derivative (FrOPID) controllers have achieved a significant interest in the last few decades. In fact, FrOPID provides more flexibility in controller design procedure than standard integer order PID controllers, because FrOPID provides five degrees of freedom. The fractional order calculus theory is used

to design the PI controller, although the classical PID controller is predominant in control development. The fractional order controllers (FrOC) provides the isodamping property which shows constant phase invariant to gain changes. The isodamping property gives the constant phase at the ω_c. The tuning of FrOC involves the approximation techniques, such as Oustaloup approximation [41, 42].

In [43], the authors used a multirate model reference adaptive system to estimate the rotor time constant for the IFOC which is highly dependent on rotor time constant. Reference [44] used the adaptive sliding mode controller with recurrent radial basis function networks to control the speed of the induction motor in IFOC scheme.

2.12.1. Robust Control Strategies for AC Drives

The electric machine is an integral part of the drive system where the controller is used to keep the desired performance of motor. The controllers are tuned mostly offline using the nominal machine parameters at nominal operating conditions. The online tuning requires a continuous monitoring of the machine parameters, which in turn increases the controller efficiency at the cost of computational overhead. Different controller schemes are used to control the machine and all of the schemes have their own merits and limitations. Each of the control schemes is dependent on different machine parameters, for example, IFOC depends in R_r and L_m while DTC depends on the R_s [45]. Various state of the art robust control strategies are presented in Table 2 with references and their brief description.

Table 2: Recent robust control of induction motor.

S. No.	Ref.	Techniques Established	Loop
01	[46]	Adaptive sliding mode control for global position tracking in the presence of uncertainties.	P
02	[47]	A survey presenting sliding mode control strategies for induction motor.	S, P
03	[48]	Forth order descriptor type robust Kalman filter used to estimate rotor flux and speed.	S
04	[49]	DTC-SVM offers fast dynamic response and easy to implement with adaptive parameter estimation scheme for robust speed control.	S
05	[50]	Control of six phase induction motor with combinational concept of predictive control and extended Kalman filter for robust speed control.	S
06	[51]	A robust control against speed sensors faults using hybrid fault tolerant control with PI and $H\infty$ controllers. The second architecture is based on generalized internal model control.	S
07	[52]	Interfacing multiple model extended Kalman filter is replaced by the extended Kalman filter to reduce the influence of gross external disturbance and internal estimated error.	S

Continued on next page.

Table 2 – Continued from previous page.

S. No.	Ref.	Techniques Established	Loop
08	[53]	Speed and torque control for IFOC using $H\infty$ and quantitative feedback theory immune to rotor resistance perturbation.	S, T
09	[54]	Fault diagnoses robust linear discriminator schemes, which can detect broken bar and short circuit of stator winding.	S, P
10	[55]	The block control technique quasi continuous sliding mode manifold design and the second order sliding mode super twisting algorithms is designed to track speed and flux of single phase induction motor under perturbations.	S
11	[56]	The PI sliding mode control established to increase robustness, efficiency and elimination of chattering.	S
12	[57]	Armature voltage field oriented approach combined with robust linear generalized PI observer based output feedback controller for the induction motor.	S
13	[58]	Sliding mode observer based on singular perturbation theory for IFOC, robust to rotor resistance variations.	S
14	[59]	Hybrid robust control using fuzzy logic for position control of induction motor under vector control scheme.	P
15	[10]	Auto disturbance rejection controllers without the need of estimation of rotor flux.	S

Continued on next page.

Table 2 – Continued from previous page.

S. No.	Ref.	Techniques Established	Loop
16	[60]	Flux controllers are designed using Lyapunov linearization approach associated with sliding mode control. Speed loop is designed using PI controller and Lyapunov method based on backstepping procedure.	S
17	[61]	Online estimation of the rotor resistance with online rotor resistance adaptation (R_s50% and R_r100%).	S
18	[62]	Ninth order adaptive observer estimates rotor flux and rotor resistance and a third order high gain observer for speed and acceleration.	S
19	[63]	Nonlinear robust feedback control with second order observer for rotor flux and third order high gain observer for speed and acceleration (R_r and R_s).	S
20	[64]	MRAS with observing instantaneous reactive power of magnetizing inductance immune to stator and rotor resistance thermal variations.	S
21	[65]	Variable structure control for DTC scheme.	S
22	[66]	Variable structure control with an adaptive gain for the indirect vector control.	P
23	[67]	Gain scheduled flux observer subject to parameter variations (R_r and $R_s \pm 50\%$).	S

Continued on next page.

Table 2 – Continued from previous page.

S. No.	Ref.	Techniques Established	Loop
24	[68]	Novel control strategy for stator active-reactive currents of DFIM. Since the rotor currents are not measured forming the proposed control scheme as output feedback controller.	S, P
25	[69]	Field weakening operation of induction motor under vector control scheme with modulation depth control.	S

CHAPTER 3. KHARITONOV THEOREM AND SYNTHESIS OF CONTROLLER

The system will be stable if and only if all roots of the characteristics polynomial lie in the open left of the complex plane and is known as Hurwitz stable. The question of robust stability arises when the system depends on uncertain parameters whose values are unknown but satisfy known bounds. The presence of such uncertain parameters means that the coefficients of the characteristic polynomial are unknown but bounded. This then define the family of characteristic polynomials. The system will be stabilizable if all polynomials in this family are Hurwitz stable. Kharitonov's theorem is used to assess the stability of the dynamical system for the family of polynomials. In this chapter, Kharitonov's theorem is utilized for the synthesis of the PI controller for the fifth order model of induction motor for speed loop. The closed loop characteristics polynomial involving controller unknown coefficients is solved for stability analysis using Hurwitz matrix, to obtain bounds of the coefficients of controller. The inner current loops are designed using the classical control techniques.

3.1. Introduction

The demand for high performance electric drives is steadily increasing, given the growing emphasis for electrification of the transportation industry. In many similar applications, electric drives are required to perform under tighter control requirements even when subject to widely varying ambient or operating conditions [70]. In such cases, the drift introduced in motor parameters due to such variations typically degrade the control performance, especially, in AC drives using induction motors. The degradation occurs mainly because, the mismatch between the plant and controller creates discrepancies between commanded and actual/measured values of torque and flux, which induce undesirable torque oscillations or even trigger drive instability [45, 71].

Research efforts to counteract the effects of parametric variations mainly rely on tracking drive parameters, either by measurement or observer based methods [72], [73], [74], and adapting the controller parameters via gain scheduling or using the nonlinear sliding mode controller [75]. Since PID controllers are widely used in industrial control systems, the tuning of PID controllers for induction motor drives are based on well established classical control techniques including the symmetric optimum technique [76], [45] at nominal conditions.

In contrast, we consider an alternate approach for tuning these controllers using Kharitonov's theorem. The theorem [77] provides a necessary and sufficient conditional test for Hurwitz stability when four variants of the polynomials created using the upper and the lower bounds on coefficients are strictly stable. Therefore, an immediate application of the theorem is for robust stability analysis and check the robust stability of the system in the presence of uncertainties, [78], [79]. Relatively, the theorem has fewer applications for control synthesis. An example in [80] illustrates the design of a robust power system stabilizer while [79] presents an application to CMOS manufacturing under process variations.

In this chapter, we show how Kharitonov's theorem can be exploited to determine the controller gains, if the uncertainties in key drive parameters are restricted to specified intervals. These intervals can be specified given reasonable knowledge of variations in operating or ambient conditions. For an induction machine drive, the parameters magnetizing inductance L_m and rotor resistance R_r vary in a specific range with changes in temperature [2], [45]. The resulting interval characteristic polynomials for the closed loop system obtained with the linearized induction machine model can be analyzed with Kharitonov's theorem to compute robust gains for the controllers. Therefore, the proposed tuning method obviates the need for online parameter estimation, additional instrumentation, or gain scheduling.

3.2. Problem Statement

We consider Indirect Field Oriented Control (IFOC), a vector control scheme for induction motor drives as shown in Figure 5. The scheme has three closed loops, where two internal loops for the torque producing component are overseen by the outer (third) speed control loop. The upper and lower limits for each of the controller in loop is given in Appendix (B). The scheme is sensitive to three parameters namely: rotor resistance (R_r), mutual inductance (L_m), and rotor self-inductance (L_r). A standard dynamic model for induction motor in the synchronously rotating reference frame [45], [81] is linearized to obtain the transfer function $G(s) = \frac{P(s)}{Q(s)}$ from v_{qs} to ω_m (details in Appendix (B)). The inverter is represented by an averaged model (with a single time constant and delay) [45]. The inverter transfer function $I(s)$ is noted in the Appendix (B). With $G_c(s)$ denoting the controller, the speed control loop is as shown in Figure 6.

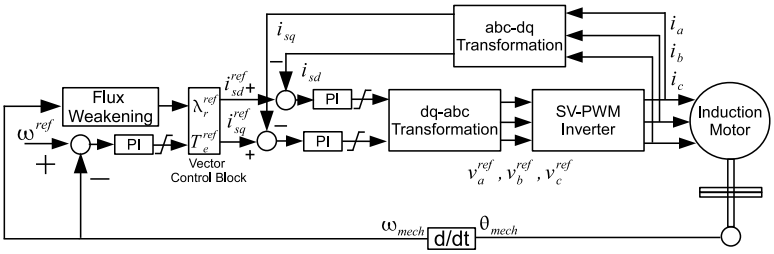

Figure 5. Block diagram of vector control with flux weakening.

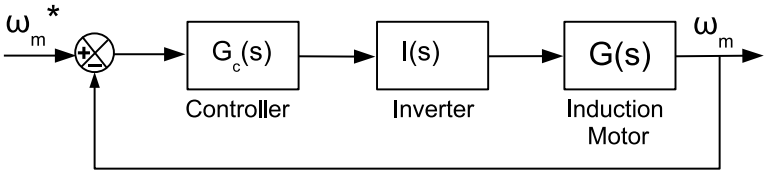

Figure 6. Block diagram of speed loop.

The closed loop transfer function between measured speed and reference speed $\frac{\omega_m}{\omega_m^*}$, is denoted by:

$$G_{cl}(s) = \frac{P_{cl}(s)}{Q_{cl}(s)} \tag{3.1}$$

The specific form of $G_{cl}(s)$ is described in the Appendix (B). The uncertainties in the motor parameters enter both the denominator and numerator of the resulting closed loop transfer function. The objective is to select the coefficients of the controller function $G_c(s) = K_P + \frac{K_I}{s}$ such that the system is robust to the parametric uncertainties as shown in Figure 7. Here, point A corresponds to operation with nominal parameters for rotor resistance and magnetizing inductance denoted by: $A : (R_r, L_m)$. Similarly, $B : (R_r, 0.8L_m)$, $C : (2R_r, 0.8L_m)$, $D : (2R_r, L_m)$.

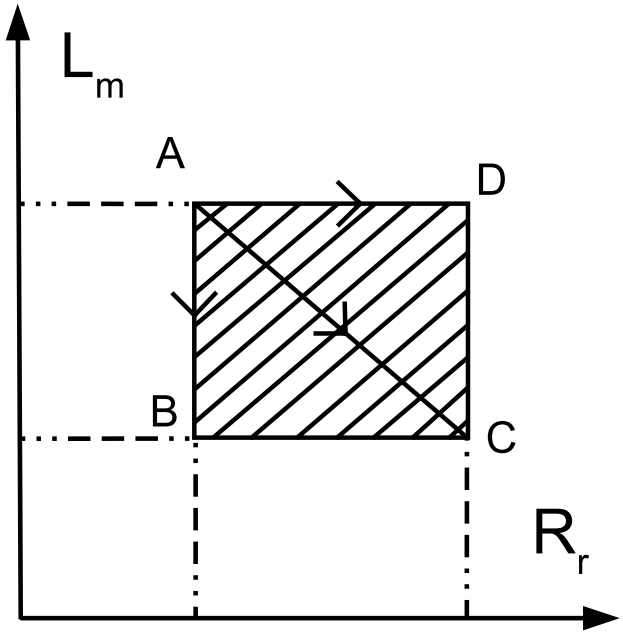

Figure 7. Parameter space.

3.3. Solution with Kharitonov's Theorem

Kharithonov's theorem provides a robust stability criterion for interval polynomial of the form:

$$G(s) = \sum_{k=1}^{n} [\underline{a_k}, \overline{a_k}] s^k, k = 0, 1, 2, ..., n \tag{3.2}$$

The theorem states that the interval polynomial (3.2) are strictly Hurwitz, if and only if four polynomials, obtained by the arrangement of upper and lower bounds on coefficients as noted in Eqn.(3.3), are strictly Hurwitz.

$$\begin{aligned}
G_1(s) &= \underline{a_0} + \underline{a_1}s + \overline{a_2}s^2 + \overline{a_3}s^3 + \underline{a_4}s^4 + \underline{a_5}s^5 \\
G_2(s) &= \overline{a_0} + \underline{a_1}s + \underline{a_2}s^2 + \overline{a_3}s^3 + \overline{a_4}s^4 + \underline{a_5}s^5 \\
G_3(s) &= \overline{a_0} + \overline{a_1}s + \underline{a_2}s^2 + \underline{a_3}s^3 + \overline{a_4}s^4 + \overline{a_5}s^5 \\
G_4(s) &= \underline{a_0} + \overline{a_1}s + \overline{a_2}s^2 + \underline{a_3}s^3 + \underline{a_4}s^4 + \overline{a_5}s^5
\end{aligned} \tag{3.3}$$

For the system considered in this chapter, the four corner polynomials generated from Eqn.(B.5) are as follows:

$$\begin{aligned}
G_1(s) &= \underline{d_0} + \underline{d_1}s + \overline{d_2}s^2 + \overline{d_3}s^3 + \underline{d_4}s^4 + \underline{d_5}s^5 \\
&\quad + \overline{d_6}s^6 + \overline{d_7}s^7 \\
G_2(s) &= \overline{d_0} + \underline{d_1}s + \underline{d_2}s^2 + \overline{d_3}s^3 + \overline{d_4}s^4 + \underline{d_5}s^5 \\
&\quad + \underline{d_6}s^6 + \overline{d_7}s^7 \\
G_3(s) &= \overline{d_0} + \overline{d_1}s + \underline{d_2}s^2 + \underline{d_3}s^3 + \overline{d_4}s^4 + \overline{d_5}s^5 \\
&\quad + \underline{d_6}s^6 + \underline{d_7}s^7 \\
G_4(s) &= \underline{d_0} + \overline{d_1}s + \overline{d_2}s^2 + \underline{d_3}s^3 + \underline{d_4}s^4 + \overline{d_5}s^5 \\
&\quad + \overline{d_6}s^6 + \underline{d_7}s^7
\end{aligned} \tag{3.4}$$

The coefficients $d_1 \dots d_7$ are functionally noted in Appendix (B). Each polynomial in 3.4 is analyzed for the Hurwitz stability where, the stability test of Hurwitz matrix generates 28 inequalities with two unknown coefficients.

3.3.1. Tuning Procedure

The four polynomials given in Eqn. 3.3 with coefficients $a_j s$ depends on the machine parameters R_r and L_m for every j. The $\min(a_j s)$ and $\max(a_j s)$ are attained at corner points of the parameter square given in Figure 7. The values of $a_j s$ is given in the table 3:

Table 3. Lower and upper bounds of $a_j s$.

	Lower Bound	**Upper Bound**
a_0	0	0
a_1	4.139e8	1.619e9
a_2	1.498e7	3.018e7
a_3	1.574e5	1.739e5
a_4	242	349.3
a_5	1	1

The numerator in the transfer function given in Eqn. B.5 has the upper and lower bound given in table 4 are given to compute the d_j coefficients.

Table 4. Lower and upper bounds of $b_j s$.

	Lower Bound	**Upper Bound**
b_0	9.049e8	1.803e9
b_1	9.56e6	1.084e7
b_2	4.189e5	6.139e8
b_3	3450	3459

Based on the values of $a_j s$ we can find the coefficients of four equations given in Eqn. 3.4. The coefficients are functions of controller parameters K_P and K_I.

$$n_4 = K_1(K_P b_3) \tag{3.5}$$

$$n_3 = K_1(K_I b_3 + K_p b_2) \tag{3.6}$$

$$n_2 = K_1(K_I b_2 + K_p b_1) \tag{3.7}$$

$$n_1 = K_1(K_I b_1 + K_p b_0) \tag{3.8}$$

$$n_0 = K_I b_0 \tag{3.9}$$

$$d_7 = 1 \tag{3.10}$$

$$d_6 = (K_2 + a_4) \tag{3.11}$$

$$d_5 = (a_4 K_2 + a_3) \tag{3.12}$$

$$d_4 = (K_2 a_3 + a_2 + K_I K_P b_3) \tag{3.13}$$

$$d_3 = (K_2 a_2 + a_1 + K_I b_3 + K_P b_2) \tag{3.14}$$

$$d_2 = (K_2 a_1 + a_0 + K_I b_2 + K_P b_1) \tag{3.15}$$

$$d_1 = (a_2 K_2 + K_I b_1 + K_P b_0) \tag{3.16}$$

$$d_0 = K_I b_0 \tag{3.17}$$

The stability of four polynomial obtained in Kharitonov's theorem guarantees the stability of the system with arbitrary R_r and L_m from square given in Figure 7. The lower and upper bounds on $d_j s$ obtained are given in table 5.

The Hurwitz matrix is generated for all of the four polynomials given in Eqn. 3.4 and the matrix is function of controller parameters K_P and K_I. The principle minors are obtained from Hurwitz matrix, which produces the 28 polynomials as a function of controller parameters.

Table 5. Lower and upper bounds of $d_j s$.

	Lower Bound	**Upper Bound**
d_0	6.7e13	1.3e14
d_1	6.3e8+9.5e6K_I+9.04e8K_P	1.2e11+1.1K_I+1.8e79K_P
d_2	1.6e12+4.2e5K_I +9.56e6K_P	6.5e12+6.1e8K_I+1.1e7K_P
d_3	6.0e10+3450K_I+4.2e5K_P	1.2e11 +3459K_I+6.1e8K_P
d_4	6.4e9+3450$K_I K_P$	7.3e9+3459$K_I K_P$
d_5	1.12e6	1.57e6
d_6	4242.9	4394.3
d_7	1	1

By using the optimization procedure the values of K_P and K_I are obtained for which all the 28 polynomials are positive. The values obtained for the K_P and K_I are then:

$$K_P = 0.8 \tag{3.18}$$

$$K_I = 2.9 \tag{3.19}$$

3.4. Tuning of PI Controller Using Classical Approach

Motion control systems often must respond to large changes in the reference values of the speed, torque, and position. For large changes, the overall system is usually nonlinear. The nonlinearity occurs due to mechanical load which is often highly nonlinear. Additional nonlinearity is introduced by voltage and current limits imposed by inverter and main supply and motor itself. The classical PI controller tuning therefore requires that the input reference change and load disturbances are small around steady-state operating point. Therefore, the system can be assumed linear around the steady-state operating point, so that the basic concepts of linear control theory can be applied. For controller design a cascade control structure shown in Figure 8 is used. The cascade control structure is commonly used for motor drives because of its flexibility. It consists of distinct control loops; the innermost current

(torque) loop is followed the speed loop. If position needs to be controlled accurately, the outer most position loop is superimposed on the speed loop. Cascade control requires that the bandwidth (speed of response) increases towards the inner loop, with the torque loop being the fastest, and the position loop being the slowest. The two loops are tuned for bandwidth of $250rad/s$ and $25rad/s$ respectively with a phase margin of 60^o for indirect field oriented controlled induction motor drive. Since, the parameters or gains of PI controller are based on machine parameters, the parameters of PI are calculated while assuming the estimation of all the machine parameters is perfect . This assumption is good, because it can create parametric mismatch between controller and induction motor under operation for detailed insight of the effect of parametric mismatch.

3.4.1. Speed Controller

In vector control block diagram shown in Figure 5 the two reference currents i_{sd}^{ref} and i_{sq}^{ref} are inputs to the flux linkage and torque controllers. The d-winding reference current i_{sd}^{ref} controls the rotor flux linkage λ_{rd}, where the q-winding current i_{sq}^{ref} controls the electromagnetic torque T_{em} developed by the motor. The reference dq winding currents (the outputs of the proportional-integral PI controllers) are converted into v_{sd}^{ref} and v_{sq}^{ref} voltage references. The dq-abc transformation produces the three voltage reference signals v_a^{ref}, v_b^{ref}, and v_c^{ref} for the inverter. The voltage controlled inverter can deliver the desired currents to the induction motor.

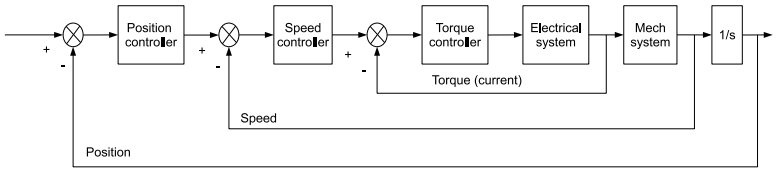

Figure 8. Cascade control of motor drive.

The outer speed loop is designed assuming unity feedback, while inner current (torque) loop is considered ideal having the gain of unity as shown in Figure 9. Since the system is assumed in steady state, and under indirect field oriented control the rotor d-axis current becomes zero(because d-axis is aligned along the rotor flux linkage) i.e., $i_{rd} = 0$ and i_{sd} is at rated value and is a constant. The d-axis flux linkage equation can be written as:

$$\begin{aligned} \lambda_{rd} &= L_r i_{rd} + L_m i_{sd} \\ \lambda_{rd} &= L_m i_{sd} \end{aligned} \tag{3.20}$$

by using $i_{rd} = 0$ and $i_{rq} = -\frac{L_m}{L_r} i_{sq}$ the electromagnetic torque equation:

$$\begin{aligned} T_{em} &= \frac{P}{2}(\lambda_{rq} i_{rd} - \lambda_{rd} i_{rq}) \\ T_{em} &= \frac{p}{2}\frac{L_m^2}{L_r} t_{sd} i_{sq} \\ T_{em} &= k i_{sq} \end{aligned} \tag{3.21}$$

where $k = \frac{p}{2}\frac{L_m^2}{L_r} i_{sd}$ is a constant. The open loop transfer function is:

$$\begin{aligned} G_{ol} &= (k_p + \frac{k_i}{s}) k (\frac{1}{s J_{eq}}) \\ G_{ol} &= \frac{k_i}{s}(1 + \frac{s}{\frac{k_i}{k_p}}) \frac{k}{s_J eq} \end{aligned} \tag{3.22}$$

So for given cutoff frequency (ω_c) and phase margin ϕ_{PM}, the k_p and k_i can be calculated such that:

$$\left(\frac{k_i k}{J_{eq}}\right)\left(\frac{1+\frac{s}{\frac{k_i}{k}}}{s^2}\right)_{s=j\omega_c} = 1 \tag{3.23}$$

$$\angle\left(\frac{k_i k}{J_{eq}}\right)\left(\frac{1+\frac{s}{\frac{k_i}{k}}}{s^2}\right)_{s=j\omega_c} = -180^o + \phi_{PM} \tag{3.24}$$

The bandwidth can be found using the closed loop transfer function G_{cl}, given as:

$$G_{cl} = \frac{G_{ol}}{1+G_{ol}} \tag{3.25}$$

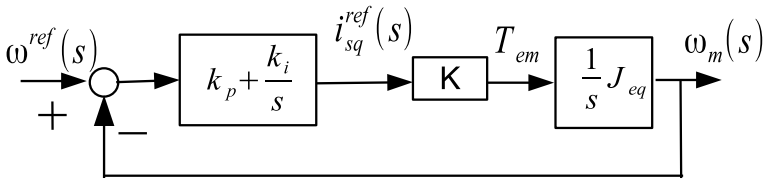

Figure 9. Block diagram of speed loop.

3.4.2. Current Control Design

Similarly the current loop shown in Figure 10 is designed for the given cutoff frequency and phase margin. Under vector control conditions and steady state operation the v_{sd}^* and v_{sq}^* can be written as:

$$v_{sd}^* = v_{sd} + v_{sd,compensated} \tag{3.26}$$

$$v_{sq}^* = v_{sq} + v_{sq,compensated} \tag{3.27}$$

where the stator d-axis and q-axis voltages are:

$$v_{sd} = Rsi_{sd} + \sigma L_s \frac{di_{sd}}{dt} \tag{3.28}$$

$$v_{sq} = Rsi_{sq} + \sigma L_s \frac{di_{sq}}{dt} \tag{3.29}$$

The Laplace transform of the equation v_{sd} and v_{sq} is given as:

$$i_{sd}(s) = \frac{1}{R_s + s\sigma L_s} v_{sd}(s) \tag{3.30}$$

$$i_{sq}(s) = \frac{1}{R_s + s\sigma L_s} v_{sq}(s) \tag{3.31}$$

Since the controller parameters are calculated based on the ideal conditions and disturbance can be avoided therefore, it is assumed that the $v_{sd,compensated}$ and $v_{sq,compensated}$ are disturbance terms and can be set to zero. The open loop transfer function for the current loop shown in Figure 10 is:

$$G_{ol} = \frac{k_p + \frac{ki}{s}}{R_s + s\sigma L_s}$$

$$G_{ol} = k_i \frac{1 + \frac{s}{\frac{k_i}{k_p}}}{s^2 \sigma L_s + s R_s} \tag{3.32}$$

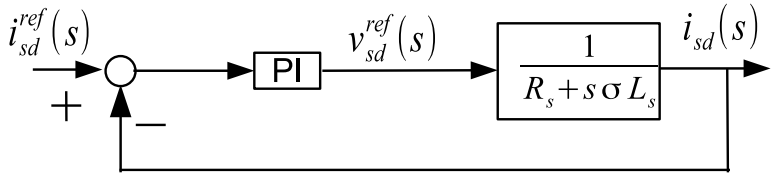

Figure 10. Block diagram of current loop.

The parameters for PI controllers for both d-axis and q-axis can be found from:

$$|G_{ol}|_{s=j\omega_c} = 1 \tag{3.33}$$

$$\angle G_{ol}|_{s=j\omega_c} = -180^o + \phi_{PM} \tag{3.34}$$

3.5. Tuning of PI Controller Using Symmetric Optimum

The magnitude and symmetric optimization techniques are two related methods for designing "optimal" linear control systems in the frequency domain. The technique is most commonly used in industries to tune the PID controller. In magnitude optimum technique the main objective is to maintain the magnitude response curve as flat as close to unity for as large bandwidth as possible for the given plant and controller. The magnitude optimum is an optimization technique to find the best controller coefficients for a given controller configuration that previously had been determined [45].

3.6. Block Diagram and its Reduction

The block diagram of the indirect vector controlled induction motor is produced by developing transfer functions of different components of the drive system shown in Figure 11. The block diagram shows the overlap between the torque current feedback loop and induced emf feedback loop. The overlap can be removed by using the block reduction techniques.

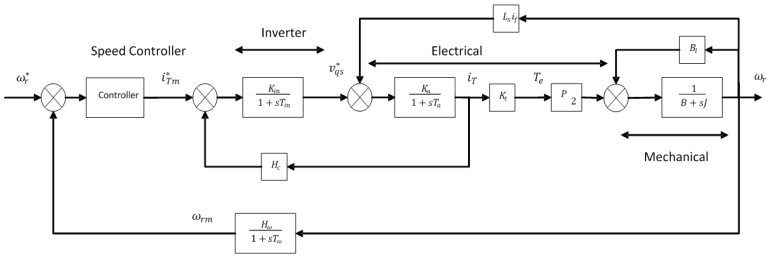

Figure 11. Block diagram of vector control induction motor with constant rotor flux.

3.6.1. Indirect Vector Controlled Induction Machine

The indirect vector controlled induction motor drive is obtained with the key assumptions of constant rotor flux linkages:

$$\lambda_r = \text{a constant} \tag{3.35}$$

$$p\lambda_r = 0 \tag{3.36}$$

where p is derivative operator. The stator equations of the induction motor are then obtained as:

$$v_{qs}^e = (R_s + L_s p)i_{qs}^e + \omega_s L_s ids^e + L_m p i_{qr}^e + \omega_s L_m i_{dr}^e \tag{3.37}$$

$$v_{ds}^e = -\omega_s L_s i_{qs}^e + (R_s + L_s p)i_{ds}^e - \omega_s L_m iqr^e + L_m p i_{dr}^e \tag{3.38}$$

since by vector controller, we have:

$$i_{qr}^e = -\frac{L_m}{L_r} i_{qs}^e \tag{3.39}$$

$$i_{dr}^e = \frac{\lambda_r}{L_r} - \frac{L_m}{L_r} i_{ds}^e \tag{3.40}$$

substituting the rotor currents in to stator voltage equations yields:

$$v_{qs}^e = (R_s + \sigma L_s p)i_{qs}^e + \sigma L_s \omega_s i_{ds}^e + \omega_s \frac{L_m}{L_r}\lambda_r \tag{3.41}$$

$$v_{ds}^e = (R_s + \sigma L_s p)ids^e - \sigma L_s \omega_s ids^e + \frac{L_m}{L_r} p\lambda_r \tag{3.42}$$

where σ is the leakage coefficient. The flux producing component of the stator current which is d axis stator current in the synchronous frames is constant in steady state and hence its derivative is also zero.

$$i_f = i_{ds}^e \tag{3.43}$$

$$p i_{ds}^e = 0 \tag{3.44}$$

The torque producing component of the stator current is the q axis current in the synchronous frames, given by:

$$i_T = i^e_{qs} \tag{3.45}$$

by plugging into q axis voltage equation gives:

$$v^e_{qs} = (R_s + \sigma L_s p) i_T + \omega_s L_a \omega_s i_f + \omega_s \frac{L_m}{L_r} \lambda_r \tag{3.46}$$

where L_a is defined as:

$$L_a = \sigma L_s = \left(L_s - \frac{L^2_m}{L_r} \right) \tag{3.47}$$

substituting $\lambda_r = L_m i_f$ gives the q axis stator voltage in synchronous reference frame:

$$v^e_{qs} = (R_s + \sigma L_s p) i_T + \omega_s L_a \omega_s i_f + \omega_s \frac{L^2_m}{L_r} i_f = R_s + L_a p i_T + \omega_s L_s i_f \tag{3.48}$$

The second stator equation is not required, the solution of either will yield i_T, which is the variable under control in the system. Now the stator frequency is represented as:

$$\omega_s = \omega_r + \frac{i_T}{i_f} (\frac{R_r}{L_r}) \tag{3.49}$$

substituting ω_s in Eqn. 3.48 gives:

$$v^e_{qs} = (R_s + \frac{R_r L_s}{L_r} + L_a p) i_T + \omega_r L_s i_f \tag{3.50}$$

From which the torque producing component of the stator current is derived as:

$$i_T = \frac{v^e_{qs} - \omega_r L_s i_f}{R_s + \frac{R_r L_s}{L_r} + L_a p} = \frac{K_a (v_{qs^e - \omega_r L_s i_f})}{1 + sTa} \tag{3.51}$$

where

$$\begin{aligned} R_a &= R_s + \frac{L_s}{L_r} R_r \\ K_a &= \frac{1}{R_a} \\ T_a &= \frac{L_a}{R_a} \end{aligned}$$

The electromagnetic torque is given as:

$$T_e = \frac{3}{2}\frac{P}{2}\frac{L_m^2}{L_r} i_f = K_t i_T \tag{3.52}$$

The load dynamics can be represented, given the electromagnetic torque and a load torque that is considered to be frictional for this particular case, as:

$$J\frac{d\omega_m}{dt} + B\omega_m = T_e - T_l = K_t i_T - B_l \omega_r \tag{3.53}$$

and hence the transfer function between the speed and the torque producing current is derived as:

$$\frac{I_T(s)}{\omega_r(s)} = \frac{K_m}{1 + sT_m} \tag{3.54}$$

where

$$K_m = \frac{P}{2}\frac{K_t}{B_t} \tag{3.55}$$

$$B_t = B + B_l \tag{3.56}$$

$$T_m = \frac{J}{B_t} \tag{3.57}$$

3.6.2. Inverter

The stator q axis voltage is delivered by the inverter with a command input that is the error between the torque-current feedback. The gain of the current controller

is considered unity. The inverter is modeled as a gain, K_in with a time lag of T_in. The gain is obtained from dc-link voltage to the inverter, V_{dc}, and maximum control voltage, V_{cm}, as:

$$K_{in} = 0.65\frac{V_{dc}}{V_{cm}} \tag{3.58}$$

The term 0.65 is introduced to account for the maximum peak fundamental voltage obtainable from the inverter with a given dc-link voltage. The time lag in the inverter is equal to the carrier switching-cycle time, which half the period, and is given in terms of PWM switching frequency as:

$$T_{in} = \frac{1}{2f_c} \tag{3.59}$$

3.6.3. Speed Controller

A PI controller is used to process the speed-reference and filtered speed feedback signals. The PI controller is given as:

$$G_s(s) = \frac{K_s(1 + sT_s)}{sT_s} \tag{3.60}$$

where K_s and T_s are the gain and time constants of the speed controller respectively. The feedback for the current signal is $G_c(s) = H_c$.

3.6.4. Speed Feedback

The speed feedback signal is processed through first order filter given by:

$$G_\omega(s) = \frac{\omega_{rm}(s)}{\omega_r} = \frac{H_\omega}{1 + sT_\omega} \tag{3.61}$$

Using the pickoff point for the electrical system can be moved to the i_T point which further can be simplified where the current loop transfer function is given by:

$$G)i(s) = \frac{K_a K_{in}(1+sT_m)}{(1+sT_{in}[(1+sT_a)(1+sT_m)+K_a K_b]+H_c K_a K_{in}(1+ST_m))} \tag{3.62}$$

where emf constant is given by $K_b = K_m L_s i_f$.

3.6.5. Simplified Current Loop Transfer Function

The third order current transfer function $\frac{i^*_{Tm}}{H_c i^*_T}$, can be approximated to a first order transfer function as follows. T_{in} is usually negligible compared to T_1,T_2, and T_m and in the vicinity of crossover frequency, the following approximation are valid:

$$\begin{aligned} 1+sT_{in} &\approx 1 \\ (1+sT_a)(1+sT_{in} &\approx 1+s(T_a+T_{in}) \approx 1+sT_{ar} \end{aligned} \tag{3.63}$$

where $T_{ar} = T_a + T_{in}$. Substituting these into $G_i(s)$ results in:

$$G_i(s) = \frac{K_a K_{in}(1+sT_m)}{(1+sT_{ar})(1+sT_m)+K_a K_b + H_c K_a K_{in}(1+sT_m)} \tag{3.64}$$

which can written in compact form as:

$$G_i(s) = \frac{T_1 T_2 K_a K_{in}}{T_{ar} T_m} \frac{(1+sT_m)}{(1+sT_1)(1+sT_2)} \tag{3.65}$$

where

$$-\frac{1}{T_1}, -\frac{1}{T_2} = \frac{-b \pm \sqrt{b^2-4ac}}{2a} \tag{3.66}$$

$$a = T_{ar} T_m \tag{3.67}$$

$$b = T_{ar} + T_m + H_c K_a K_{in} T_m \tag{3.68}$$

$$c = 1 + K_a K_b + H_c K_a K_{in} \tag{3.69}$$

The transfer function $G_i(s)$ is simplified by using the fact that $T_1 < T_2 < T_m$ and near the vicinity of the crossover frequency, the following approximations are valid:

$$1 + sT_m \approx sT_m \tag{3.70}$$

$$1 + sT_2 \approx sT_2 \tag{3.71}$$

substituting these into $G_i(s)$ yields:

$$G_i(s) = \frac{K_a K_{in} T_1}{T_{ar}} \frac{1}{(1 + sT_i)} = \frac{K_i}{(1 + sT_i)} \tag{3.72}$$

where K_i and T_i are the gain and time constant of the simplified current loop transfer function, given by:

$$K_i = \frac{K_a K_{in} T_1}{T_{ar}} \tag{3.73}$$

$$T_i = T + 1 \tag{3.74}$$

The model reduction of the current loop is necessary to synthesize the speed controller. The loop transfer function of the speed is given then by the substitution of this simplified transfer function of the current loop.

3.6.6. Speed Controller Design

The transfer function of the speed loop is given by:

$$GH(s) \approx \frac{K_s}{T_s} K_g \frac{(1 + sT_s)}{s^2(1 + sT_{\omega i})} \tag{3.75}$$

where approximation $1 + sT_m \approx sT_m$ is made and the current loop time constant and speed filter time constant are combined into an equivalent time constant:

$$T_{\omega i} = -T_{\omega} + T_i \tag{3.76}$$

$$K_g = K_i K_m \frac{H_{\omega}}{T_m} \tag{3.77}$$

The transfer function of the speed to its command is derived as:

$$\frac{\omega_r(s)}{\omega_r^*} = \frac{1}{H_{\omega}} \left(\frac{1 + sT_s}{1 + sT_s + \frac{T_s}{K_g K_s} s^2 + \frac{T_s T_{omegai}}{K_g K_s} s^3} \right) \tag{3.78}$$

By equating the coefficient of the denominator polynomial to the coefficient of the symmetric optimum function, K_s and T_s can be evaluated:

$$\frac{1_s T_s}{1 + (T_s)s + (\frac{3}{8} T_s^2)s^2 + (\frac{1}{16} T_s^3)s^3} \tag{3.79}$$

The symmetric optimum function found is for a damping ratio of 0.707. From which the speed controller constants are derived as:

$$T_s = 6T_{\omega i} \tag{3.80}$$

$$K_s = \frac{4}{9} \frac{1}{K_g T_{\omega i}} \tag{3.81}$$

The proportional and integral gains of the speed controller are, respectively, then obtained as:

$$K_p = K_s = \frac{4}{9} \frac{1}{K_g T_{\omega i}} \tag{3.82}$$

$$K_i = \frac{K_s}{T_s} = \frac{2}{27} \frac{1}{K_g T_{\omega i}^2} \tag{3.83}$$

The symmetric optimum controller gains for the motor given parameter are:

$$K_p = 0.28 \tag{3.84}$$

$$K_I = 16.715 \tag{3.85}$$

The constant gain as expected can be observed in the Figure 12.

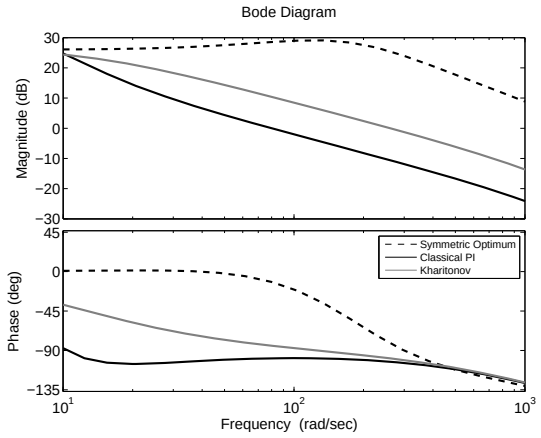

Figure 12. Symmetric optimum speed controller.

3.7. Results

We consider a 3 phase induction motor drive system with parameters (from [71]) as noted in Appendix (B). We consider variations in two key parameters namely: rotor resistance R_r and mutual inductance (L_m) as noted earlier, in Figure (7). The speed controller tuned via Kharitonov's theorem is compared with a standard tuning procedure - the Symmetric Optimum [76] popularly used in industrial drives and the classical method. The controller settings obtained with these three approaches are shown in Table. 6.

Table 6. Controller parameters for different tuning techniques.

	K_p	K_i
Classical PI	0.24	3.53
Symmetric Optimum	0.28	16.715
Kharitonov Theorem	0.8	2.9

3.7.1. Small Signal Analysis

The eigenvalues of the drive system at rated values are given in Table 7, while Table 8 shows eigenvalues for L_m at 80% and R_r at 200%. The induction machine contributes to five eigenvalues whereas the inverter and controller contribute to one eigenvalue each. The first pair of eigenvalues correspond to the electromechanical oscillatory mode associated with the rotor. The last eigenvalue corresponds to the fast acting inverter dynamics. From the eigenvalue results, it can be noted that the dynamics are well damped with nominal values, for all three control settings. At condition C, the symmetric optimum based controller is poorly damped compared to settings with the classical and proposed methods. The actual dynamic performance with these controllers is verified with dynamic simulations described in the next section.

Table 7. Poles location for classical PI and proposed PI (Kharitonov theorem) at rated values.

λ	Classical Method	Symmetric Optimum	Kharitonov Theorem
1	-65.86+j388.27	-40.892+j383.49	-60.176+j431.87
2	-65.86-j388.27	-40.892-j383.49	-60.176-j431.87
3	-2.86+j12.43	-50.112+j52.455	-10.646+j25.06
4	-2.86-j12.43	-50.112-j52.455	-10.646-j25.06
5	-66.04	-53.422	-84.206
6	-35.43	-3.3976	-4.0825
7	-4004	-4004	-4013

Table 8. Poles location for classical PI and proposed PI (Kharitonov theorem) for L_m at 80% and R_r at 200%.

λ	Classical Method	Symmetric Optimum	Kharitonov Theorem
1	-66.89+j380.09	-64.016+j382.78	-66.433+j425.66
2	-66.89+j380.09	-64.016-j382.78	-66.433-j425.66
3	-2.04+j8.45	-107.84+j8.396	-21.331
4	-2.04+j8.45	-107.84-j8.396	-5.0693
5	-120.98	-0.51098+j17.782	-143.28
6	-86.413	-0.51098+j17.782	-33.576
7	-4004	-4004	-4013

3.7.2. Small Signal Disturbance Dynamic Response

The small signal analysis can be compared with the following simulation setup:

- The simulation starts with full load and machine parameters R_r at 200% and L_m at 80% of the rated values.
- The small load torque change is applied at 4 seconds.
- The load torque is set back to full load torque.

The simulation results shows that the with small disturbance and the with L_m at 80% and R_r at 200% the drive is still stable and small disturbance does not make system unstable.

3.7.3. Dynamic Simulations

To assess control performance, dynamic simulations are conducted on the full system with the 5th order nonlinear induction motor model [82], with machine parameters as described in Appendix (B). Control saturation is represented for all the controllers as shown in Figure 6. The simulations are configured as follows:

1. First, the motor starts with full load torque and attains steady state.
2. At 3 sec, the load torque is reduced to $\frac{1}{2}$ while retaining nominal parameters.

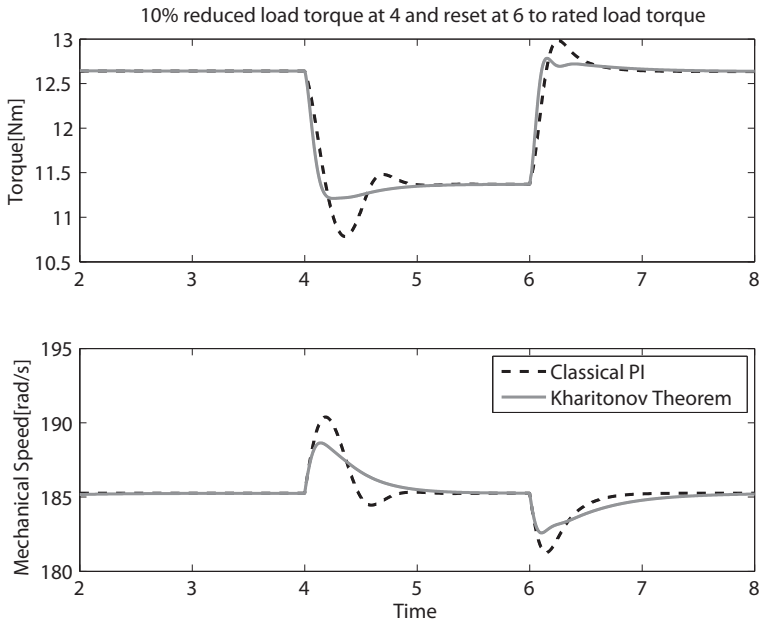

Figure 13. Torque and speed response.

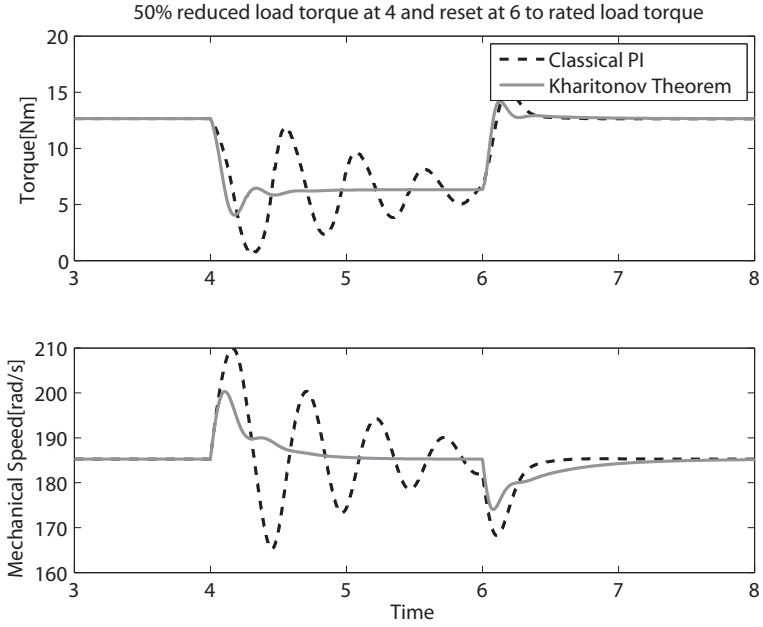

Figure 14. Torque and speed response.

3. At 5 sec, parameter variations (noted earlier in Sec. 3.2) are introduced as a step-input, while parameter drifts occur gradually in practice, a harsh step change is considered to assess the dynamic performance as a worst case scenario.

The dynamic response with nominal parameters is shown in Figure 15. The response is well damped with all three controllers as corroborated with the eigenvalue results in Table. 7. Doubling the rotor resistance while keeping all other parameters fixed, produces the dynamic response as shown in Figure 16. While the response is stable and damped with all three control settings, the proposed controller displays superior dynamic performance via reduced overshoots in torque and speed with faster settling time. Dropping the magnetizing inductance to 80 % of its nominal value while keeping all other parameters fixed, produces the dynamic response as shown in Figure 17. Here, the dynamic performance is considerably degraded for controllers tuned traditionally and via symmetric optimum, as shown by the oscillatory response. However, the response is well damped with the proposed controller in terms of overshoot and settling time. Dropping the magnetizing inductance to 80 % and doubling the rotor resistance produces the dynamic response as shown in Figure 18. In this case, the dynamic performance of the proposed controller is superior to the classical PI and symmetric optimum as in the previous cases.

The selection of parameters of the PI controller parameter are further verified by random selection of rotor resistance and magnetizing inductance within the shaded region of parametric space shown in Figure 7. The dynamic response for these selection of controller parameters is shown in Figure 19. The dynamic response with proposed and classical PI controller shows the stable response having more damping than classical PI. The response becomes unstable by using symmetric optimum.

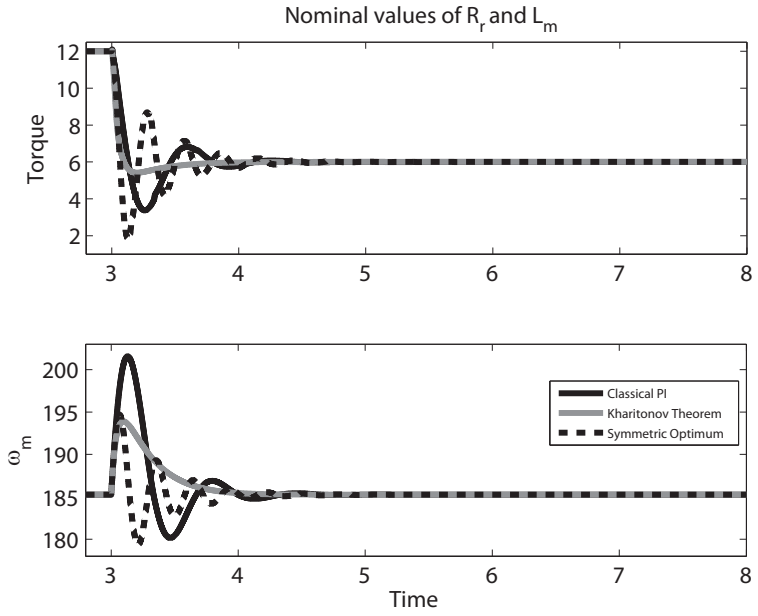

Figure 15. Torque and speed response.

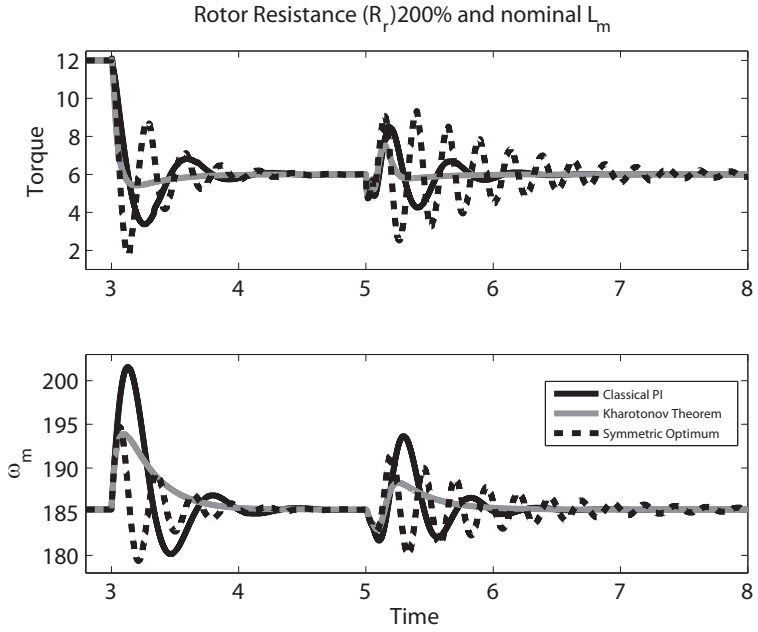

Figure 16. Torque and speed response for D.

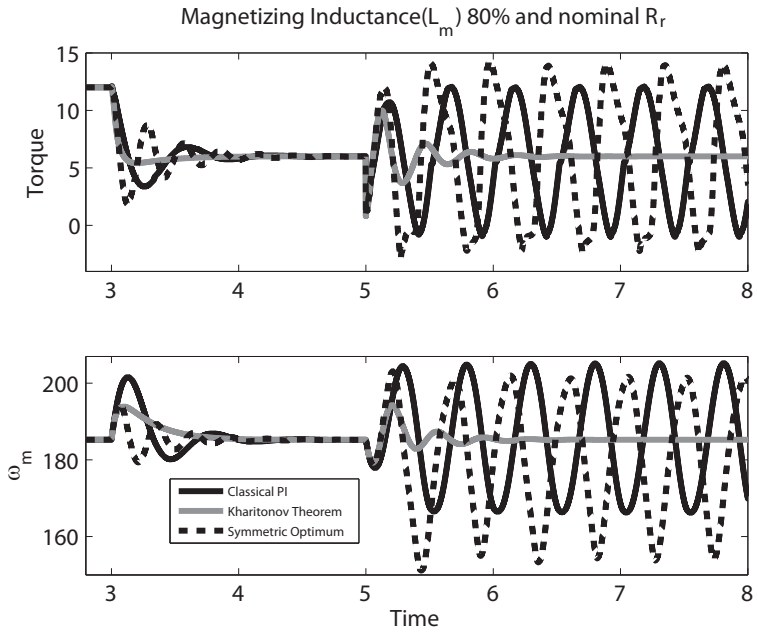

Figure 17. Torque and speed response for B.

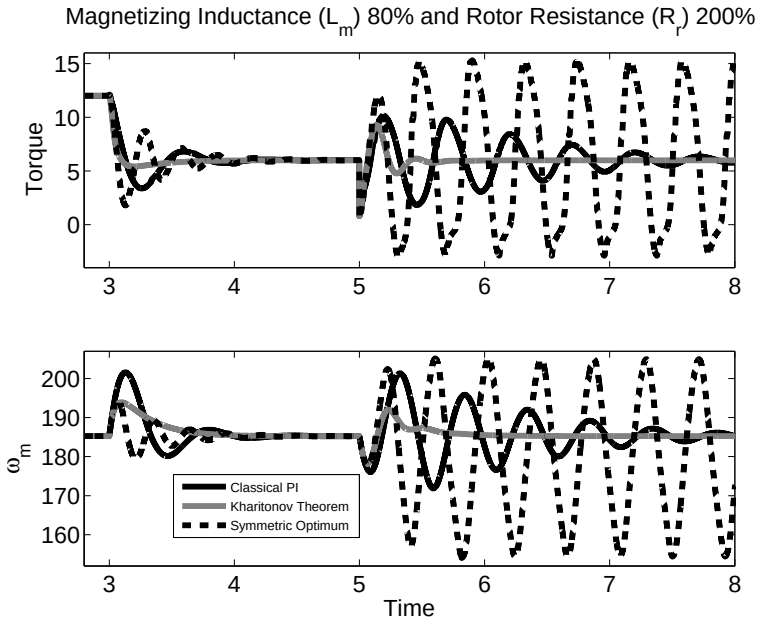

Figure 18. Torque and speed response for C.

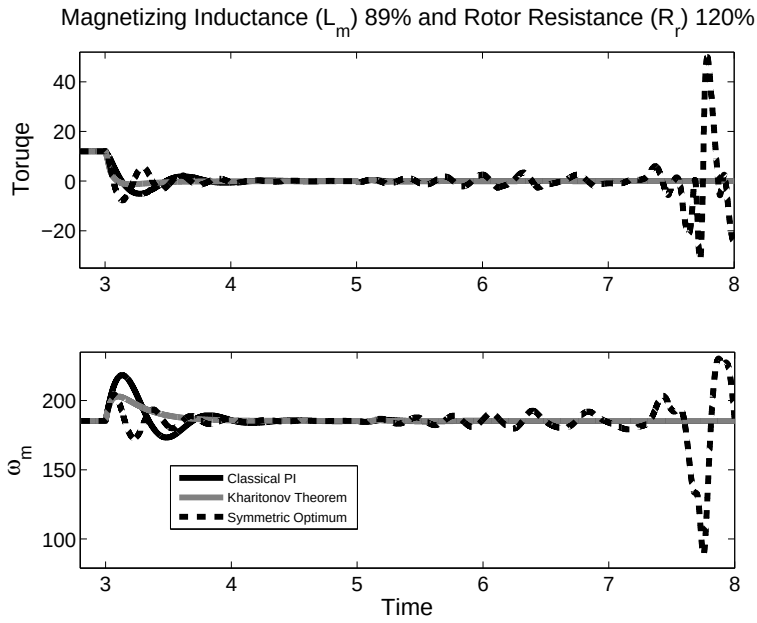

Figure 19. Torque and speed response at 89% rated value of L_m and 120% rated value of R_r, corresponding to point inside shaded region.

Figure 22 shows input power and air gap power and corresponding efficiency of controller tuned using classical PI and Kharitonov's theorem. The efficiency of the motor is approximately same as before the introduction of parameter mismatch as disturbance. Figures 20 and 21 shows the unstable response and hence efficiency can not be obtained.

3.7.4. Quantitative Analysis of Dynamic Simulation

From previous section we can conclude that the controller synthesis using Kharitonov's theorem produces the better results and are verified with in the parametric space shown in Figure 7. The simulations results for the stable case are considered to produce the quantitative analysis for the controller. The results for classical PI and PI synthesized using Kharitonov's theorem are presented in the Figures 23, 24, 25, and 26.

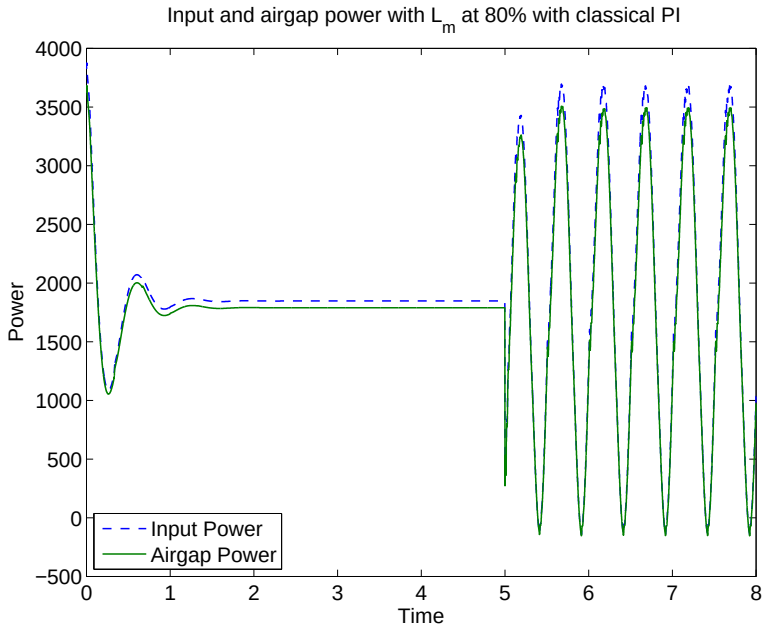

Figure 20. Input and airgap power with magnetizing inductance reduced to 80% of the rated value with classical PI control configuration.

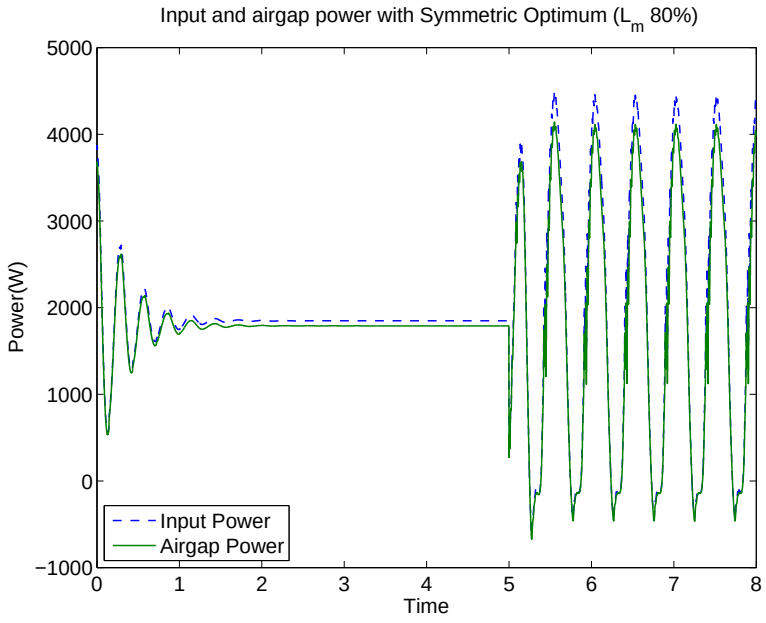

Figure 21. Input and airgap power with magnetizing inductance reduced to 80% of the rated value with symmetric optimum PI control configuration.

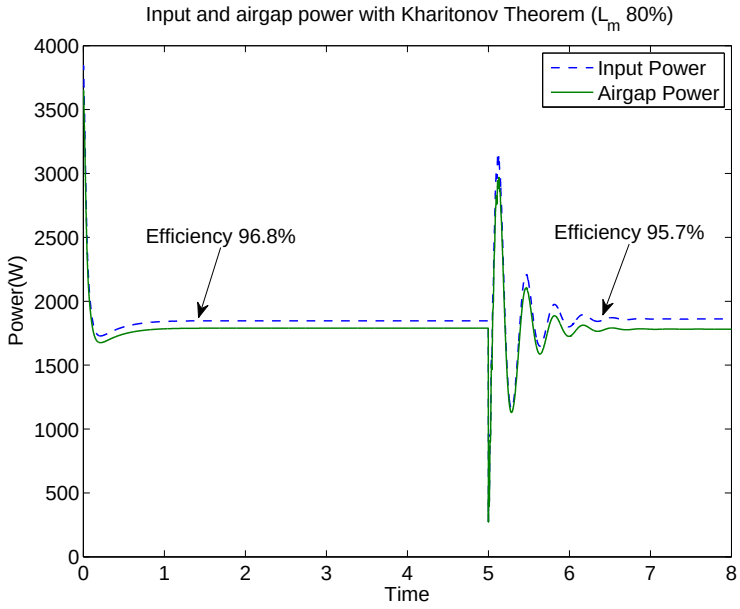

Figure 22. Input and airgap power with magnetizing inductance reduced to 80% of the rated value with Kharitonov theorem PI control configuration.

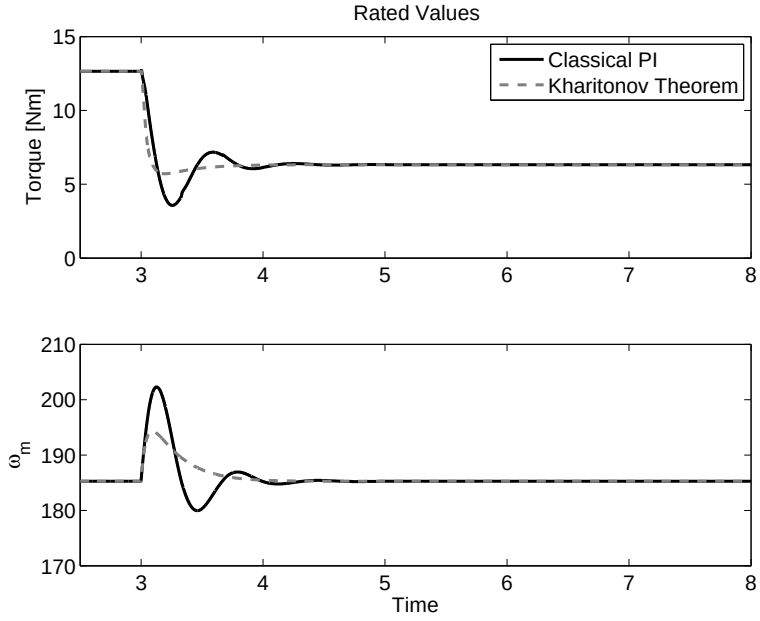

Figure 23. Torque and speed response at nominal values of R_r and L_m (Point A).

Table 9. Quantitative analysis at rated values with step change in load torque.

	Settling Time	**Overshoot**	**Rise Time**
Torque (PI)	1.4s	14.3%	1.2s
Torque (KT)	0.2	0%	0.2s
Speed (PI)	1.4s	9%	1.4s
Speed (KT)	0.9s	4.8%	0.06s

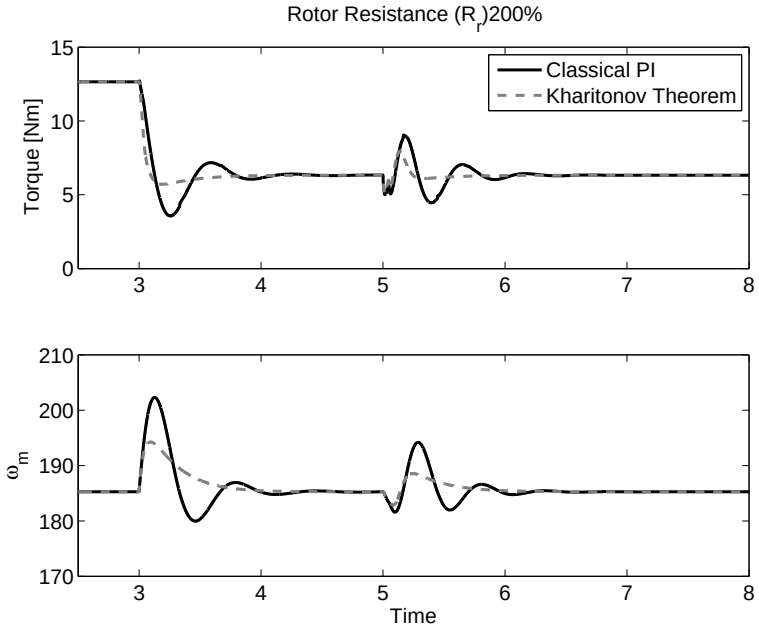

Figure 24. Torque and speed response at 200% rated value of R_r and nominal L_m, (point D).

Table 10. Quantitative analysis at rated values with R_r as step change.

	Settling Time	**Overshoot**	**Rise Time**
Torque (PI)	1.25s	43.6%	1.17s
Torque (KT)	0.5s	26.9%	0.3s
Speed (PI)	1.25s	4.6%	1.27s
Speed (KT)	1.25s	1.7%	0.72s

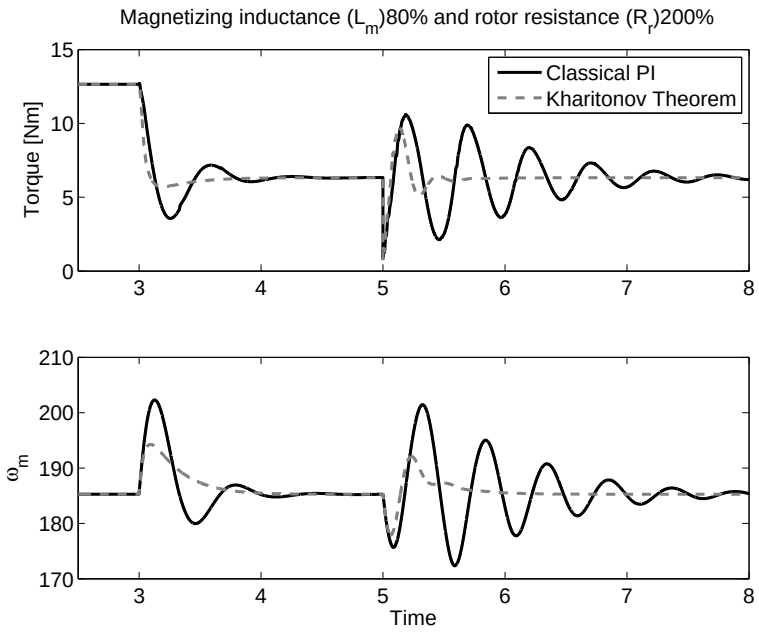

Figure 25. Torque and speed response at 80% rated value of L_m and 200% rated value of R_r, (point C).

Table 11. Quantitative analysis at rated values with 80% rated value of L_m and 200% rated value of R_r.

	Settling Time	**Overshoot**	**Rise Time**
Torque (PI)	3s	68.3%	0.17s
Torque (KT)	0.74s	54.3%	0.14s
Speed (PI)	3s	8.7%	1.3s
Speed (KT)	0.8s	3.6%	0.22s

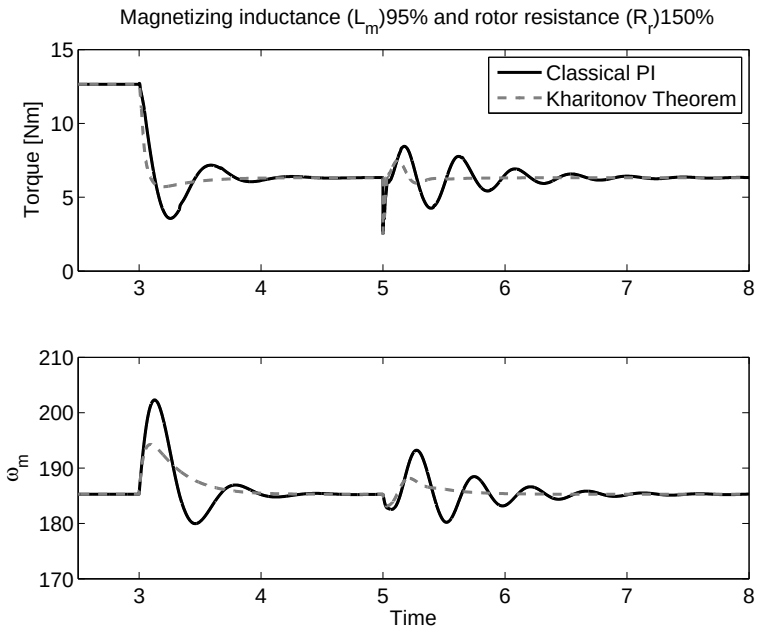

Figure 26. Torque and speed response at 95% rated value of L_m and 150% rated value of R_r, corresponding to point inside shaded region.

Table 12. Quantitative analysis at rated values with R_r and L_m as step change.

	Settling Time	**Overshoot**	**Rise Time**
Torque (PI)	2s	34.12%	0.25s
Torque (KT)	0.5s	19.8%	0.12s
Speed (PI)	2s	4.26%	0.25s
Speed (KT)	1s	1.5%	0.12s

3.8. Parameter Mismatch Reference and Generated Signals Analysis

All simulations consider the machine under full (rated) load torque (assumed as a constant torque load). The sensitivity of the system is evaluated with respect to two parameters: rotor resistance (R_r) and magnetization (L_m) which will drift with temperature variations. The eigenvalue results for "local" stability and dynamic simulations with the nonlinear model show that the performance of the drive system is most sensitive to L_m.

The mismatch between reference and generated torques at nominal parameters and when $L_m = 80\%$ of nominal are shown for a PI controller: **(a)** tuned traditionally, **(b)** tuned with symmetric optimum and **(c)** tuned with the proposed method. All the results are shown in the Figures from 27-38. The simulation results clearly show a pronounced mismatch when $L_m = 80\%$ of its nominal value.

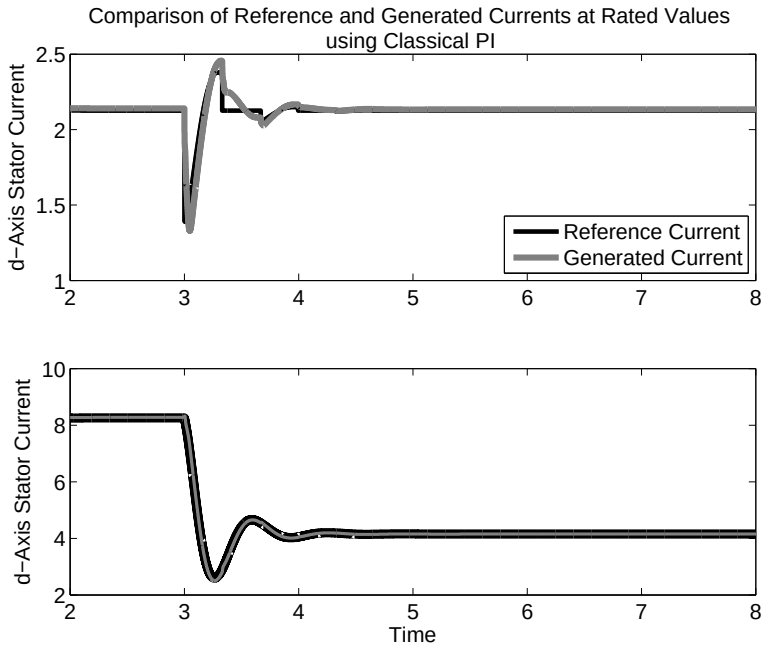

Figure 27. dq-axis reference stator currents classical PI.

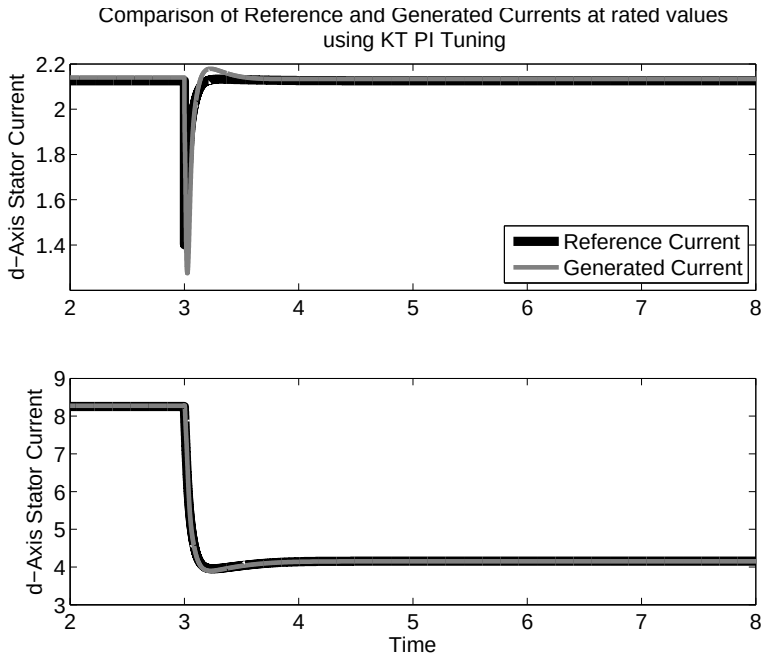

Figure 28. dq-axis reference stator currents Kharitonov theorem PI.

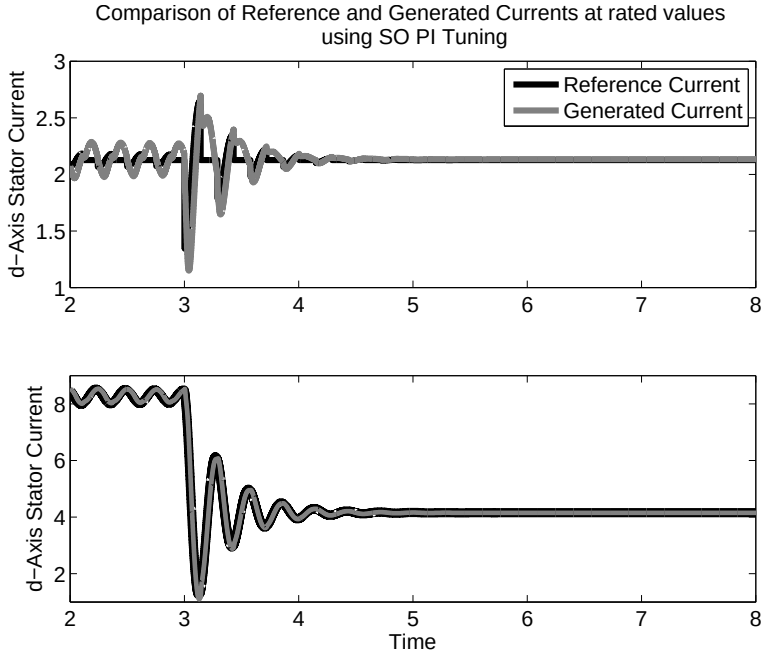

Figure 29. dq-axis reference stator currents symmetric optimum PI.

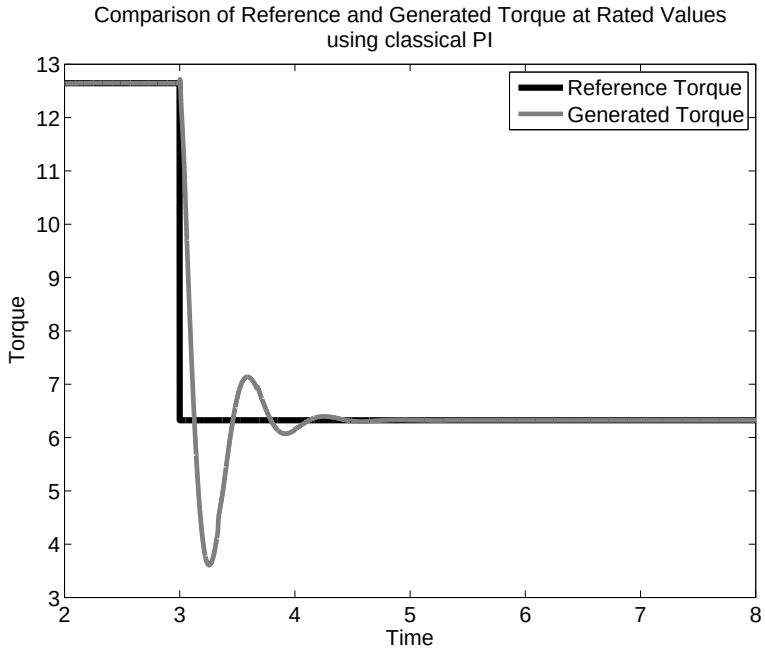

Figure 30. Torque reference classical PI.

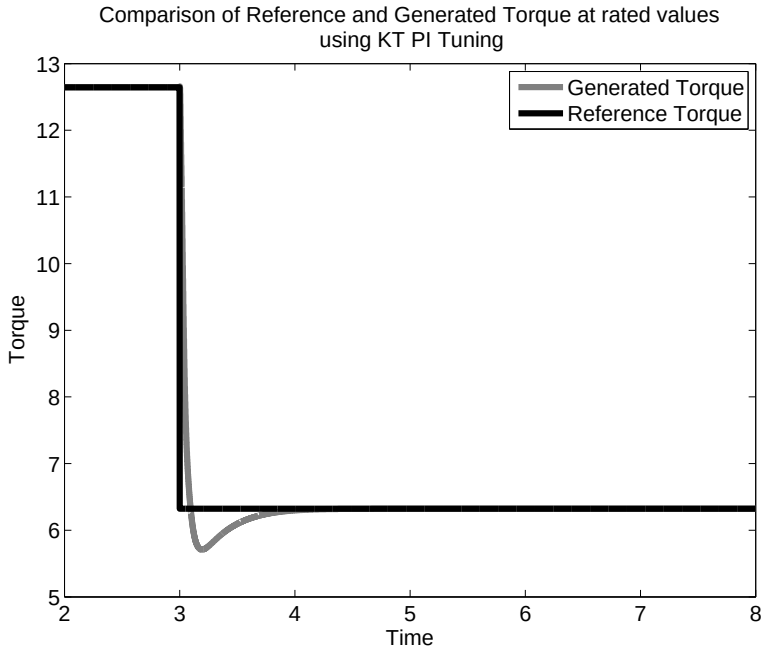

Figure 31. Torque reference Kharitonov theorem PI.

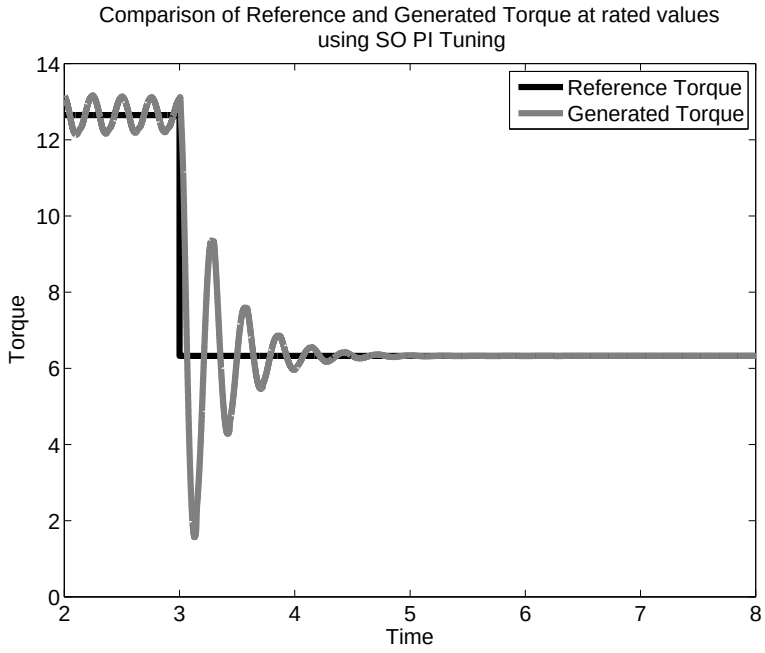

Figure 32. Torque reference symmetric optimum PI.

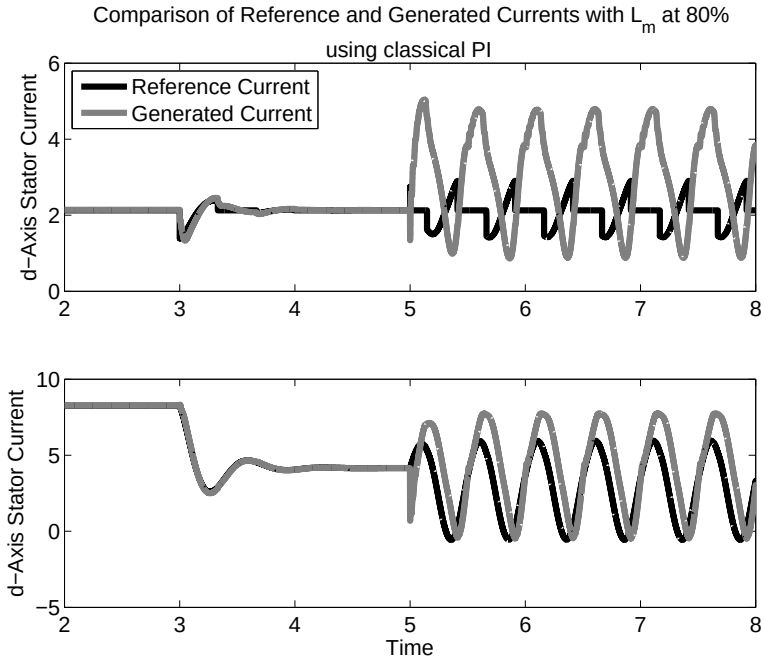

Figure 33. dq-axis reference stator currents classical PI with L_m at 80%.

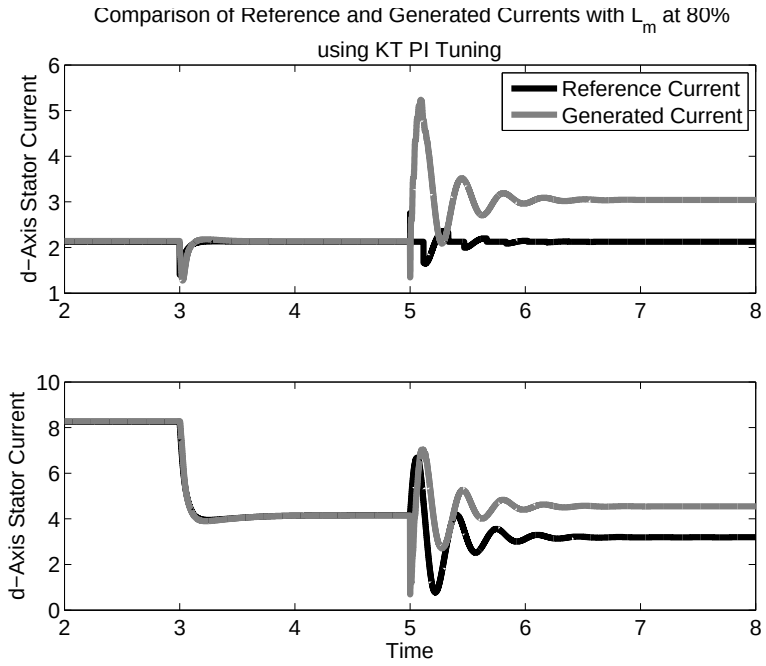

Figure 34. dq-axis reference stator currents Kharitonov theorem PI with L_m at 80%.

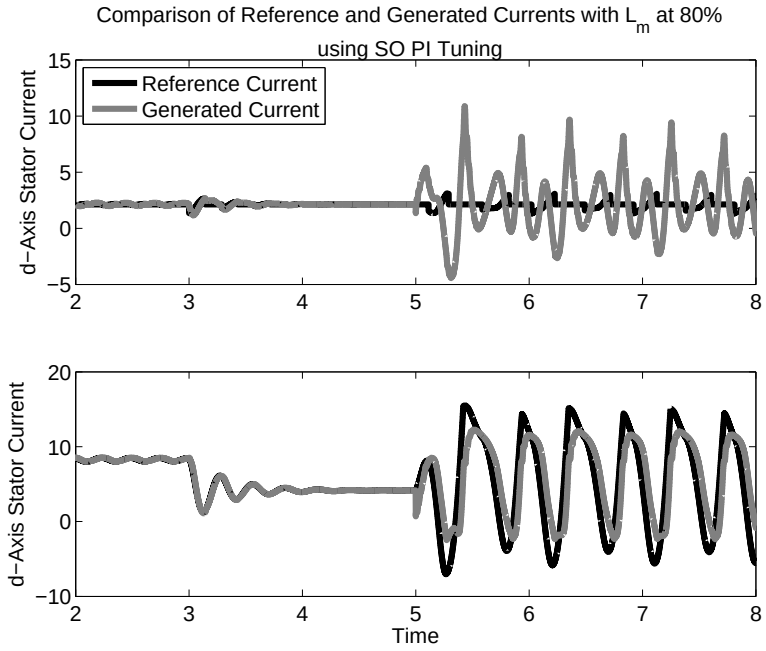

Figure 35. dq-axis reference stator currents symmetric optimum PI with L_m at 80%.

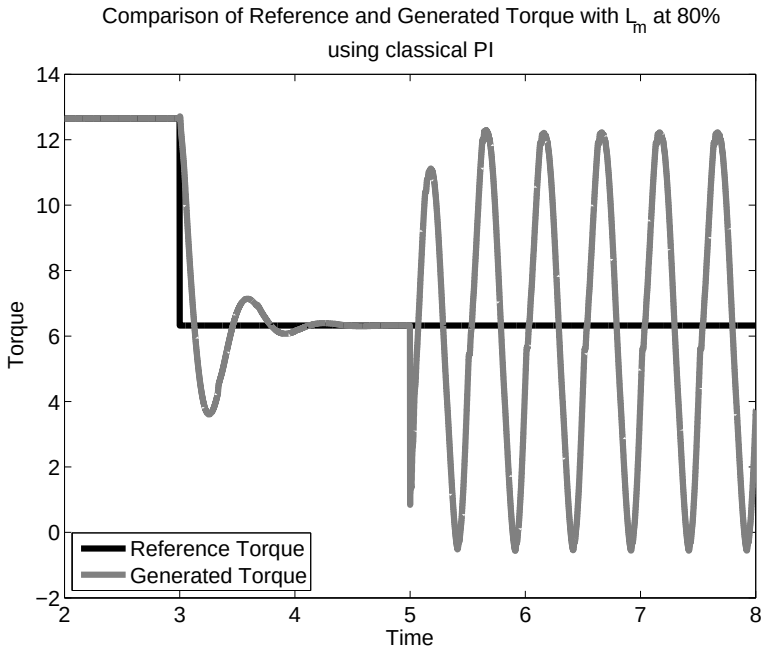

Figure 36. Torque reference classical PI with L_m at 80%.

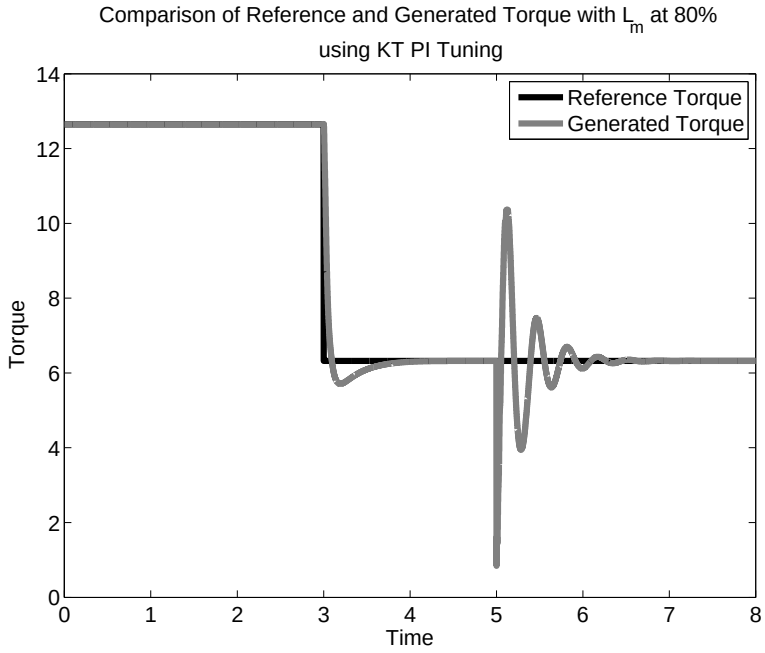

Figure 37. Torque reference Kharitonov theorem PI with L_m at 80%.

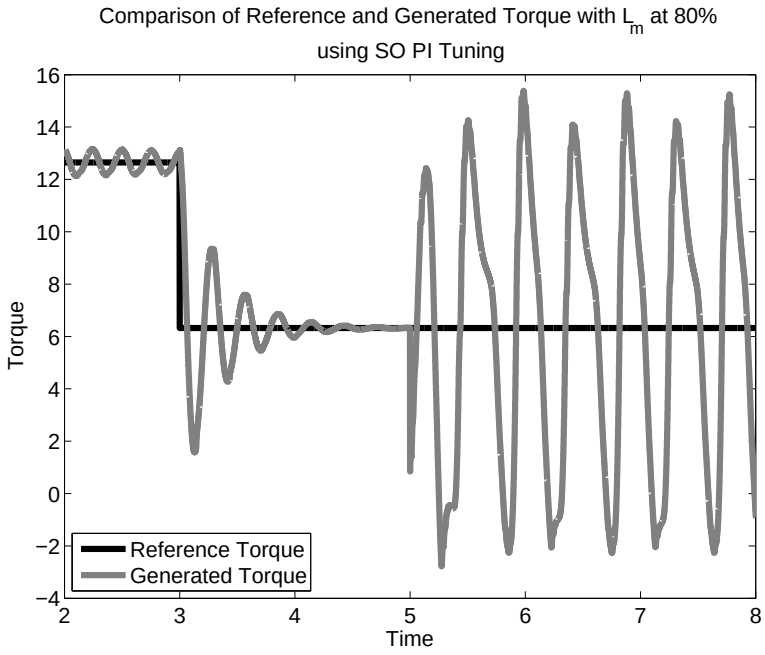

Figure 38. Torque reference symmetric optimum PI with L_m at 80%.

3.9. Performance at Low Speed

Simulation results are shown for speeds at 10%, 20% and 50% of rated speeds. The parameter Lm is considered at nominal and 80% of nominal at each of these speeds. The results show that the control performance is not adversely affected at low speeds. This is because our method does not rely on speed as an explicit or implicit input unlike in sensorless control applications which rely on parameter estimation.

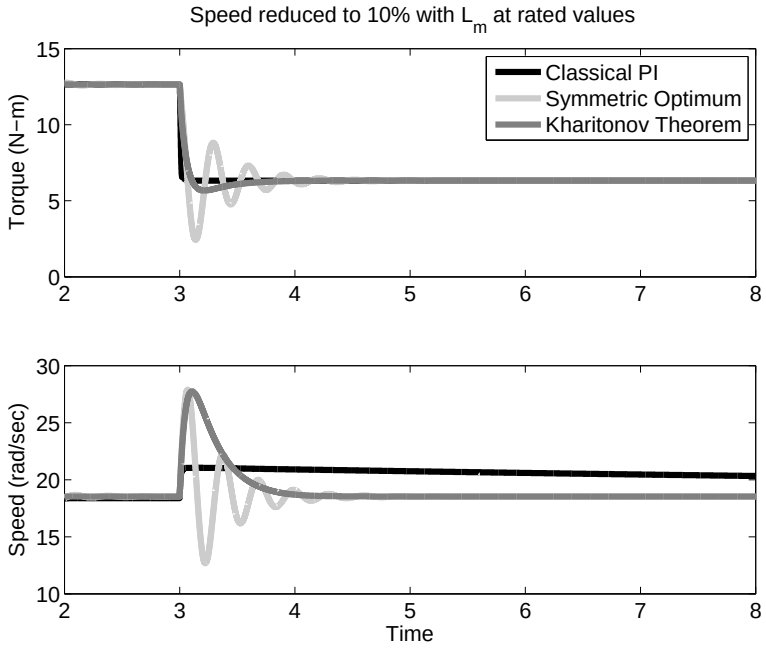

Figure 39. Speed reduced to 10% at rated values.

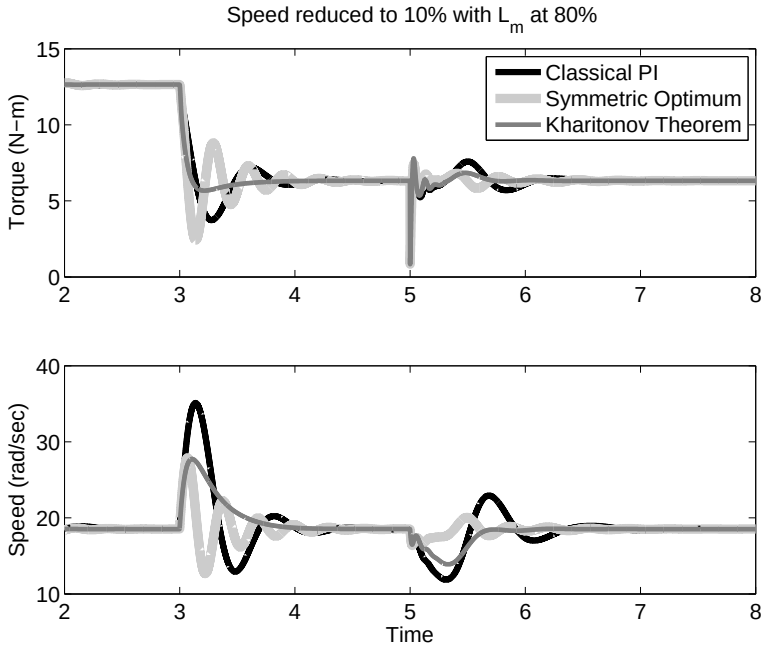

Figure 40. Speed reduced to 10% with L_m at 80%.

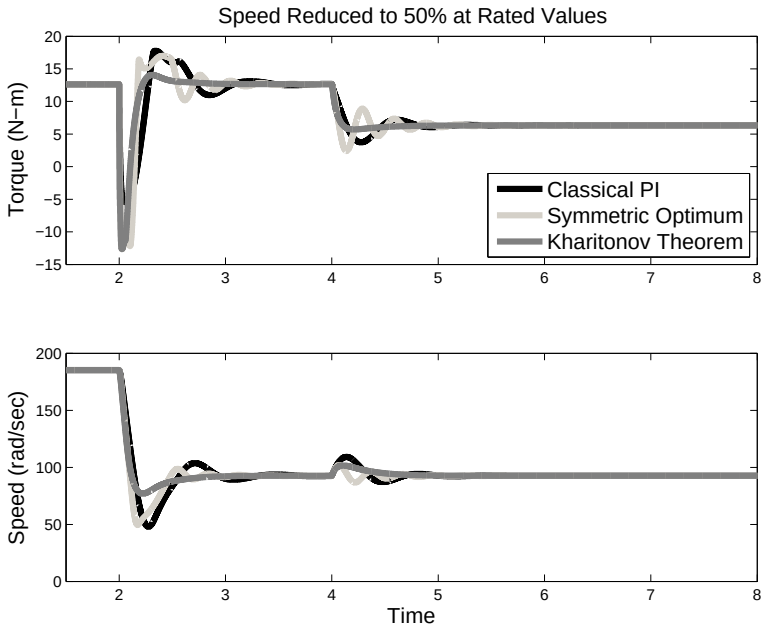

Figure 41. Speed reduced to 50% at rated values.

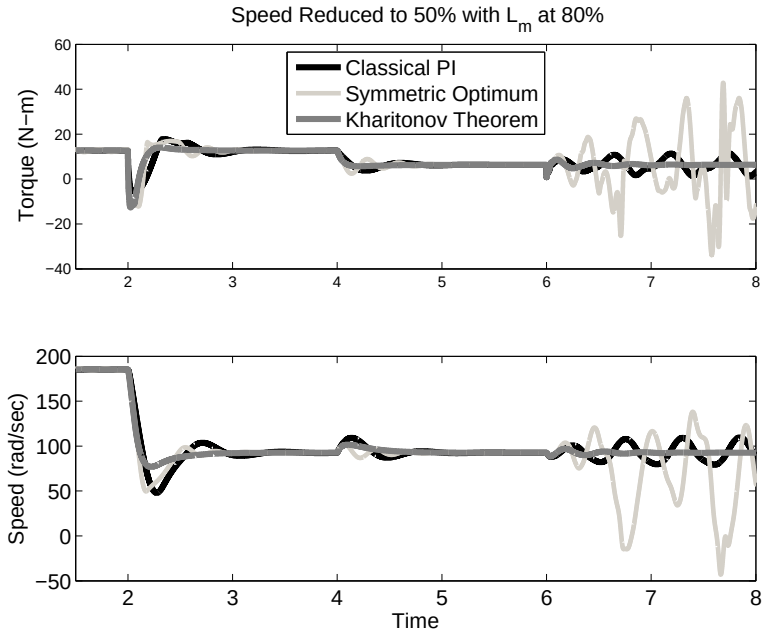

Figure 42. Speed reduced to 50% with L_m at 80%.

3.10. Root Locus of Linearized Model at Different Speeds

The root locus captures the behavior of the poles with the variation in certain parameters. The root locus is generated to have insight in small signal analysis for different set of variable combinations, such as speed (ω_m), magnetizing inductance (L_m), and rotor resistance (R_r). Following are the different set-up of parameter combinations are established to find out controller performance:

- Rated speed, L_m fixed, and vary R_r from rated to 200% using classical PI (Figure 43), symmetric optimum (Figure 44), and Kharitonov's theorem (Figure 45) and corresponding poles are shown in tab;e 13.

- Rated speed, R_r fixed, and vary L_m from rated to 70% using classical PI (Figure 46), symmetric optimum (Figure 47), and Kharitonov's theorem (Figure 48) and corresponding poles are shown in table 14.

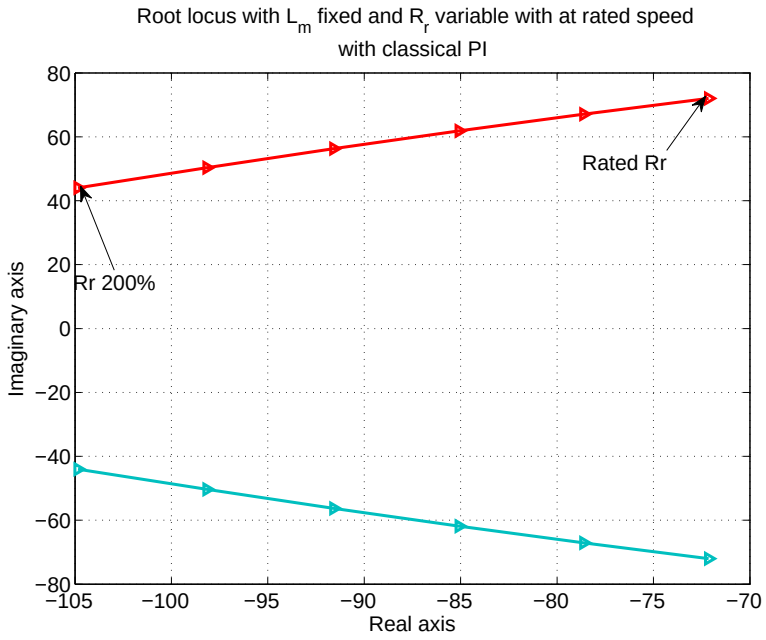

Figure 43. Root locus with L_m fixed and varying R_r with classical PI at rated speed.

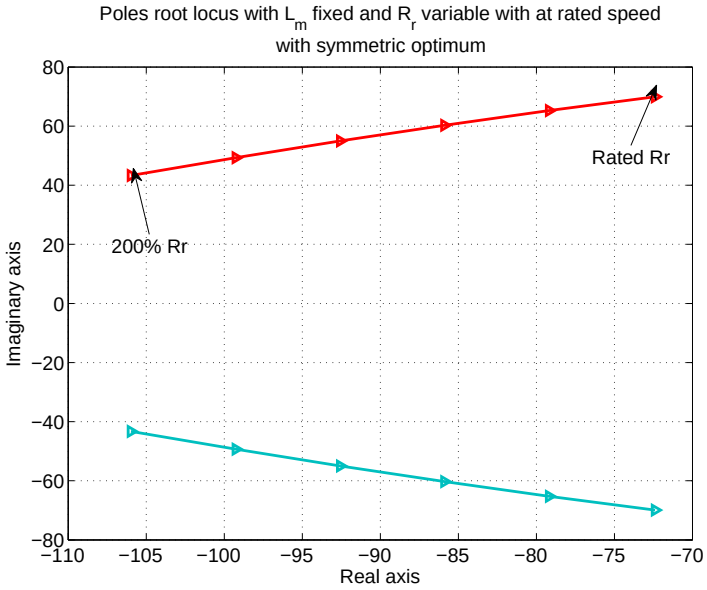

Figure 44. Root locus with L_m fixed and varying R_r with symmetric optimum at rated speed.

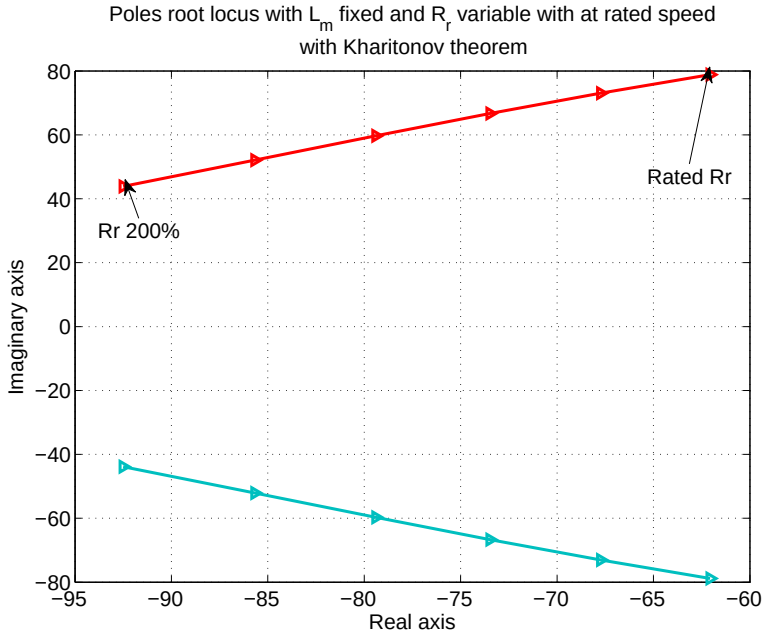

Figure 45. Root locus with L_m fixed and varying R_r with Kharitonov theorem at rated speed.

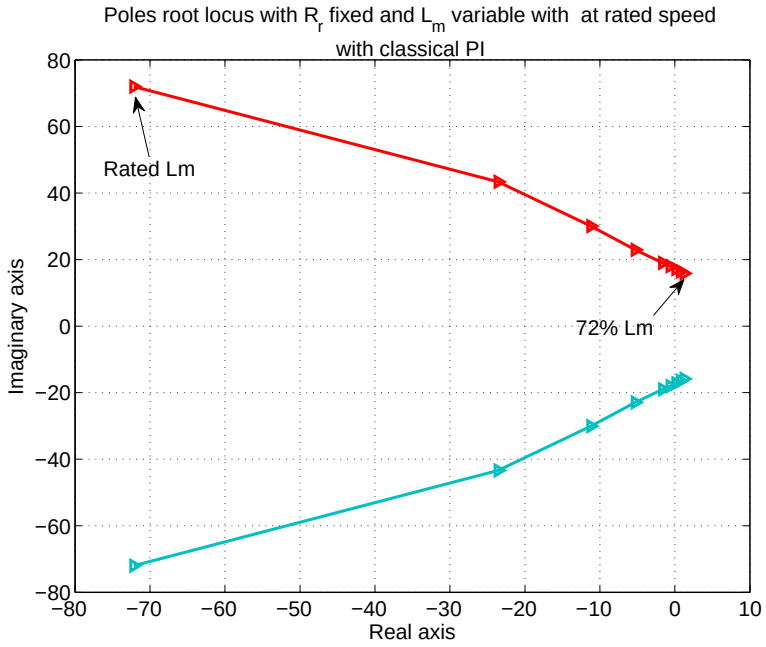

Figure 46. Root locus with R_r fixed and varying L_m with classical PI at rated speed.

Table 13. Dominant poles with L_m fixed and varying R_r.

	Rated	**1.2**R_r	**1.4**R_r	**1.6**R_r	**1.8**R_r	**2**R_r
PI	-72±71j	-78±67j	-85±62j	-91±56j	-98±50j	104±44j
SO	-72±69j	-79±65j	-85±60j	-92±54j	-99±49j	-105±43j
KT	-62±78j	-67±73j	-73±66j	-79±59j	-85±52j	-92±43j

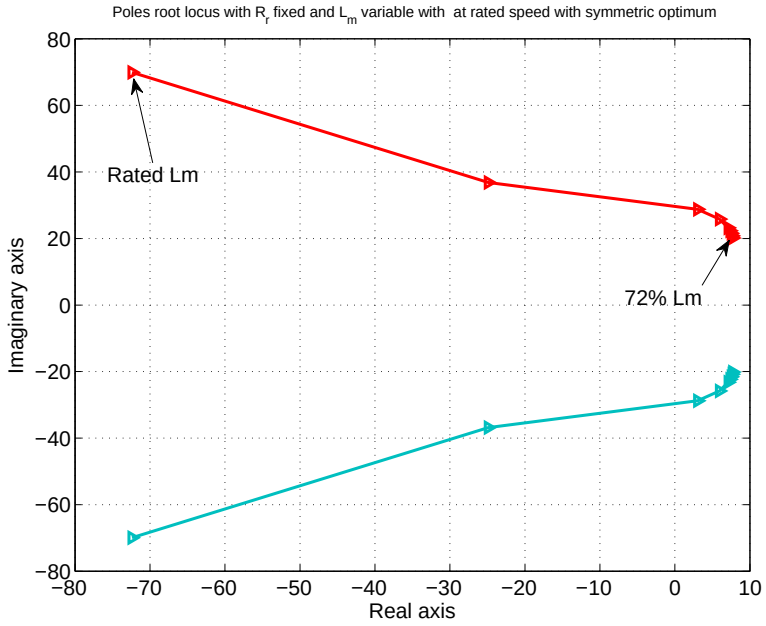

Figure 47. Root locus with R_r fixed and varying L_m with symmetric optimum at rated speed.

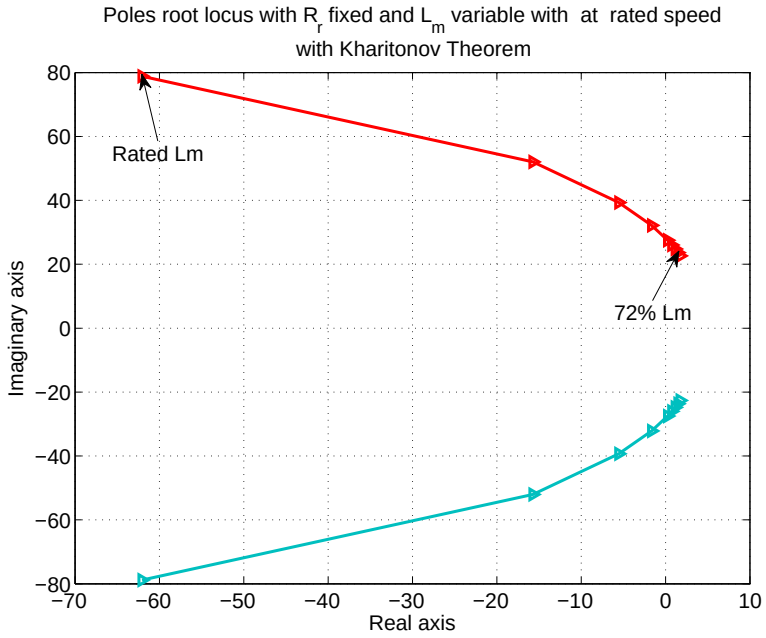

Figure 48. Root locus with R_r fixed and varying L_m with Kharitonov theorem at rated speed.

Table 14. Dominant poles with R_r fixed and varying L_m.

	Rated	**0.95**L_m	**0.90**L_m	**0.80**L_m	**0.78**L_m	**0.74**L_m	**0.72**L_m
PI	-72±71j	-23±43j	-11±30j	-2±19j	-0.6±18j	0.7±16	1.2±15
SO	-72±69j	-24±36j	3±28j	7±23j	7±22j	7±20j	7±19j
KT	-62±78j	-15±52j	-5±39j	0.2±27j	0.7±26j	1.4±23j	1.7±22j

3.10.1. Discussion on Linear Analysis

The root locus for the above mentioned cases shows that the drive system is sensitive to L_m. The drive reaches the instability with L_m below 79% of the rated value, while the root locus is insensitive to rotor resistance R_r.

3.11. Conclusion

A method to determine PI controller parameters of an induction motor drive system (employing indirect field oriented control) based on Kharitonov's theorem is presented in this chapter. Variations in two parameters: namely R_r and L_m are specified in *a priori* ranges and the controller gains are selected to ensure the stability the corner polynomials corresponding to the parametric square. An eigenvalue analysis indicates excellent damping for all the modes with control settings obtained with the proposed method. Dynamic simulations with the full nonlinear model considering control saturation confirm the robustness and superior damping benefits with the proposed controller compared to traditional and symmetric optimum based tuning methods.

The proposed method thus provides a systematic approach to robustify control settings that arise in several drive systems subject to similar parametric variations. The proposed method provided with the better result than the classical PI and symmetric optimum tuned PI, because the proposed scheme utilized the fifth order model while the other two techniques used reduced order pant model.

CHAPTER 4. FRACTIONAL ORDER CALCULUS AND DERIVATION OF FRACTIONAL CONTROLLER

It is known that the nth order derivative of a function $f(t)$ can be mathematically described by $\frac{d^n y}{ds^n}$. With this notation, one may ask "What does $n = \frac{1}{2}$ mean in the notation?" Actually, this was the question asked in a letter by the French mathematician Guillaume François Antoine L'Höpital to one of the inventors of calculus, the French mathematician Gottrfied Wilhelm Leibnitz said: "It will lead to a paradox, from which one day useful consequences will be drawn." This marks the beginning of the fractional calculus. In the field of control it is more desirable to have fractional order controller instead of fractional order systems. This is due to the fact that the plant model may have already been obtained as an integer order model in classical sense. In most cases, the objective is to improve the performance of the system using fractional order controller.

In AC drive systems, the speed, torque and/or position of machines are controlled using some type of device, for example, hydraulic pump, linear actuator, or an electric motor, generally a servo. Speed control is a typical task in AC drive systems. In this chapter, the speed control of AC drive system in vector controlled closed loop mode of operation are focused. The fractional order PI controller is generalized for speed control of induction motor. For simplification, the gains of PI controller are obtained using classical control strategy with integral order assumed to be unity. In order to improve the control performance of AC drive systems with integer order mathematical model fractional order PI controller is proposed and designed in this chapter.

4.1. Introduction

Fractional order calculus is an area of mathematics that deals with the derivatives and integrals from non-integer order. The fractional order proportional, integral,

and derivative (FrOPID) controllers have achieved a significant interest in the last few decades. In fact, FrOPID provides more flexibility in controller design procedure than standard integer order PID controllers, because FrOPID provides five degrees of freedom. The fractional order calculus theory is used to design the PI controller, although the classical PID controller is predominant in control development. The fractional order controllers (FrOC) provides the isodamping property which shows constant phase invariant to gain changes. The isodamping property gives the constant phase at the ω_c, i.e.:

$$\frac{d\angle G(s)}{ds}_{s=j\omega_c} = 0 \tag{4.1}$$

where ω_c is critical frequency. Also $G(s)$ is the open loop transfer function containing both plant $P(s)$ and controller $K(s)$.

Applications of fractional calculus in control are numerous. The fractional order control (FrOC) scheme [83] and [84] gives the simulation results for permanent magnet DC motor and proposed hardware realization using fractance circuit and with microprocessor. The authors in [85] discussed the use of FrOC for Buck converter and verified the results with simulations and experiments. In [86] the relay feedback with artificial delay is used to tune the fractional order PID.

The reset of chapter is organized as follows: In section 4.2 classical definition of fractional operator is introduced. Section 4.3 introduces about the fractional order controller and approximation technique for implementation of FrOC. Section 4.4 includes the simulation results for DC motor showing the iso-damping property. The relation between overshoot and phase margin is given in section 4.5. The simulation and tuning of fractional order controller for AC drive under indirect field oriented control is presented in section 4.6 and 4.8. The conclusion is presented in section 4.10.

4.2. Fractional Calculus

Fractional calculus defines the branch of calculus where derivatives and integrals are classified as noninteger. Fractional Calculus came into existence nearly at the same time as integerorder calculus and is generalization of integerorder calculus. The differentiation and integrals can be defined as:

$$ {}_aD_t^r = \begin{cases} \dfrac{d^r}{dt^r} & \Re(r) > 0 \\ 1 & \Re(r) = 1 \\ \int_a^t d(\tau)^{-r} & \Re(r) < 0 \end{cases} \tag{4.2} $$

where ${}_aD_t^r$ is non-integer fractional-order operator with a and t as the limits of operation, and r is the order of operation.

4.3. Fractional Order Controller

The fractional order controller (FrOC) forms a class of controllers based on the fractional calculus. The most common form of a fractional order PID controller is the $PI^{\lambda}D^{\delta}$ [87], involving an integrator of order λ and a differentiator of order δ, where λ and $\delta \in \Re$. The transfer function of the fractional order $PI^{\lambda}D^{\delta}$ controller is of the form:

$$ C(s) = \frac{U(s)}{E(s)} = K_p + K_i s^{-\lambda} + K_d s^{\delta} \tag{4.3} $$

where $(\lambda, \delta > 0)$. If $\lambda = 1$ and $\delta = 1$ the classical PID is obtained. Similarly as in classical control theory, $PI^{\lambda}, PD^{\delta}, PI^{\lambda}D^{\delta}$ controllers can be obtained by keeping any of the values to zero, depending upon the requirements of the plant or process. The fractional order controller $PI^{\lambda}D^{\delta}$ enhances the performance because it behaves like an infinite dimensional linear filter, due to noninteger integrator and differentiation.

4.3.1. Continuous Approximation of FrOC

To implement fractional order control an infinite memory is required, it is necessary to obtain an approximate band limited controller. The band should be carefully selected so that all frequencies of interest stay in range. The Oustaloups recursion algorithm [88] and [89] is proposed for simulation purposes as it gives the frequency response more closely like ideal bode. The approximation is based on selection of band limits for the system. The transfer function of the type can be used to find the approximation of fractional order transfer function:

$$H(s) = s^r, r \in \Re, r \in [-1:1] \tag{4.4}$$

The band limit (ω_l, ω_h) is defined, where

ω_l is low frequency limit

ω_h is high frequency limit

The Oustaloup's approximation is then given as:

$$\hat{H}(s) = C_0 \prod_{k=-N}^{N} \frac{s + \omega'_k}{s + \omega_k} \tag{4.5}$$

where the gains, poles, and zeros are defined as:

$$\begin{aligned} w'_k &= w_l(\frac{\omega_h}{\omega_l})^{\frac{k+N+0.5(1-r}{2N+1}} \\ w_k &= w_l(\frac{\omega_h}{\omega_l})^{\frac{k+N+0.5(1+r}{2N+1}} \\ C_0 &= (\frac{\omega_h}{\omega_l})^{\frac{-r}{2}} \prod_{k=-N}^{N} \frac{\omega_k}{\omega'_k} \end{aligned} \tag{4.6}$$

The implementation of Oustaloups in MATLab is given as function $oraf oc()$ by [18]. The approximate transfer function using $\omega_l = .01$ and $\omega_h = 1000$ and

selecting the transfer function as $H(s) = s^{\frac{-1}{s}}$ with $N = 5$ and $r = \dfrac{-1}{3}$. The bode plot of the approximate transfer function is shown in figure 49. The bode plot of the approximated transfer function closely matches the ideal bode transfer function $G(s) = \dfrac{k}{s^{\alpha}}$. The step response is also shown in figure 50.

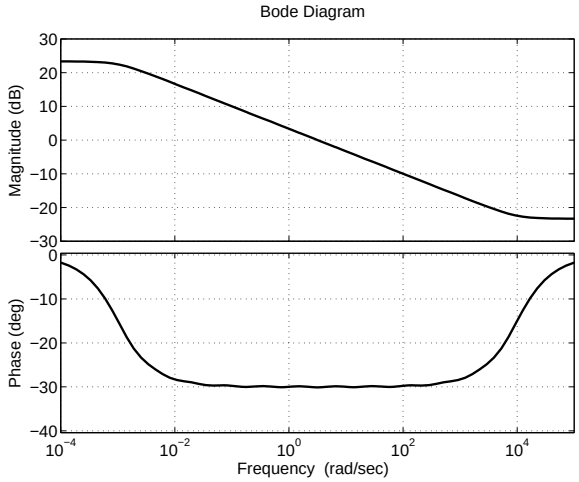

Figure 49. Frequency response of approximated fractional order transfer function.

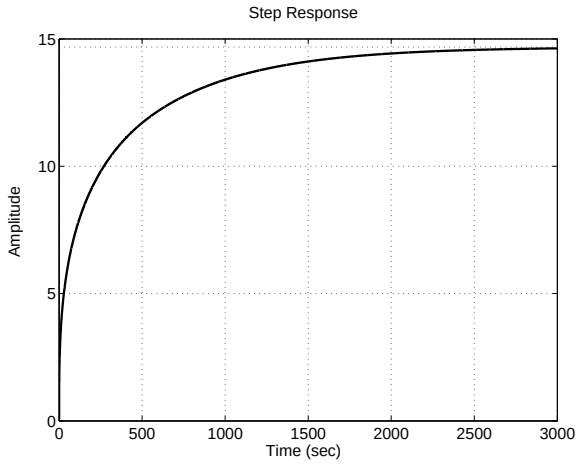

Figure 50. Step response of approximated fractional order transfer function.

4.4. Simulation Results of DC Motor and AC Motor

The DC motor is used to test the fractional controller for isodamping property by changing the variation in parameters of the DC- motor. Block diagram of the DC motor in closed loop with fractional order control is shown in figure 3. The transfer function obtained for the dc motor is given as:

$$G_{DCM}(s) = \frac{\theta(s)}{V_a(s)} = \frac{K_m}{s[(Ls+R)(Js+K_f)+K_bK_m]} \tag{4.7}$$

Assuming time constant of the DC motor armature negligible, above model can be simplified as:

$$G_{DCM}(s) = \frac{\theta(s)}{V_a(s)} = \frac{K_m}{s[R(Js+K_f)+K_bK_m]} \tag{4.8}$$

$$G_{DCM}(s) = \frac{\theta(s)}{V_a(s)} = \frac{K_m/RK_f + K_bK_m}{s(\tau s+1)} \tag{4.9}$$

$$G_{DCM}(s) = \frac{\theta(s)}{V_a(s)} = \frac{K_{DCM}}{\tau s^2+s)} \tag{4.10}$$

The rated values of the machine parameters are $R = 6\Omega, K_m = K_b = 0.1, K_f = 0.2Nms, J = 0.01kgm^2/s^2$ The transfer function of DC motor becomes:

$$G_{DCM}(s) = \frac{\theta(s)}{V_a(s)} = \frac{0.08}{s(0.05s+1)} \tag{4.11}$$

The controller used is of the form $D^\lambda I^\delta$. The λ and δ are selected based on ideal bode with phase margin $\phi_m = \pi(1+r)\pi/2$ and remains constant showing the ISO damping property. For constant phase margin the controller has the following form [90] and [83].

$$C(s) = K_1 \frac{K_2 s + 1}{S^r} \tag{4.12}$$

where $K_1 = 1/K_{DCM}$ and $K_1 = /\tau$. The constant phase margin obtained from controller is:

$$\phi_m = arg[C(j\omega)G_{DCM}(j\omega)] + \pi \tag{4.13}$$

which yields to

$$\phi_m = \pi - (1 + r)\pi/2 \tag{4.14}$$

For $r = -1/3$ the phase margin obtained is

$$\phi_m = \pi - (1 - \frac{1}{3})\pi/2 = 150 \tag{4.15}$$

so from 4.12 the controller gets the form as:

$$C(s) = \frac{\tau}{K_{DCM}} s^{0.5} + \frac{1}{K_{DCM} s^{0.5}} \tag{4.16}$$

hence

$$C(s) = 0.625 d^{0.5} + \frac{12.5}{s^{0.5}} \tag{4.17}$$

For $K_{DCM} = 0.08$ and $\tau = 0.05$, the r is the slope of the ideal bode. The step response for variation in parameter R from 50% to 150% of its rated value is shown in figure 51. The isodamping property can be clearly observed in the bode plot of the DC motor by visualizing the constant phase over the desired frequency range in figure 52.

The same model is used to obtain the step response and frequency response with classical PI controller shown in figure 53 and 54.

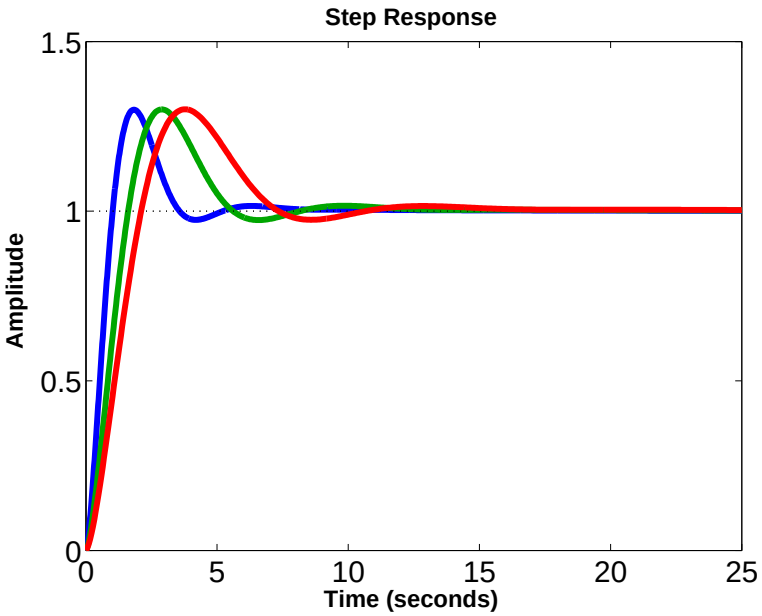

Figure 51. Step response of DC motor with iso-damping property.

By comparing the simulation results, with fractional order controller and classical PI controller, it is clear that constant overshoot is obtained with fractional order controller exhibiting the isodamping property. The four quadrant operation for DC motor is shown in figure 55. The simulation of speed tracking for a particular trajectory is performed using Oustaloups recursive algorithm shown in 55. The system shows a slight difference in settling time of system, with increased settling time with $npid()$ function and fast settling time with Oustaloups recursive algorithm, but the isodamping property with both the algorithms is same and shows the robustness over the parameter variations.

4.5. Relation Between Overshoot and Phase Margin

Consider a system with transfer function $G(s)$ with a feedback loop as shown in fig 56. The closed loop gain is given as:

$$G_{CL}(s) = \frac{G(s)}{1 + KG(s)} \tag{4.18}$$

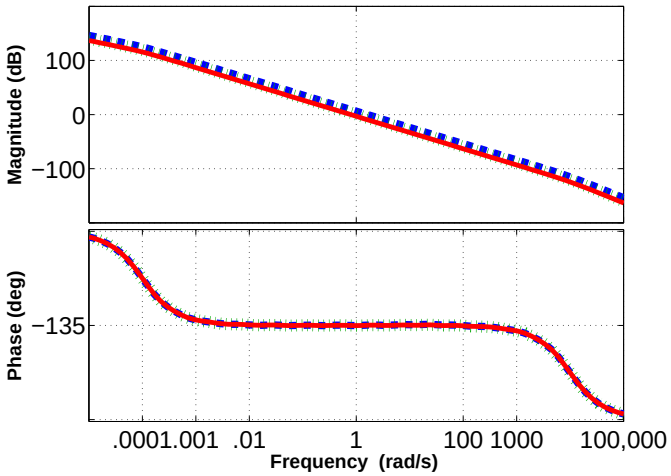

Figure 52. Bode plot of DC motor with iso-damping property.

4.5.1. Phase Margin

The phase margin is a measure of how close the phase of the loop is to -180^o, when the magnitude of the loop gain is one. The phase margin is additional phase required to bring the phase of the loop gain to -180^o.

$$\text{Phase Margin} = \text{Phase of loop gain} - 180^o$$

Consider the loop gain has a dominant pole at ω_{p1}. The higher order poles can be represented by an equivalent pole at ω_{eq}. The system $G(s)$ can then be approximated as:

$$G(s) = \frac{K_o}{(1+\frac{s}{\omega_{p1}})(1+\frac{s}{\omega_{eq}})} \tag{4.19}$$

Since, the frequencies of interest where the loop gain magnitude is close to unity, $\omega_{eq} > \omega_{p1}$. Therefore, we can approximate G(s) as:

$$G(s) = \frac{K_0\omega_{p1}}{s(1+\frac{s}{\omega_{eq}})} \tag{4.20}$$

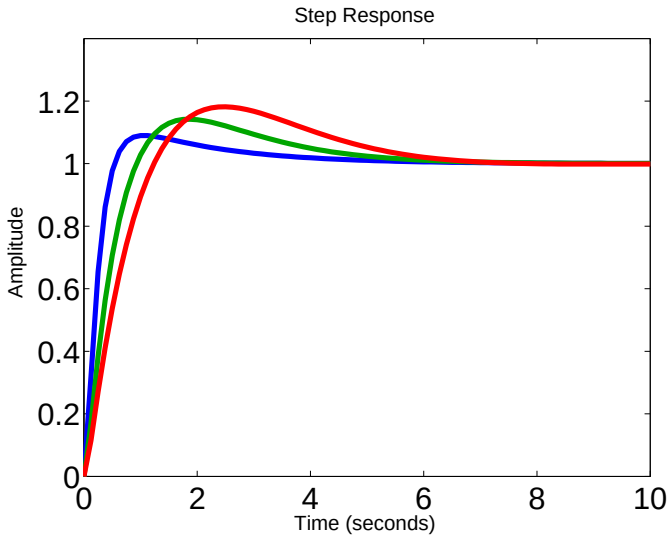

Figure 53. Step response of DC motor showing variable overshoot with PI controller.

where

$$\frac{1}{\omega_{eq}} = \frac{1}{\omega_{p2}} + \frac{1}{\omega_{p3}} + \cdots \tag{4.21}$$

Let $\omega_{ta} = K_o\omega_{p1}$. For frequencies of interest, close to the unity gain frequency, $G(s)$ can be written as:

$$G(s) = \frac{\omega_{ta}}{s(1 + \frac{s}{\omega_{eq}})} \tag{4.22}$$

Plugging Eqn. 4.22 in to Eqn. 4.18, for closed loop system:

$$G_{CL}(s) = \frac{\frac{1}{K}}{1 + \frac{s}{\omega_{ta}K} + \frac{s^2}{\omega_{ta}K\omega eq}} \tag{4.23}$$

The Eqn. 4.23 is the transfer function for a second order system. The general form for the response of the second order system, where system properties are described by its Q and resonant frequencies ω_n is given in Eqn. 4.24.

$$G_{CL}(s) = \frac{K}{1 + \frac{s}{Q\omega_n} + \frac{s^2}{\omega_n^2}} \tag{4.24}$$

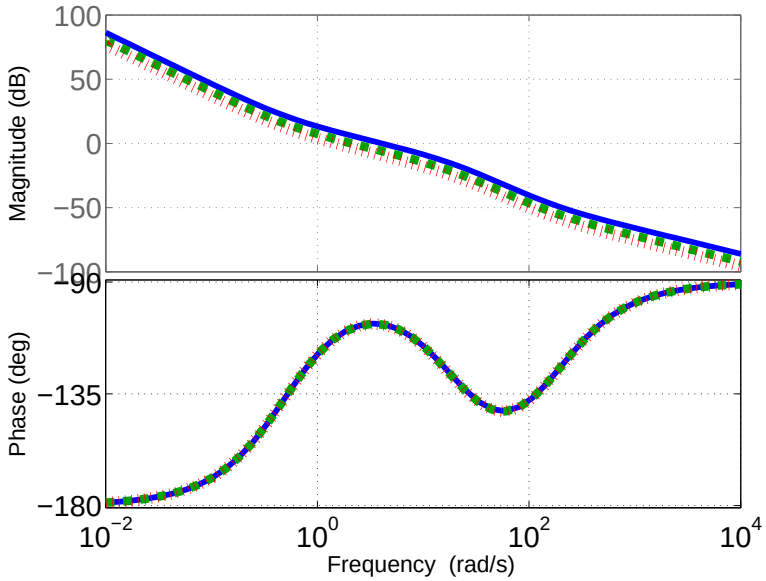

Figure 54. Bode plot of DC motor with PI controller.

By comparing Eqns. 4.23 and 4.24, we can define:

$$\omega_n = \sqrt{K\omega_{ta}\omega eq} \tag{4.25}$$

$$Q = \sqrt{\frac{K\omega_{ta}}{\omega eq}} \tag{4.26}$$

The loop gain of the system is defined as the product of the gain of the feed forward path and gain of feedback path and for the system given in Figure 56 and is given as:

$$KG(s) = \frac{K\omega ta}{a(1 + \frac{s}{\omega eq})} \tag{4.27}$$

The phase margin is function of the phase of the loop gain at the frequency where the magnitude of the loop gain is unity.

$$KG(\omega_t) = 1 \tag{4.28}$$

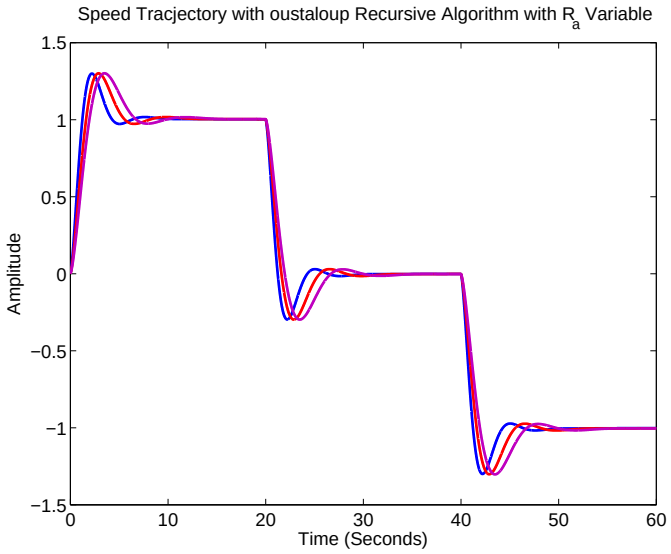

Figure 55. Reference tracking with Oustaloup approximation.

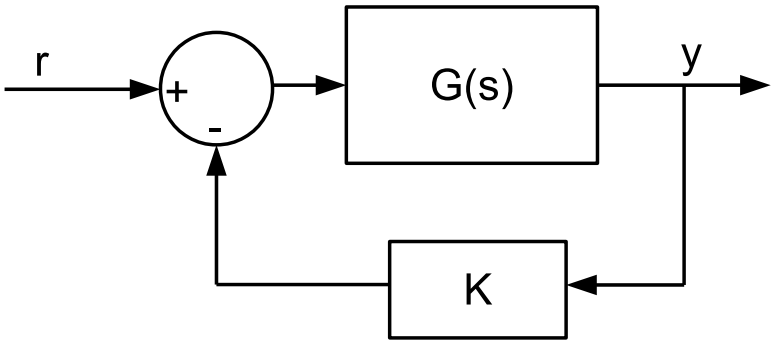

Figure 56. Block diagram of a system with feedback.

The ω_t is the loop unity gain frequency. So, from Eqns. 4.27 and 4.28, we get:

$$K^2\omega_{ta}^2 = \omega_t^2(1 + \frac{\omega_t^2}{\omega_{eq}^2}) \tag{4.29}$$

$$\frac{\omega_{ta}}{\omega_{eq}} = \frac{\omega_t}{K\omega_{eq}}(\sqrt{1 + \frac{\omega_t^2}{\omega_{eq}^2}}) \tag{4.30}$$

From Eqns. 4.25 and 4.29, we can write;

$$Q = \sqrt{\frac{\omega_t}{K\omega_{eq}}(1 + \frac{\omega_T^2}{\omega_{eq}^2})^{\frac{1}{2}}} \tag{4.31}$$

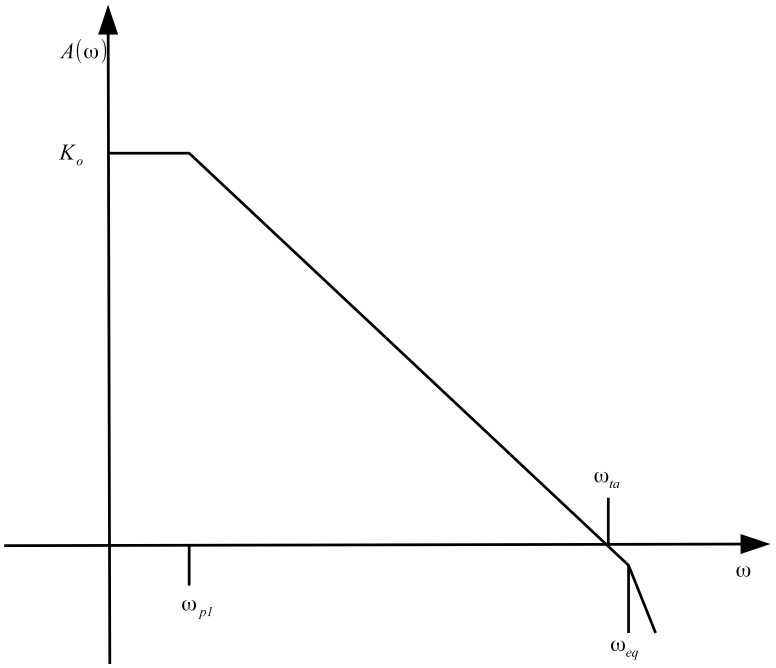

Figure 57. Frequency plot.

Table 15. Overshoot and phase margin.

PM	$\frac{\omega_t}{\omega_{eq}}$	Q	%OS
55^o	0.700	0.925	13.3%
60^o	0.580	0.817	8.7%
65^o	0.470	0.717	4.7%

The phase of the loop gain is:

$$Phase of loop gain = -90^o - tan^{-1}(\frac{\omega_t}{\omega_{eq}}) \tag{4.32}$$

A well known property of second order systems is that the percent overshoot is a function of the Q and is given by:

$$OS = e^{-\frac{\pi}{\sqrt{4Q^2-1}}} \tag{4.33}$$

Both phase margin 4.31 and Q 4.32 are a function of $\frac{\omega_t}{\omega_{eq}}$. This allows us to use 4.33 to create table of percent overshoot as a function of phase margin as given in Table 15.

4.6. Vector Control and Problem Formulation for Induction Motor

The vector control scheme, as shown in Figure 58 is used for decoupling the torque and field producing current components, thereby permitting great flexibility over wide ranges of torque and speed. The induction machine has well established 5th order nonlinear model [45, 81] that is used for simulations and is given in Appendix A. This scheme depends on machine parameters to compute reference (or commanded) values of torque and speed. However, variations in operating/ambient conditions, cause a mismatch between reference and measured signals which produces undesirable torque oscillations. The reference values are computed through via PID controllers represented by dashed boxes in Figure 58. The scheme contains three closed loops, two internal loops for torque producing components and one for the field producing component of current. These internal loops are overseen by an outer loop with a flux-weakening block - for operation beyond rated speed. Each loop contains a controller which can be switched between either PI or FrOC, indicated by the solid and dashed boxes in Figure 58 respectively. The reference signals for the current loops are generated from the vector control block using Eqns. (4.34) and (4.35).

$$i_{ds}^{ref} = \frac{1}{L_m}(\frac{L_r}{R_r}\frac{d}{dt}\lambda_r^{ref} + \lambda_r^{ref}) \tag{4.34}$$

$$i_{qs}^{ref} = \frac{4}{3P}\frac{T_e^{ref}}{\lambda_r^{ref}}\frac{L_r}{L_m} \tag{4.35}$$

where i_{sd}^{ref} is the stator d-axis reference current, i_{sq}^{ref} is the stator q-axis reference current, L_m is magnetizing inductance, L_r is rotor inductance, R_r is rotor resistance,

λ_r^{ref} is rotor reference flux linkage, T_e^{ref} is reference torque and P is the number of poles of machine. The speed tracking loop is fed through desired speed trajectory, while the flux weakening block is a lookup table to generate reference flux λ_r^{ref}, for field producing current component. Instead of adapting control parameters by constantly tracking machine parameters (and monitoring ambient conditions), we show next, how a fractional order can compensate for parametric variations without compromising the dynamic performance.

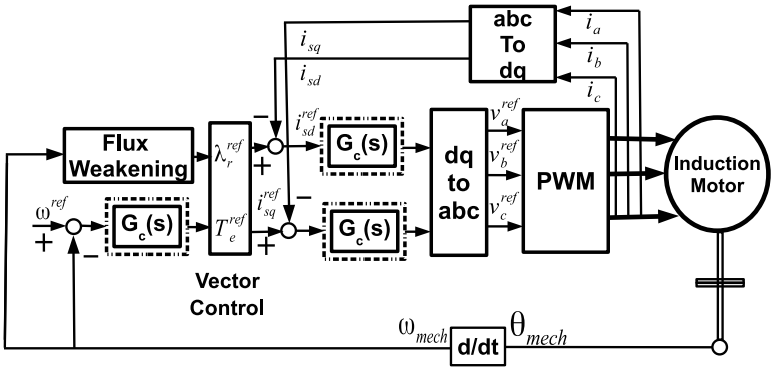

Figure 58. Block diagram of indirect field oriented control with flux weakening.

4.6.1. Tuning of Fractional Order Controller

The FrOC is tuned using a graphical approach (phase shaping) based on frequency response of an ideal integrator. The following are the steps required for tuning the FrOC:

- The gains K_P and K_I are obtained based on classical PI controller design technique.
- The parameter 'r' in Eqns. (4.4) and (4.5) is selected such that phase of FrOC closely matches to ideal integrator.

- The parameter N defines the order of approximated FrOC in Eqns. (4.4) and (4.5). The N is selected by number of iteration to match the phase of FrOC to ideal bode. It gives a trade off between order of the controller and performance.

- The bandwidth is selected on the requirement of system, for speed loop of induction motor the bandwidth required is 25rad/s. So we can select the lower frequency $\omega_l = .1$ and upper frequency $\omega_h = 25$ [81].

4.6.2. Selection of N

The selection of N is a trade off between the flatness of the system frequency response and order of the controller. The lower the order of controller gives the easy implementation. The frequency response for the $N = 1, 3,$, and 5 is shown in figure 59. The frequency response shows that even with $N = 1$ the system behaves close to ideal bode of integral, while increasing N does not significantly flattens the bode. This iteration suggests the selection of $N = 1$.

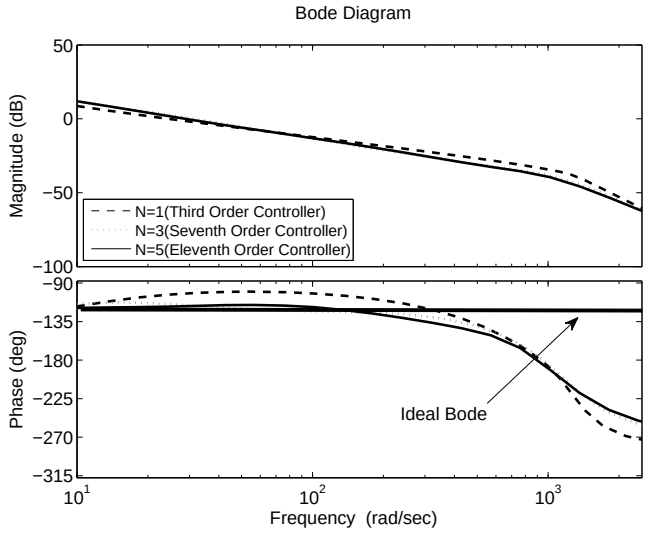

Figure 59. Frequency response with varying N.

The speed and torque response are shown in the figure 60, where the performance is comparable with $N = 1$. The N can be increased to obtain the better settling time and overshoot but at the expense of higher order controller.

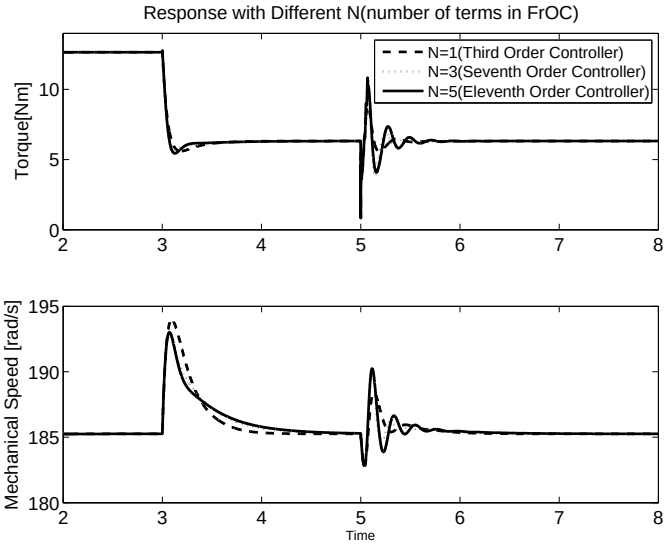

Figure 60. Torque and speed response with varying N.

4.7. Dynamic Simulation Results

Simulations are carried out for variations in two critical and temperature sensitive parameters namely the rotor resistance and the magnetizing inductance. The rotor resistance R_r and magnetizing inductance L_m are set to 200 and 80 % of their nominal values, respectively. After initialization, a speed is increased by 50%, thus activating the flux-weakening mode with a step change in load torque applied at 3s, followed by parametric changes at 5s. Finally, a further 50% increase in reference speed is commanded at 7s. The PI controllers are tuned with a bandwidth of 250 rad/sec for the current loop and 25 rad/sec for the speed controller with a phase margin of 60 degrees (obtaining dynamic response with no oscillation it is recommended to select the phase above 45 degree) [81]. The other commonly used techniques to tune PI controller are the SO explained in previous chapter.

The dynamic response with both sets of controllers is shown in Figs. 61 - 64 and frequency response in figure 65. It can be observed that the dynamic response (speed and torque oscillations) is degraded with the PI controller while the FrOC yields a stable dynamic response.

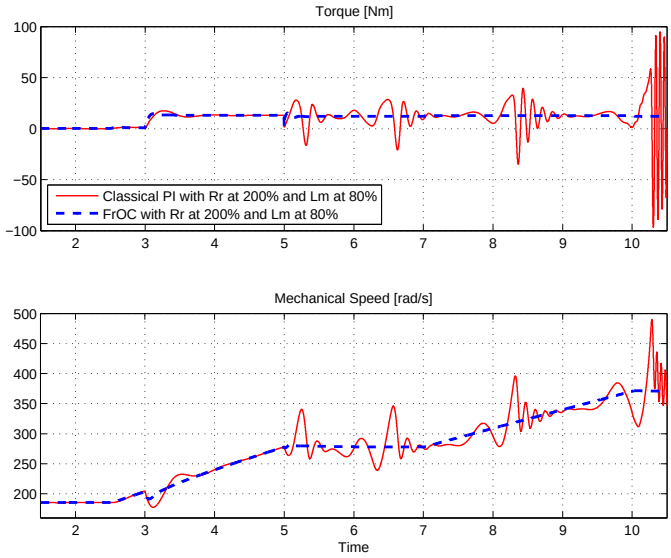

Figure 61. Torque and speed response using FrOC (dotted blue line) and classical PI (solid red line).

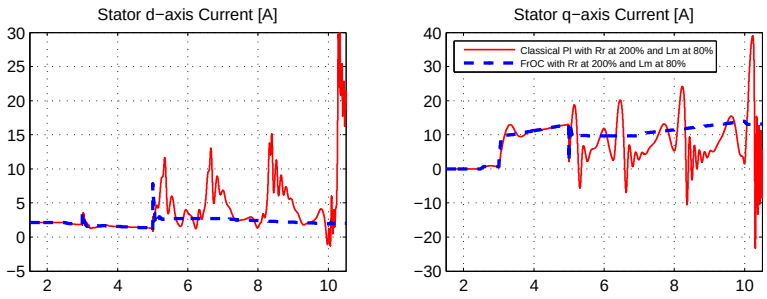

Figure 62. Stator dq-axis currents using FrOC (dotted blue line) and classical PI (solid red line).

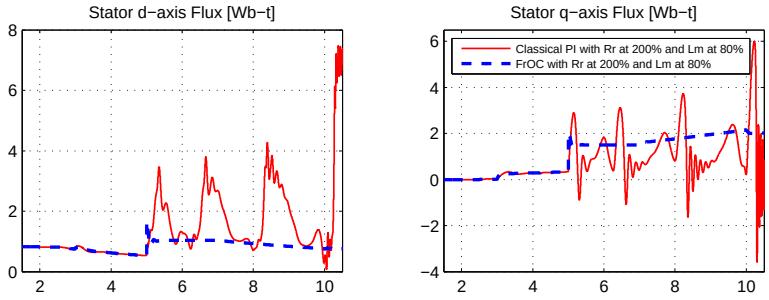

Figure 63. Stator dq-axes flux using FrOC (dotted blue line) and classical PI (solid red line).

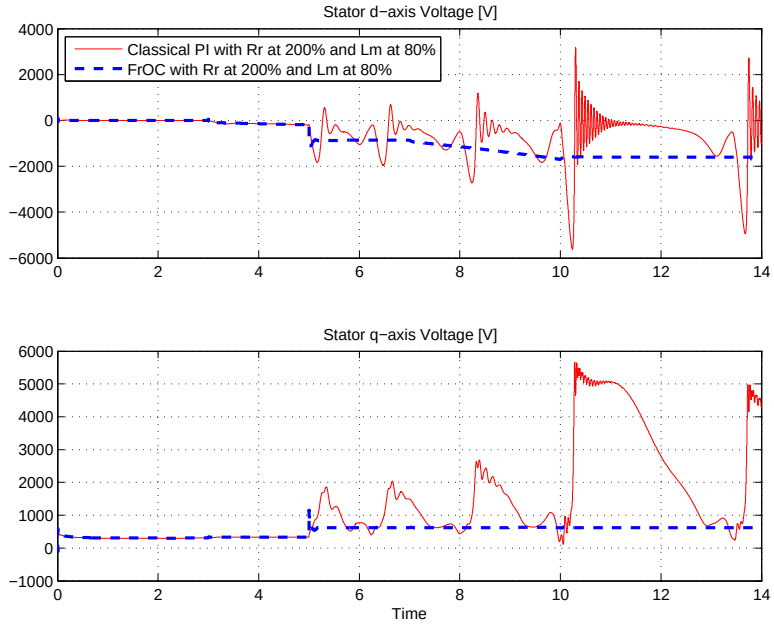

Figure 64. dq-axes voltages using FrOC (dotted blue line) and classical PI (solid red line).

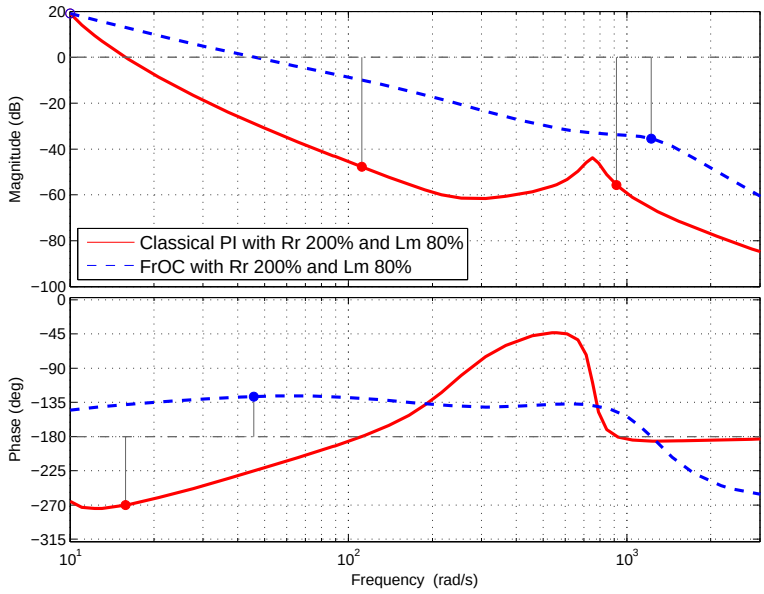

Figure 65. Frequency response (bode plot) using FrOC (dotted blue line) and classical PI (solid red line).

The unstable dynamic response occurs because of the mismatch in the reference signal and generated signals from the plant 58. Since, tuning of PI controller is tedious process and it is mostly performed for the nominal plant parameters, any change in the parameters of the plant above certain range degrades the performance of the PI controller unless it is manually tuned or through supervisory control [91]. The supervisory PI control is a redundant and is expensive option for the parameter compensation of the drives. The FrOC produces the stable and robust response because of constant phase response as shown in Fig. 65. But due to highly nonlinear nature of the induction motor the phase response is almost constant and produces the ISO-damping property.

The table 16 shows the poles of the drive system with decreasing L_m using classical PI controller. The behavior of the poles shows that the system reaches instability with $L_m = 78\%$ of the rated value, while the poles of the drive system

using FrOC shows very slow movement with decreasing L_m towards right half plane as shown in table 17. Thus, keeping the drive in stable region.

Table 16. Eigenvalues of machine with PI controller.

L_m	$\lambda_{1,2}$	$\lambda_{3,4}$	$\lambda_{5,6}$	λ_7	λ_8
Rated	-218.42±449.48j	-78±68.6j	-1.6±12.7j	-6.6	-4
0.95	-95.4±417.5j	-27.6±40.8j	-1.4±11.8j	-4.6	-2.7
0.90	-62.8±403.6j	-14.8±27.45j	-1.58±12j	-3.26+0.17j	-3.26-0.17j
0.85	-47.6±396.2j	-9.1±19.4j	-1.7±12.6j	-3.1+0.7j	-3.1-0.7j
0.80	-38.9±391.7j	-6.9±13.3j	-0.6±14.1j	-3.1+0.9j	-3.1-0.9j
0.79	-37.5±391j	-0.18±14.2j	-6.9±12.5j	-3.11+0.98j	-3.1-0.98j
0.78	-36.3±390.3j	0.22±14.2j	-6.9±11.8j	-3.1+1j	-3.1-1j
0.77	-35.2±389j	0.58±14.1j	-6.8±11.2j	-3.1+1j	-3.1-1j

Table 17. Eigenvalues of machine with FrOC.

L_m	$\lambda_{1,2}$	$\lambda_{3,4}$	$\lambda_{5,6}$	λ_7	λ_8	λ_9
Rated	-579.1±2773.6j	-621.7±2391.5j	-7.78±14.45j	-5.9	-4.2	-857
0.95	-456.3±1845.9j	-539.6±1471.1j	-6.78±6.18j	-6.7	-3.3	-857
0.90	-416.0±1501j	-526.5 ±1127.7j	-5.65±3.9j	-8.6	-2.9	-857
0.85	-392.9±1308.3j	-525.9±935.36j	-4.89±3.35j	-9.8	-2.7	-857
0.80	-376.6±1181.8j	-527.7±808.93j	-4.51±3.18j	-10.1	-2.6	-857
0.79	-373.8±1161.4j	-528.4±788.53j	-4.46±3.16j	-10.1	-2.6	-857
0.78	-371.2±1142.3j	-529.2±769.37j	-4.41±3.15j	-10.1	-2.6	-857
0.77	-68.69±1124.3j	-529.9±751.35j	-4.36±3.13j	-10.1	-2.5	-857

4.7.1. Load Torque as Pulse Disturbance

The small signal analysis can be compared with the following simulation setup:

- The simulation starts with full load and machine parameters R_r at 200% and L_m at 80% of the rated values.
- The small load torque change is applied at four seconds when machine reaches is in steady state.
- The load torque is set back to full load torque at six seconds.

Figure 67 shows that with small disturbance of 10% decrease in load torque, the system stays in stable region. The figure 67 where the large disturbance is created by reducing load torque to 50% of rated value. The PI controller tuned with classical technique shows the stable response with decreasing oscillations, while FrOC stabilizes quickly.

The 68 shows the 10% step reduction in load torque for different values of N. The dynamic response with 10% reduced load torque and L_m at 78% of the rated value, in figure 69 shows that the PI controller tuned using classical technique lost the tracking. The dq-axis currents and flux are shown in figures 70 and 71 respectively.

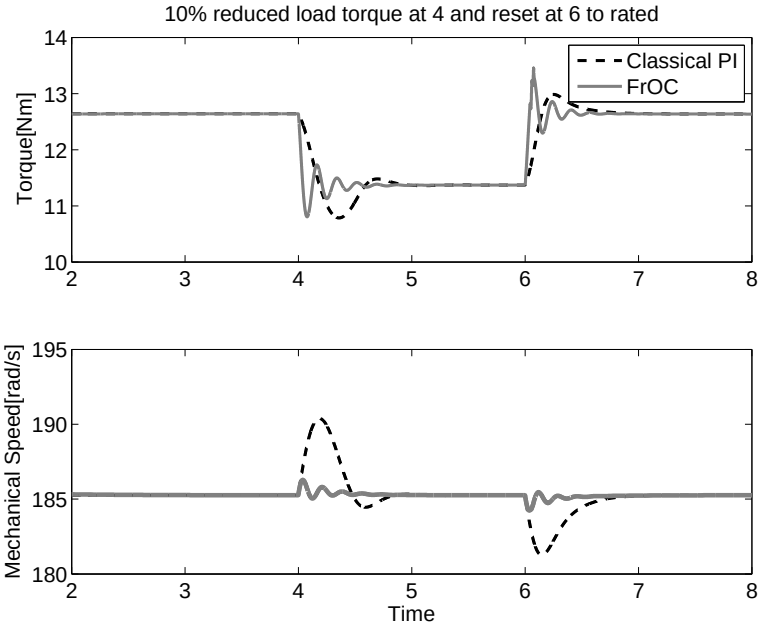

Figure 66. Torque and speed response with load torque reduced by 10% with $L_m = 80\%$, $R_r = 200\%$, and $N = 1$.

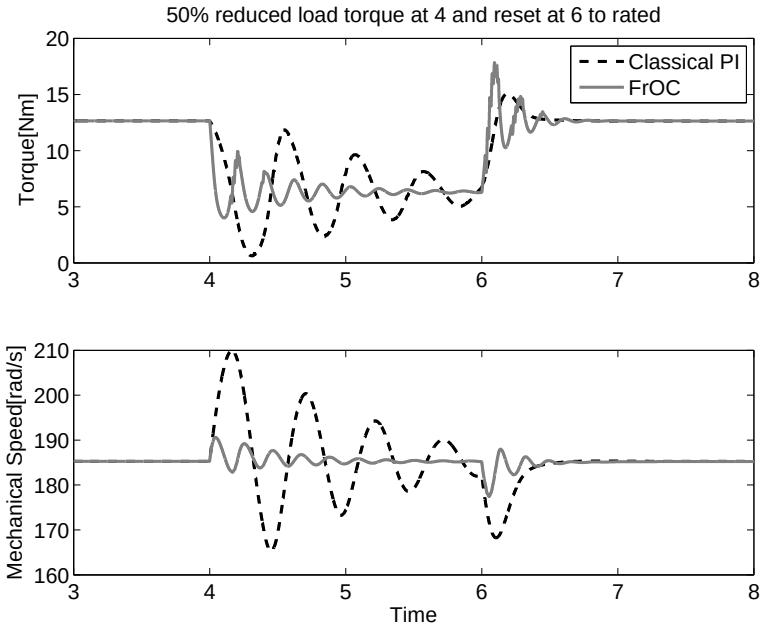

Figure 67. Torque and speed response with load torque reduced by 50% with $L_m = 80\%$ and $R_r = 200\%$ and $N = 1$.

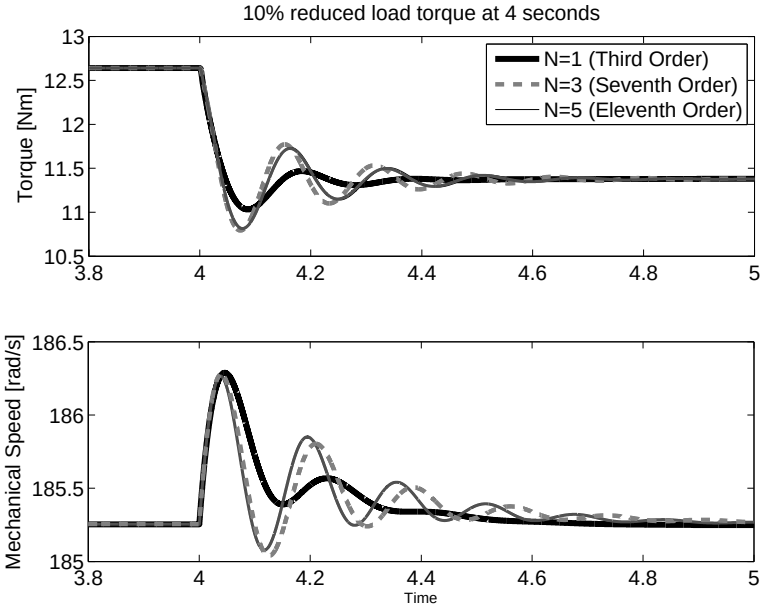

Figure 68. Torque and speed response with load torque reduced by 10% with $L_m = 80\%$ and $R_r = 200\%$ for different N.

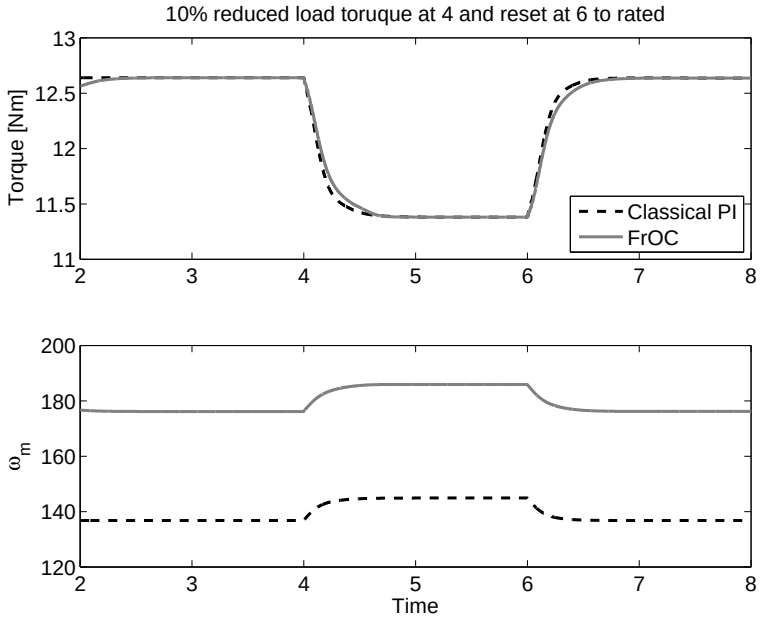

Figure 69. Torque and speed response with load torque reduced by 10% with $L_m = 75\%$, $R_r = 200\%$, and $N = 1$.

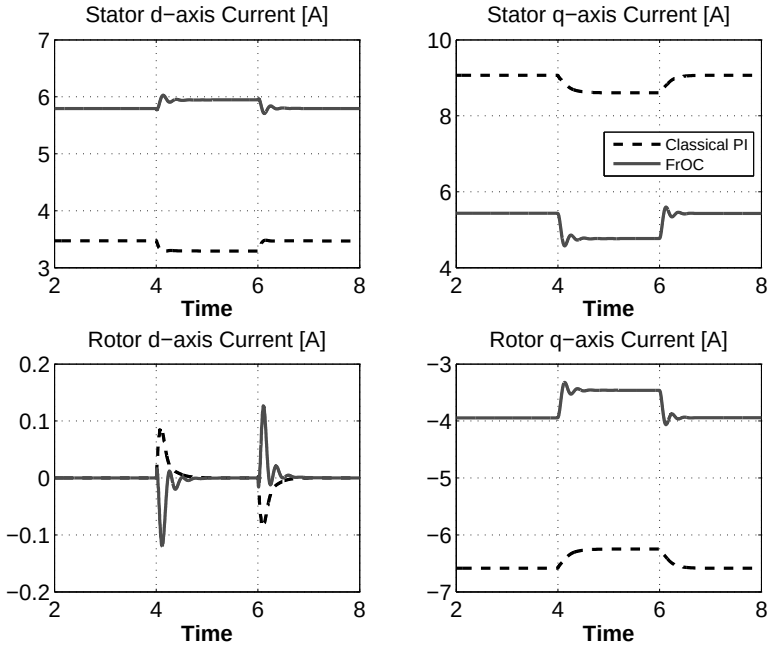

Figure 70. dq-currents with load torque reduced by 10% with $L_m = 75\%$, $R_r = 200\%$, and $N = 1$.

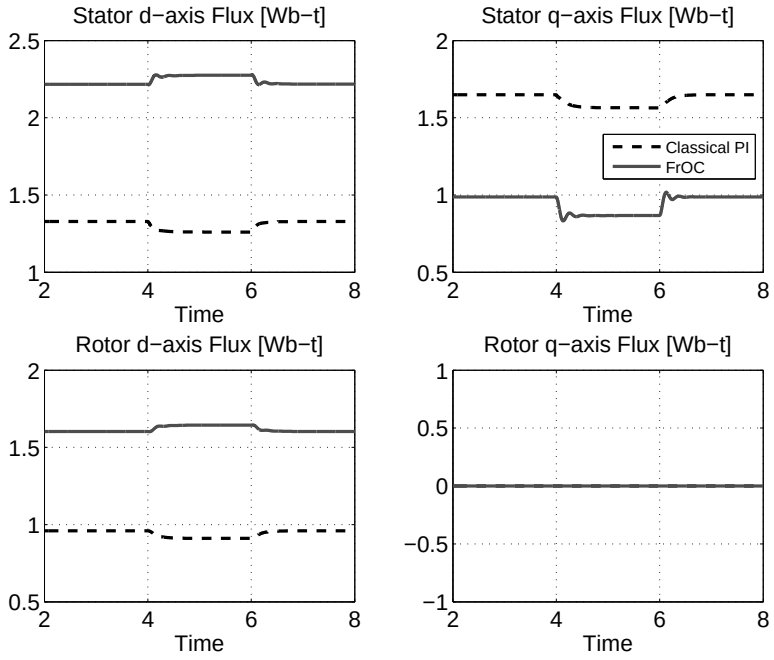

Figure 71. dq-flux with load torque reduced by 10% with $L_m = 75\%$ $R_r = 200\%$, and $N = 1$.

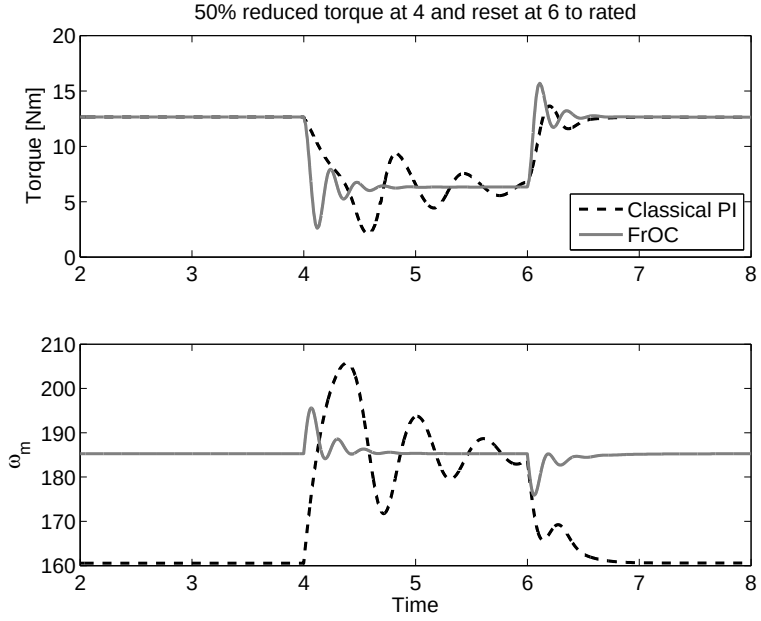

Figure 72. Torque and speed response with load torque reduced by 50% with $L_m = 75\%$, $R_r = 200\%$, and $N = 1$.

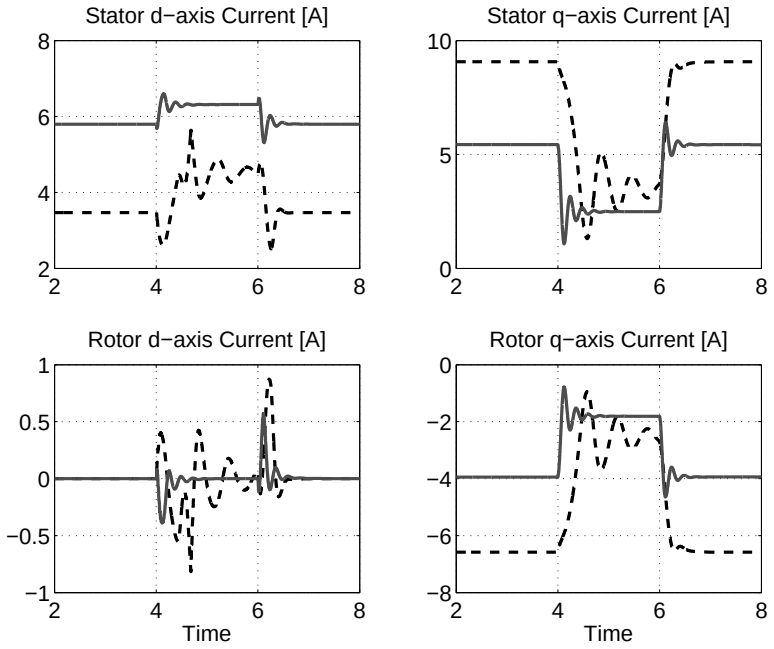

Figure 73. dq-currents with load torque reduced by 50% with $L_m = 75\%$, $R_r = 200\%$, and $N = 1$.

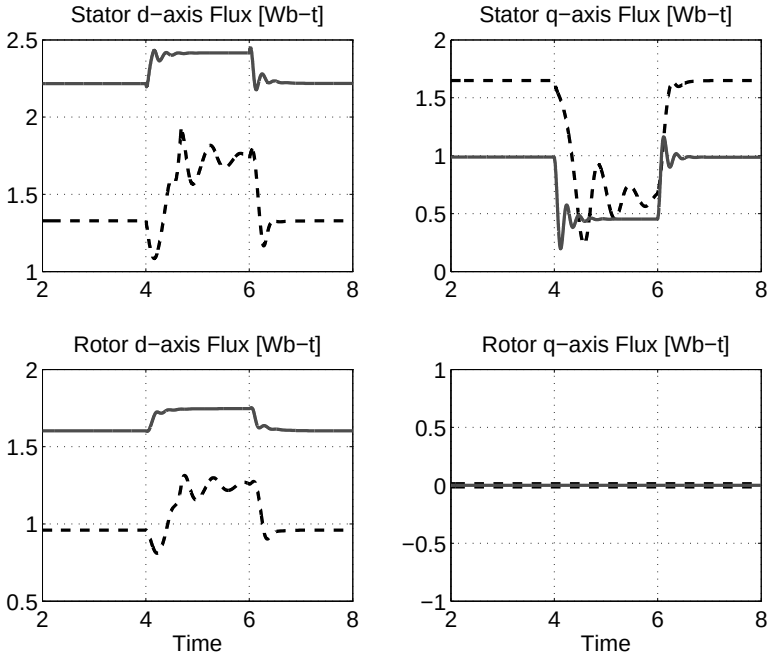

Figure 74. dq-flux with load torque reduced by 50% with $L_m = 75\%$, $R_r = 200\%$, and $N = 1$.

4.7.2. Quantitative Analysis of Dynamic Simulation

From previous section we can conclude that the controller synthesis using FrOC produces the excellent results. The Simulations results for the stable cases are considered for the quantitative analysis for classical PI controller and FrOC of third order ($N = 1$). The results for classical PI and FrOC are presented in the Figures 75 and 76 along with the analysis in tables 18 and 19 respectively.

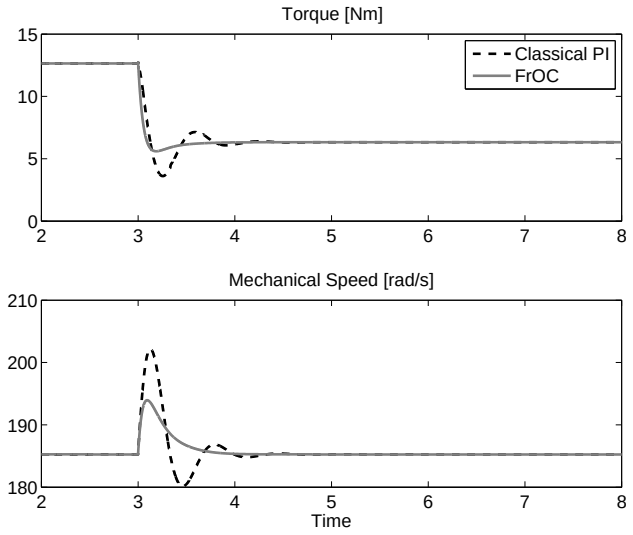

Figure 75. Torque and speed response at nominal values of R_r, L_m, and FrOC with $N = 1$.

Table 18. Quantitative analysis at rated values with step change in load torque.

	$SettlingTime$	$Overshoot$	$RiseTime$
Torque (PI)	1.4s	14.3%	1.2s
Torque (FrOC)	0.2	0%	0.2s
Speed (PI)	1.4s	9.2%	1.3s
Speed (FrOC)	0.9s	4.6%	0.06s

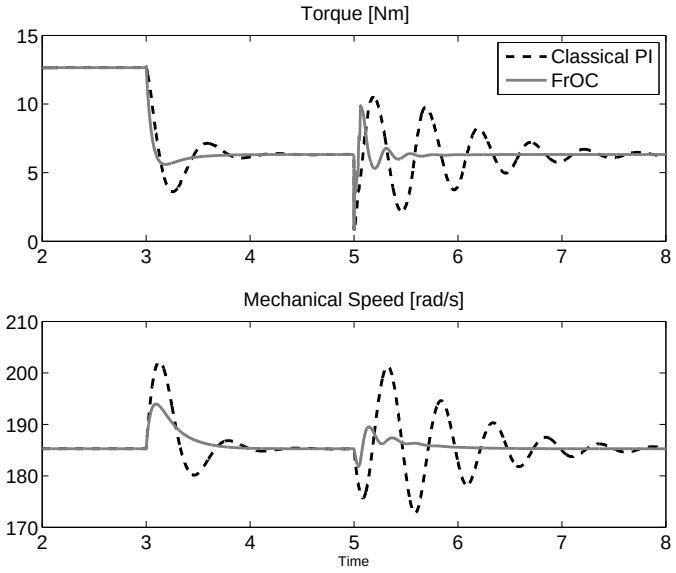

Figure 76. Torque and speed response at 200% rated value of R_r and 80% rated value of L_m and FrOC with $N = 1$.

Table 19. Quantitative analysis at rated values with R_r as step change.

	$SettlingTime$	$Overshoot$	$RiseTime$
Torque (PI)	2.3s	68.2%	0.16s
Torque (FrOC)	0.5s	59.1%	0.06s
Speed (PI)	2.25s	10.21%	0.3s
Speed (FrOC)	0.75s	3.2%	0.12s

4.8. Extended Simulation Results

Further Simulations are carried out to examine the validity and robustness of the FrOC. Different parameter variations introduced are compared for classical PI controller and FrOC. The parameters in extended simulations are varied in the wide range to observe the performance of controllers. Also some hypothetical scenarios are created to put controllers under worst conditions to comprehend the performance of controllers. The simulations are carried out for the following conditions apart from mentioned in previous section:

1. R_r increased by 100% of its nominal value.

2. L_r increased by 20% of its nominal value.

The motor is assumed to run under no load condition, and in each case the load torque is applied at the 3 seconds as a step change.To create the mismatch between parameters in indirect field oriented control block and induction motor the step change in parameters is introduced at 5s.

The case where R_r is changed to 200% of its nominal value with step change in rotor resistance R_r is shown in figures 77, 78, 79, and 80.

The step change of rotor resistance R_r at 5 seconds does not cause any instability, but variations in R_r has a deep impact on the rotor time constant $\frac{L_r}{R_r}$. Since any oscillations produced in the torque are damped based on the rotor time constant. The frequency response is shown in figure 81.

The hypothetical cased created to examine the worst case performance of the fractional order controller created by increasing L_r by 20% of its rated value. The results for variation in L_r are shown if figures 82, 83, 84, and 85. The bode plot is shown in figure 86.

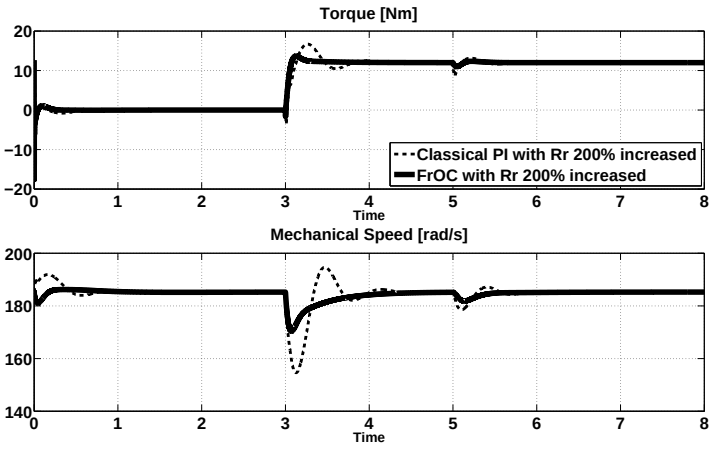

Figure 77. Torque and speed response of induction motor with R_r at 200% of rated value.

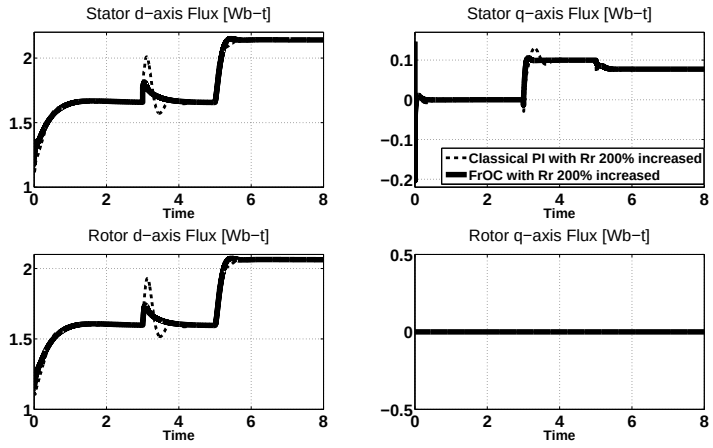

Figure 78. dq-flux for stator and rotor of induction motor with R_r at 200% of rated value.

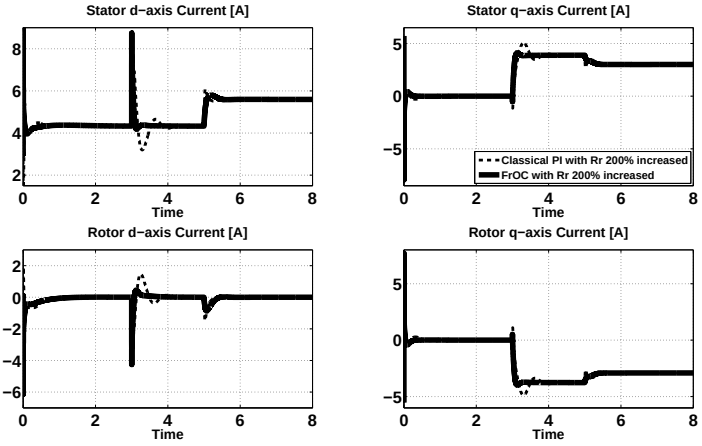

Figure 79. dq-currents for stator and rotor of induction motor with R_r at 200% of rated value.

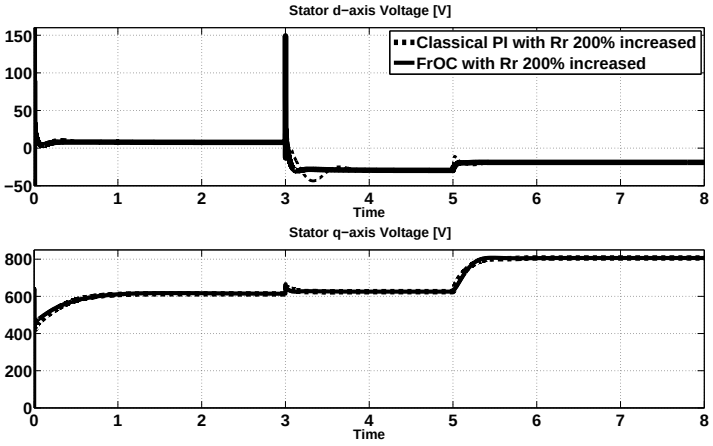

Figure 80. dq-voltages of induction motor with R_r at 200% of rated value.

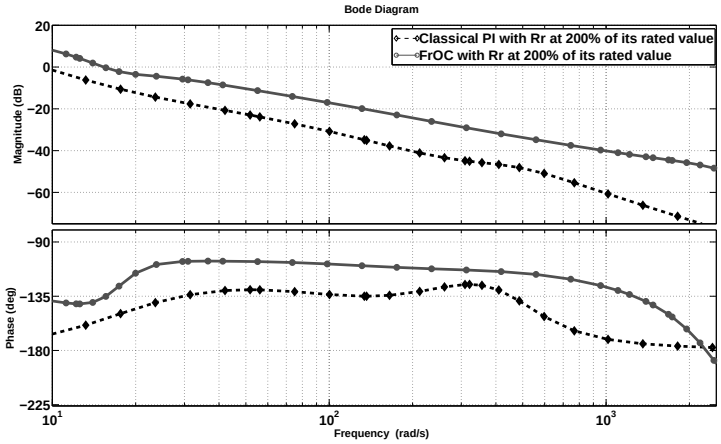

Figure 81. Frequency response showing the iso-damping property R_r at 200% of rated value.

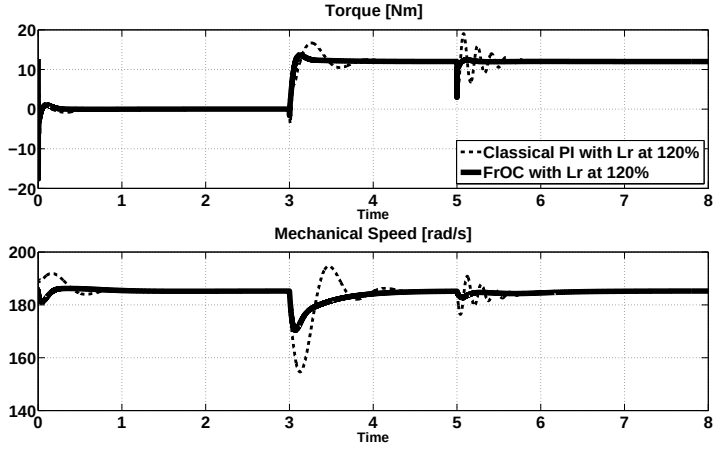

Figure 82. Torque and speed response of induction motor with L_r at 120% of rated value.

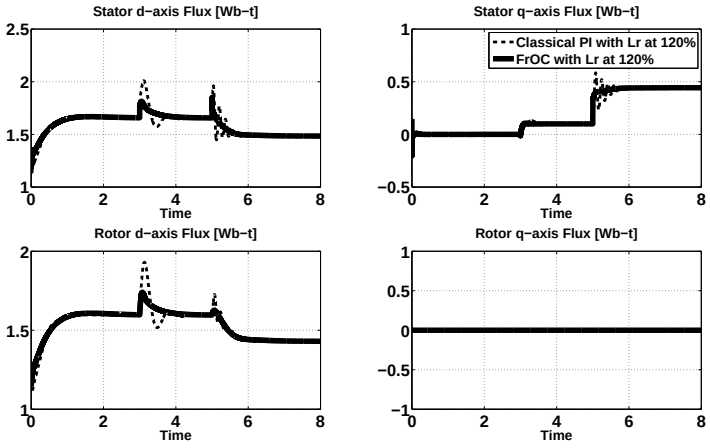

Figure 83. dq-flux for stator and rotor of induction motor with L_r at 120% of rated value.

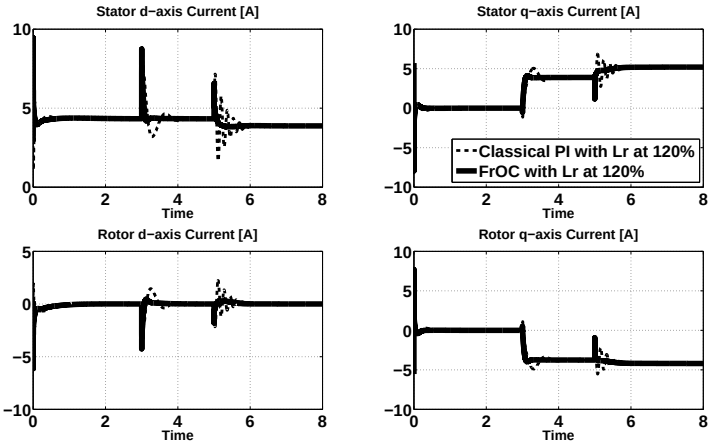

Figure 84. dq-currents for stator and rotor of induction motor with R_r at 120% of rated value.

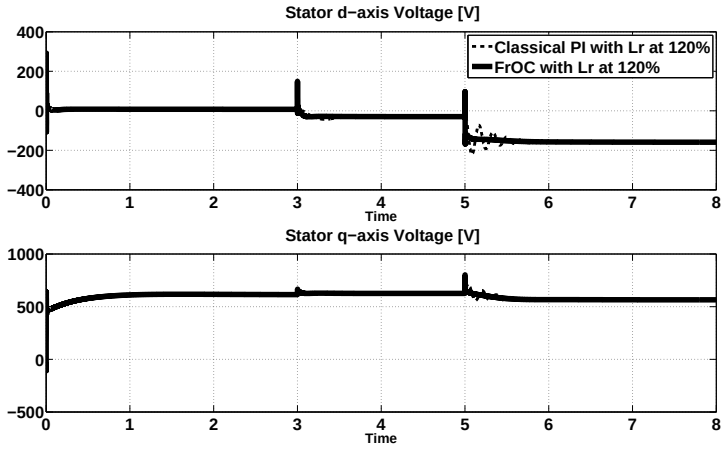

Figure 85. dq-voltages of induction motor with L_r at 120% of rated value.

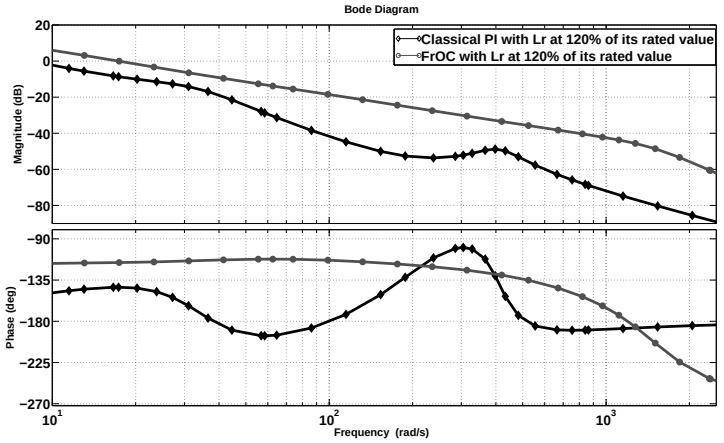

Figure 86. Frequency response showing the iso-damping property L_r at 120% of rated value.

4.8.1. Discussion

The results obtained using simulation for induction motor with classical PI controller and FrOC, with varying L_m and R_r, are supported through the damping ratio analysis. The damping ratio of corresponding mode depicts the damped oscillatory behavior of the system.

The damping ratio of the induction motor (without any controller) in table 20 clearly shows that, as the magnetizing inductance L_m decreases the damping ratio corresponding to mode start decreasing. Similarly the rotor resistance R_r in table 21, is varied over 200% to 60% of its rated value shows the similar behavior.

Table 20. Damping ratio variation of induction motor (with variation in L_m).

L_m	Mode 1	Mode 2	Mode 3
L_{mr}	0.27	1	0.19
$0.9L_m$	0.15	1	0.05
$0.8L_m$	0.11	1	0.03
$0.7L_m$	0.09	1	0.02

Table 21. Damping ratio variation of induction motor (with variation in R_r).

R_r	Mode 1	Mode 2	Mode 3
$2.0R_r$	0.56	1	0.19
$1.8Rr$	0.50	1	0.19
$1.6R_r$	0.44	1	0.19
$1.4R_r$	0.38	1	0.19
$1.2R_r$	0..32	1	0.19
R_{rr}	0.27	1	0.19
$0.8R_r$	0.21	1	0.19
$0.6R_r$	0.16	1	0.19

Table 22. Damping ratio variation (with variation in L_m) with classical PI controller.

L_m	Mode 1	Mode 2	Mode 3
L_{mr}	0.75	0.45	0.76
$0.9L_m$	0.46	0.16	1
$0.8L_m$	0.35	0.10	1
$0.7L_m$	0.27	0.08	1

The table 22 show the damping ratios of the indirect field oriented control with classical PI controller. The decrease in the damping ratio of mode 1 and mode 2 clearly shows that system under PI controller have more oscillation as the magnetizing inductance decreases.

Table 23. Damping ratio variation (with variation in L_m) using FrOC.

L_m	Mode 1	Mode 2	Mode 3
L_{mr}	1	1	0.41
$0.9L_m$	0.99	0.97	0.79
$0.8L_m$	0.99	0.89	0.96
$0.7L_m$	0.99	0.85	0.99

Similarly table 23 shows the damping ratios using FrOC. The decrease in magnetizing inductance clearly shows that the damping ratio increases for mode 3, while the decrease in damping ratio for mode 2 is comparatively slow over the expected variation of magnetizing inductance.

The tables 24, 25, and 26 shows comparisons for FrOC and classical PI for different parameter variations.

Table 24. Comparison of damping ratio variation (with variation in L_m at 80% and R_r at 200%) using FrOC.

	Mode 1	Mode 2	Mode 3
PI	0.61	0.10	1
$FrOC$	0.99	0.89	1

Table 25. Damping ratio variation (with variation in R_r) using classical PI controller.

R_r	Mode 1	Mode 2	Mode 3
$2.0R_r$	0.94	0.94	0.49
$1.8Rr$	0.91	0.92	0.45
$1.6R_r$	0.88	0.88	0.46
$1.4R_r$	0.85	0.84	0.47
$1.2R_r$	0..81	0.80	0.47
R_{rr}	0.76	0.75	0.48
$0.5R_r$	0.63	0.60	0.49

Table 26. Damping ratio variation (with variation in R_r) using FrOC.

R_r	Mode 1	Mode 2	Mode 3
$2.0R_r$	0.50	0.99	0.40
$1.8Rr$	0.50	0.99	0.41
$1.6R_r$	0.49	0.99	0.41
$1.4R_r$	0.49	0.99	0.41
$1.2R_r$	0..41	0.99	0.41
R_{rr}	0.49	0.99	0.41
$0.5R_r$	0.50	0.99	0.41

4.9. High Order Control (H_2 and H_∞ Controllers)

The optimal controllers are known because they minimize a given performance criterion. This means they achieve the best possible result in what that criterion is concerned. Of course, should the criterion be poorly chosen the controller's performance would probably be unsatisfactory, even though it would still be optimal in the sense above. Controllers minimizing the H_2 or the H_∞ norm of suitable loop transfer function involving the plant to control are in use. The idea is to minimize one of the above norms, ensuring that the input is never amplified to such an extent that instability will arise. It is usual to choose weights, that is shaping transfer functions, in the control loop so that control efforts be exerted at those frequencies desired by control designer. The weights can be found out adequately such that H_2 orH_∞ norm is minimized for stable and robust controller. These are expected to cause a worse performance but not instability.

H_2 and H_∞ controllers make use of the control structures of the block diagrams shown in figure 87, where K is the controller, A, B, C, and are the matrices of the state space representation of the plant P, and L models how noise affects the states. Vector w collects all inputs and saves the control actions u. Vector z collects all variables showing the performance of the control system, namely outputs and control actions. Weights W_1 to W_4 are usually transfer functions, and are used to shape the result by telling the loop in what frequencies control actions, outputs, etc., have to be large or small.

4.9.1. Plug-in H_∞ Controller

A plug-in compensator enhances the system robustness without affecting the nominal tracking performance. In [9] the authors used the H_∞ loop-shaping design technique, which will be discussed in this theses as a high order controller to compare with FrOC. Theoretically, this technique is optimal in dealing with unstructured

uncertainty described by the gap metric or ν-metric. Practically it is effective in cases when the uncertainty has unknown sources and is hard to measure. Comparing to other H_∞ controller design methods, such as mixed sensitivity optimization, the loop shaping design turns the different task of external weighting function selection into relatively easy choice of loop-shaping functions and eliminates the time consuming γ-iteration, which us required in usual H_∞ optimization, in the computation of the optimal controller.

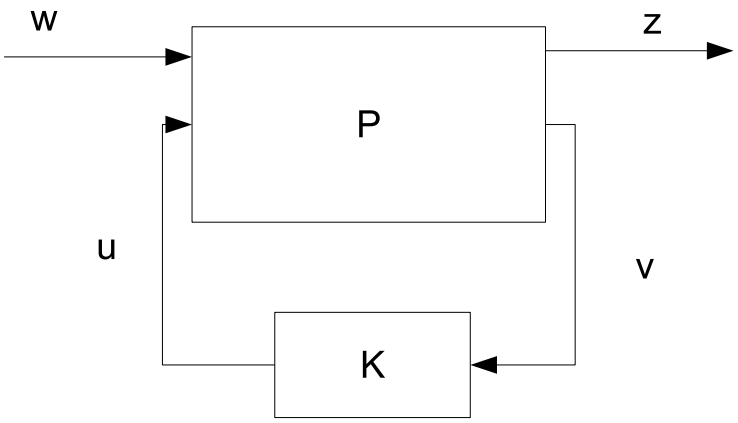

Figure 87. Block diagram of H_2 and H_∞ controller.

Figure 88 shows the linearized block diagram of induction motor. In the diagram $u = T_e$ is the command torque input, y is the system output which speed and $d = T_L$ is external disturbance, and T_L is assumed to be a constant load torque. The variation in the parameters J_m and B_m is common in real applications. For instance, the bearing friction will change after the motor has run for a period of time.

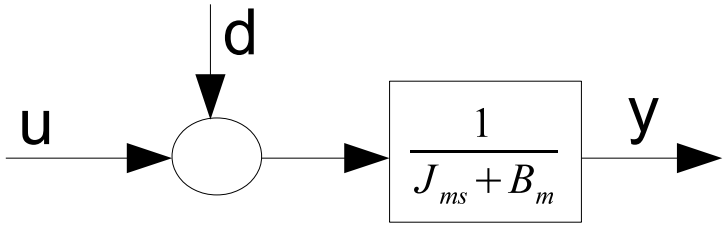

Figure 88. Linearized induction motor model.

4.9.2. Controller Design

Usually the exact plant model is not known for controller design problems. The control engineer only knows a nominal plant and a simple controller can be designed to achieve a satisfactory tracking performance for the nominal plant. The plug-in compensation requires that the controller is already designed and working well under the nominal operation of the plant. The H_∞ loop shaping technique is used to design the plug-in compensator without dismantling the existing controller.

4.9.3. Controller Structure

Figure 89 shows a P plant single input single output (SISO) strictly proper nominal system and $K = [K_1 - K_2]$ is a 2DOF controller. Initially we have already designed controller $K = C = [C_1 - C_2]$ with satisfactory nominal tracking performance, such that transfer function from reference r to output y is satisfactory and given as:

$$\frac{Y}{R} = \frac{C_1 P}{1 + C_2 P} \tag{4.36}$$

The C is already a designed PI controller using the classical tuning technique discussed in the previous chapter. Let the co-prime factorization of P be given as:

$$P = \frac{N}{M} \tag{4.37}$$

where $M,\ N\ \epsilon\ H_\infty$. Since C is stablilizing 2DOF controller for P, for any coprime factorization:

$$C = \frac{[X_1 - X_2]}{Y_o} \tag{4.38}$$

where X_1, X_2, and $Y_o\ \epsilon\ H_\infty$. The 2DOF stabilizing controller can be parameterized as:

$$[K_1 - K_2] = \frac{S - (X_2 + QM)}{Y_o - QN} \tag{4.39}$$

where $Q \epsilon H_\infty$ and $S \epsilon H_\infty$ are strictly stable systems. The nominal controller is obtained with $Q = 0$ and $S = X_1$. The transfer function from r to y, which determines the nominal tracking performance is:

$$\frac{Y}{R} = \frac{NS}{Y_o M - X_2 N} \tag{4.40}$$

which is independent of Q. Therefore, the set of all stabilizing 2DOF controllers which gives the same nominal tracking performance is given by:

$$[K_1 - K_2] = \frac{[X_1 - (X_2 + QM)]}{Y_o - QN} \tag{4.41}$$

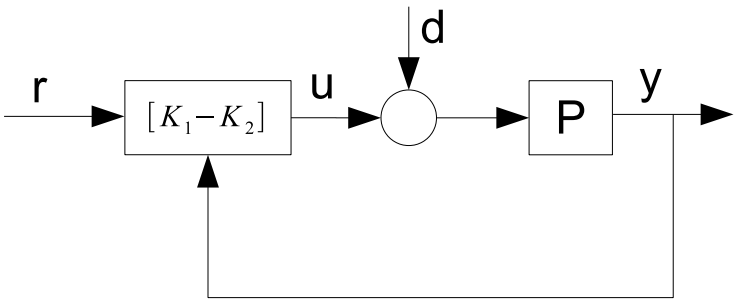

Figure 89. General 2DOF controller.

The loop property of the feedback system, which depends on K_2 and P only, now depends on Q only. For any stable system Q, which can even be nonlinear and time varying, the tracking performance is unaffected and the closed loop stability is guaranteed.

4.9.4. H_∞ Plugin Compensator and Simulations

Since the purpose of Q is to improve the loop property of the feedback system, the tracking issue is not of common in its design. Figure 90 is showing the feedback loop with the whole system redrawn and can be simplified to Figure 91 with $K_2 = (X_2 + QM/Y_o - QN)$.

The idea in the design of a stable Q is to design a satisfactory K_2 and then back substitute to get Q using:

$$Q = \frac{K_2 Y_o - X_2}{M + K_2 N} \tag{4.42}$$

which is obtained from Eqn. 4.39. All stabilizing K_2 are obtained over all stable Q from:

$$K_2 = \frac{X_2 + QM}{Y_o + QN} \tag{4.43}$$

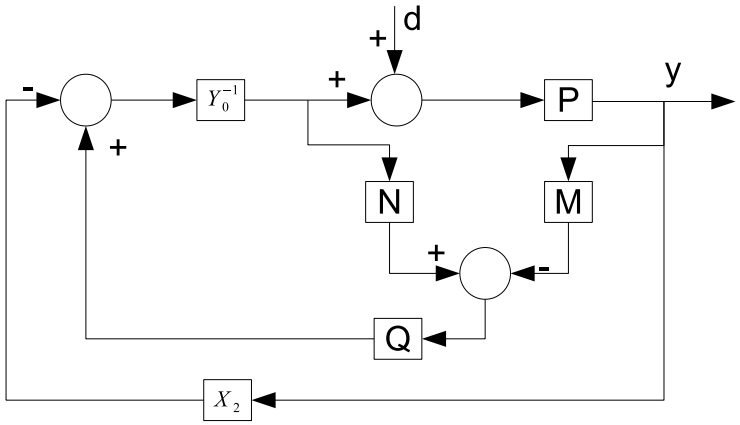

Figure 90. Block diagram for the design of the plug-in compensator Q.

The design of the controller K_2 is further divided into two steps. The first step is to choose a proper pre-filter W_1 and post filter W_2, so that the shaped plant $P_s = W_1 P W_2$ has a desired open loop frequency response. The H_{infty} optimal robust controller K_3 is found to minimize:

$$\left\| \begin{bmatrix} I \\ K_3 \end{bmatrix} (I + P_s K_3)^{-1} \begin{bmatrix} I & P_s \end{bmatrix} \right\|_\infty \tag{4.44}$$

This can be done using the command *ncfsyn* of MATLAB μ-Analysis and Synthesis Toolbox. The controller K_2 is a combination of per-filter W_1, post-filter W_2 and the H_∞ controller K_3 as $K_2 = W_1 K_3 W_2$. Figure 92 shows the design procedure of H_∞ loop-shaping controller. Finally the Q can be found from Eqn. 4.42.

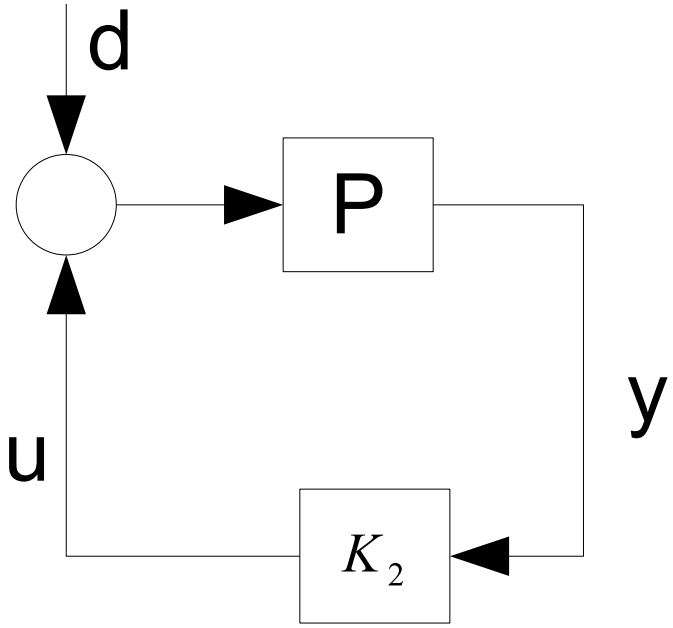

Figure 91. Standard feedback configuration.

4.9.5. Speed Controller Design for the IM

The classical PI controller tuned in the last chapter

$$[C_1(s) - C_2(s)] = \frac{1}{s}[C_{10}s + C_{11} - (C_{20}s + C_{21})] \tag{4.45}$$

is employed as nominal controller tuned to obtain to track a step reference and reject a constant external disturbance. For speed control, our plant is SISO strictly proper stable system. It follows that $M(s) = 1$ and $N(s) = P(s)$ can be assigned and $P(s) = (1/J_m s + B_m)$ is the nominal plant model. Now the problem reduces to select the proper pre-filter and post-filter. For a SISO system we can have $W_2(s) = 1$ and only put the emphasis on the choice of $W_1(s)$. As a nominal controller $C_2(s)$ has

already an integrator to reject the constant disturbance, the choice of $W_1(s)$ here is equal to $\alpha C_2(s)$ so that the nominal loop frequency response can be optimized according to the norm in Eqn. 4.44, and α is constant used to adjust the bandwidth of the shaped plant. In this design we have:

$$Y_0(s) = \frac{s}{c_{20}s + c_(21)} \tag{4.46}$$

where $c_{20} = K_P$ and $c_{21} = K_I$.

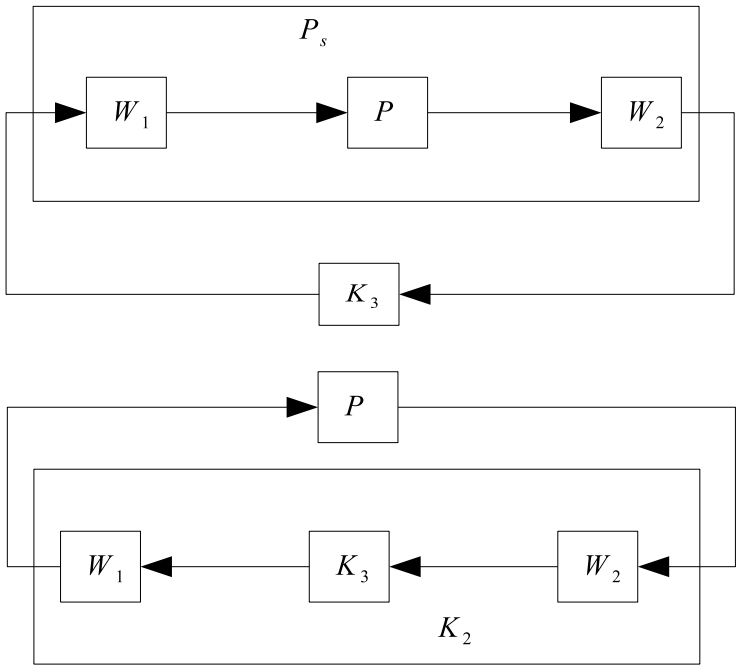

Figure 92. H_∞ loop-shaping controller design procedure.

$$X_1(s) = \frac{C_{10}s + C_{11}}{(C_{20}s + C_{21}} \tag{4.47}$$

$$X_2(s) = 1 \tag{4.48}$$

$$P(s) = \frac{\frac{1}{J_m}}{s + \frac{B_m}{J_m}} \tag{4.49}$$

$$W_1(s) = \alpha \frac{c_{20}s + C_{21}}{s} \tag{4.50}$$

$$P_s(s) = \alpha \frac{c_{20}s + C_{21}}{s(J_m s + B_m)} \tag{4.51}$$

where $P_s(s)$ is the shaped plant.

The $C_2(s)$ is defined as the classical PI tuned controller and is given as:

$$C_2(s) = \frac{K_P s + K_I}{s} \tag{4.52}$$

where $K_P = 0.24$ and $K_I = 3.53$.

For the design of block Q defined in Eqn. 4.42, the pre-filter

$$W_1(s) = \alpha \left(\frac{K_P s + K_I}{s} \right) \tag{4.53}$$

is selected, which is a constant α times PI controller. The constant α is chosen to be 8 so that the crossover should be adequate for torque rejection loop. By using the command *ncfsyn* of MATLAB μ-Analysis and Synthesis Toolbox ($[K, CL, GAM, INFO] = ncfsyn(P, -W1, W2);$), $K_3(s)$ found is:

$$K_3 = \frac{1.1508(s + 10.98)}{s + 14.54} \tag{4.54}$$

which is H_∞ robust controller.

The K_2 as given in Figure 92 is $K_2 = W_1 K_3 W_2$ and is found to be:

$$\frac{2.2096(s + 14.71)}{s + 10.98} \tag{4.55}$$

In the last Q can then be found from Eqn. 4.42 and after canceling the common poles and zeros we get Q as:

$$Q(s) = \frac{8.2066s(s + 10.54)(s + 0.02942)}{(s + 75.32)(s + 15)(s + 12.63)} \tag{4.56}$$

In the following dynamic simulation the results are compared for classical PI, FrOC, and plug-in robust compensator. The simulation is setup as:

- The simulation starts with full load and at the rated machine parameters.
- The simulation starts with full load and machine parameters R_r at 200% and L_m at 80% of the rated values.
- The small load torque change is applied at 4 seconds.
- The load torque is set back to full load torque.
- The above steps are repeated for 10% and 50% load torque reduction as a disturbance.

The load torque is reduced by 10% of the rated value as an external disturbance for which the dynamic simulation response are shown in Figure 93 for rated values of L_m and R_r. The simulation results shows that the disturbance tracking is comparable for the three controller types of controllers tuned. Similarly the load torque reduction by 50% gives the same intuition. Furthermore, the dynamic simulation results for L_m at 80% and R_r at 200% of the rated values and applying the load torque as external disturbance produces the stable response and the controller results are almost similar as shown in Figures 95 and 96.

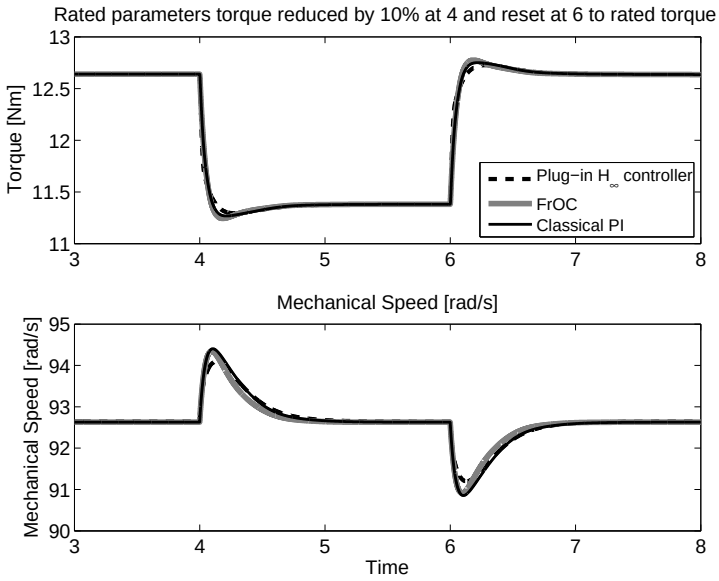

Figure 93. Torque and speed response load torque reduced by 10%.

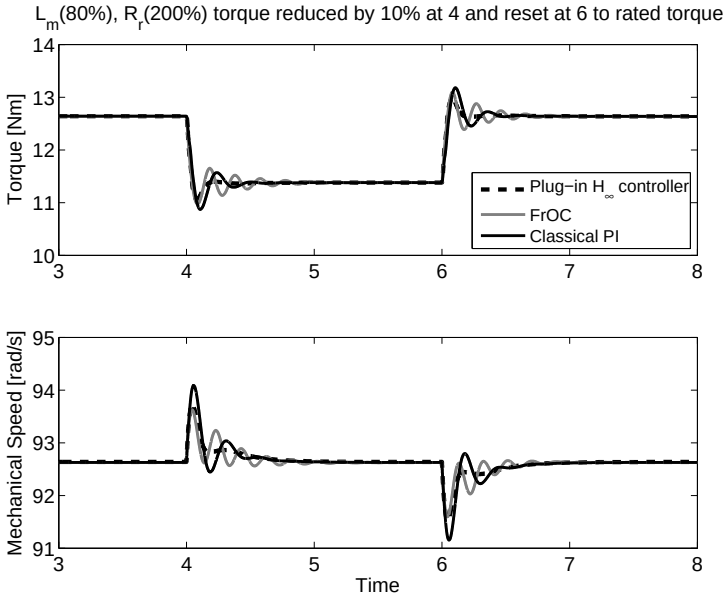

Figure 94. Torque and speed response load torque reduced by 10%.

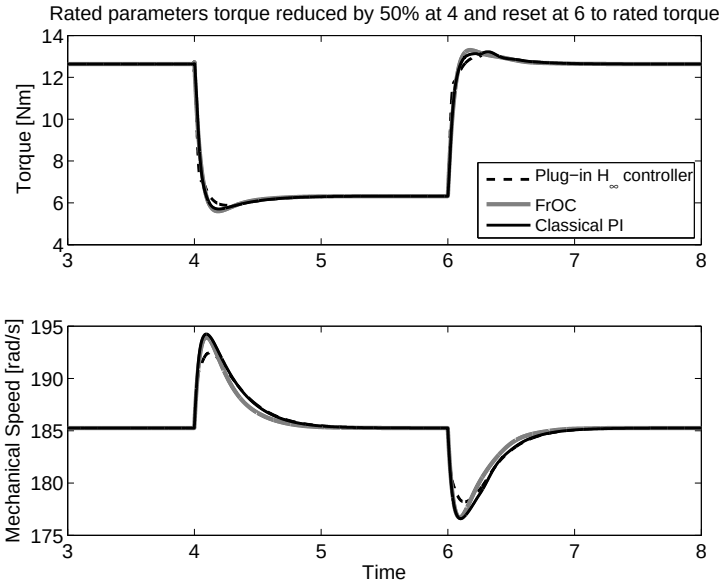

Figure 95. Torque and speed response load torque reduced by 50%.

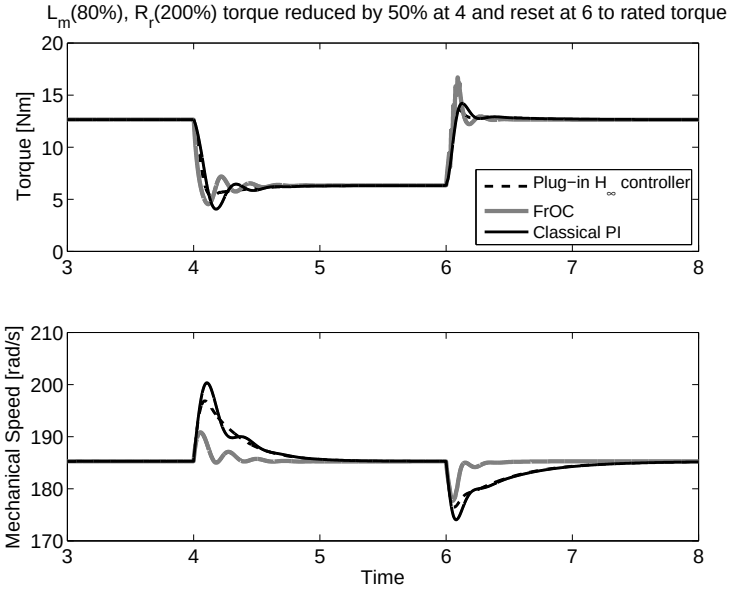

Figure 96. Torque and speed response load torque reduced by 50%.

4.10. Conclusion

Robustness to parameter variations is an important factor that dictates control performance in electric drives. In this chapter, a third order fractional order controller implemented with Oustaloup's approximation [42] was substituted for traditional PID controllers used in the current and speed control loops of a vector controlled induction motor drive. Dynamic simulations are presented when the drive system is subject to variations in two critical parameters - rotor resistance and magnetizing inductance. Unlike the PI controller, the simulations show that control performance is not degraded with the proposed fractional controller despite substantial variations in motor parameters. The results are encouraging and indicate that fractional order controllers provide a promising alternative for the design of robust controllers in electric drives applications.

CHAPTER 5. EXPERIMENTAL RESULTS

The experiments are carried out for the dc motor in speed control loop and for induction motor for V/f method. The dSpace DS1104 is used for the real time experiments. There are four major components of the dSpce DSP-based drives, used for the experiments in the dissertation. They are as follows: **1)** Motor coupling system, **2)** Power Electronics Drive Board, **3)** DSP based DS1104 research and development controller card and CP 1104 I/O board and **4)** MATLAB Simulink and Control-desk. The block diagram of the hardware setup is shown in Figure 97.

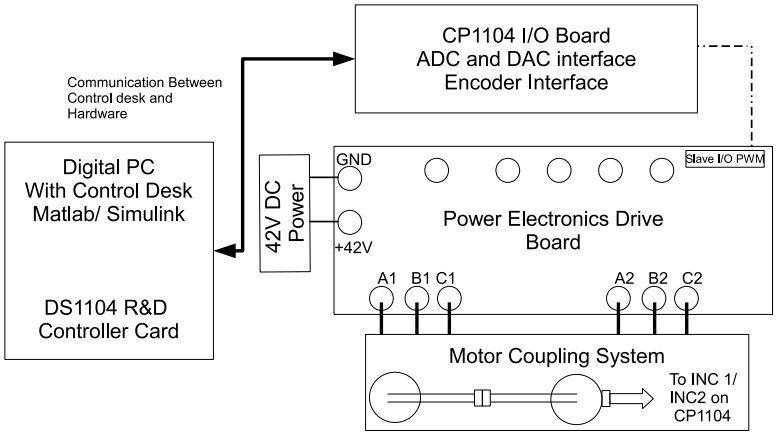

Figure 97. Block diagram for hardware setup.

5.1. Experimental Results for DC Motor

DC motor is setup for the speed control with the cascade control structure with similar tuning procedure is used to tune the current and speed loops of the DC motor as discussed in chapter 3. The hardware in loop experimental results are obtained for the two set of controllers namely: the classical PI tuned controller and and the fractional order controller (with similar tuning procedure given in chapter 4.

The speed response with both controllers shows that the dc motor has good reference tracking performance even under load as shown in the Figures 98, 99, 100, 101, 102, and 103.

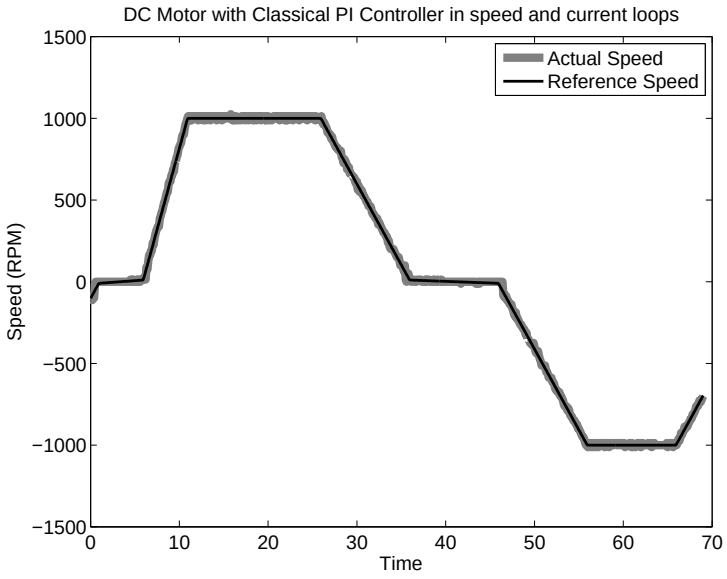

Figure 98. DC motor speed using PI controller.

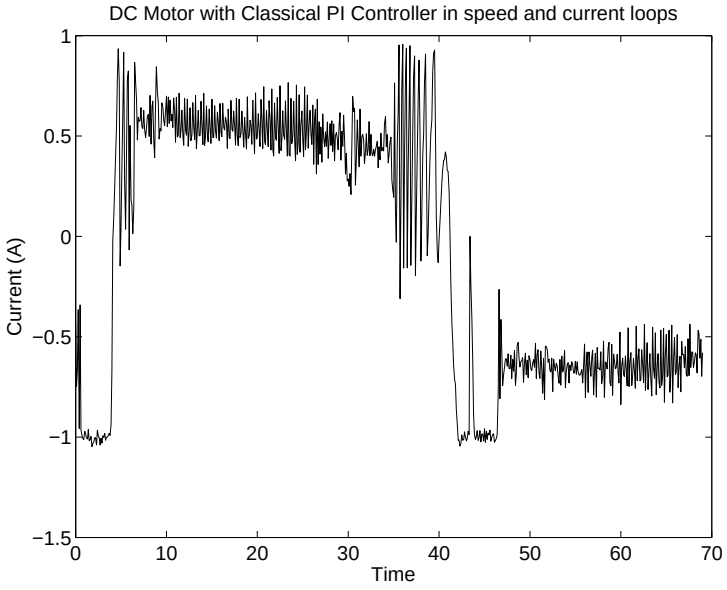

Figure 99. DC motor armature current with PI controller.

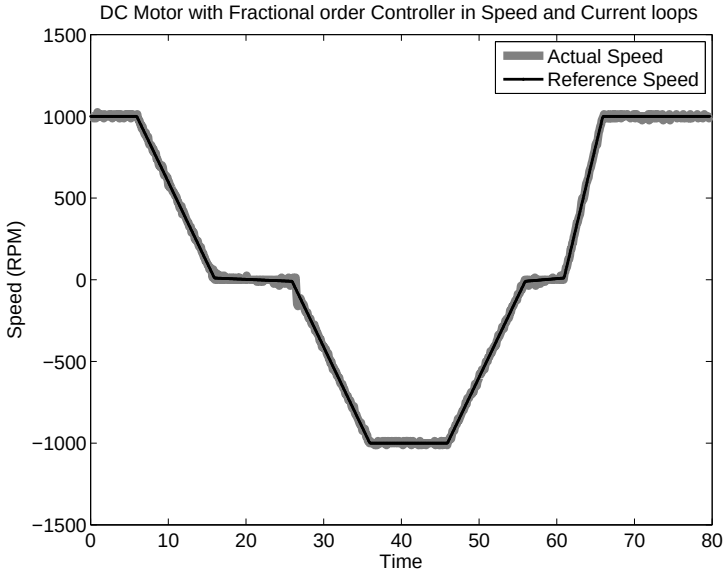

Figure 100. DC motor speed with fractional order controller.

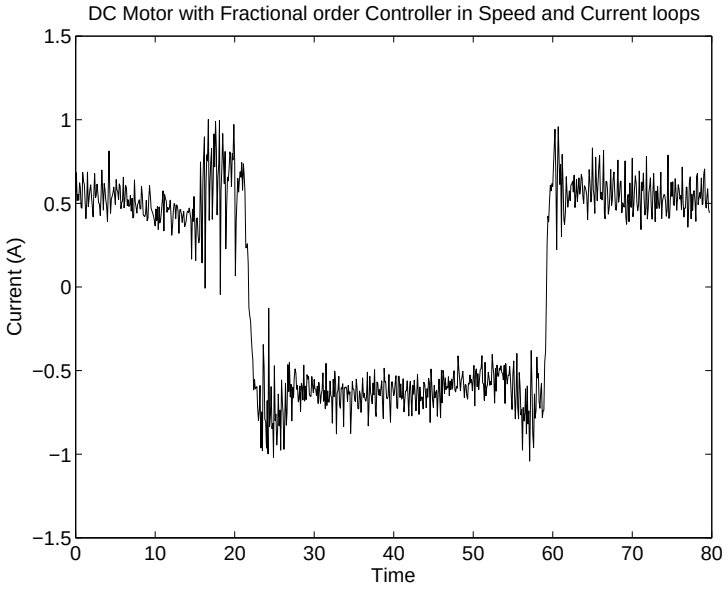

Figure 101. DC motor armature current with fractional order controller.

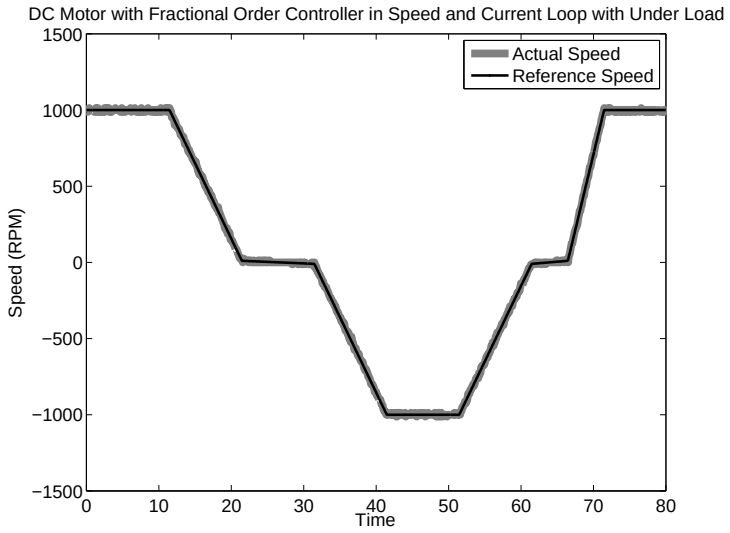

Figure 102. DC motor speed with fractional order controller under load of $0.1Nm$.

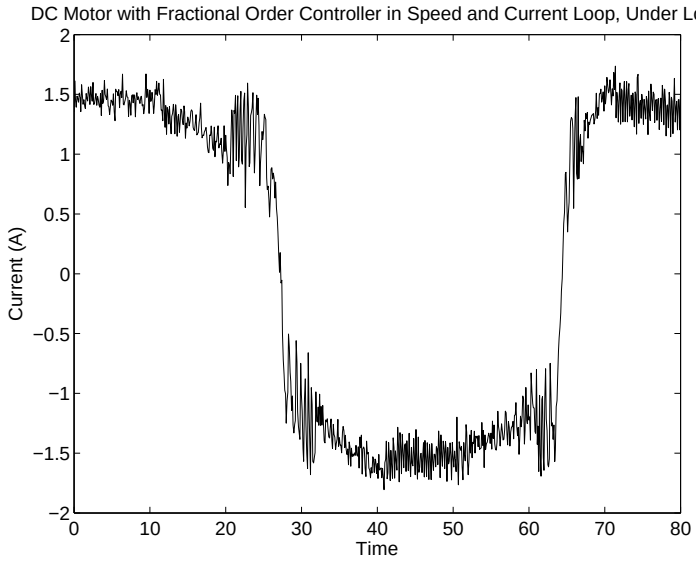

Figure 103. DC motor armature current with fractional order controller under load of $0.1Nm$.

5.2. Experiment Results for Induction Motor

The three phase induction motor is setup for the speed control loop with scalar control (V/f) scheme using the two sets of controller, the classical tuned PI controller and fractional order controller. The experimental results shows that at nominal operation the induction motor with FrOC gives a better reference tracking 104 than classical PI controller 105.

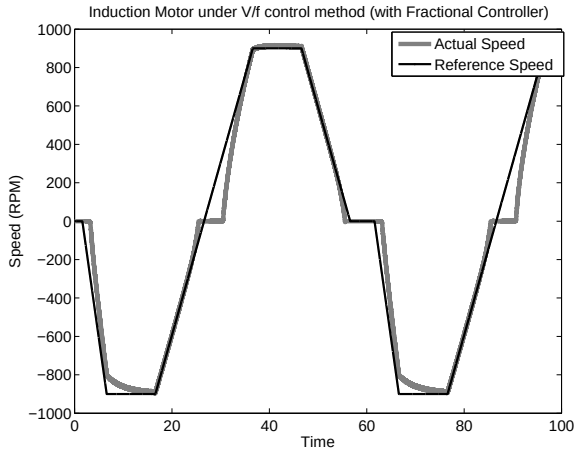

Figure 104. Induction motor speed V/f method using fractional order controller four quadrant.

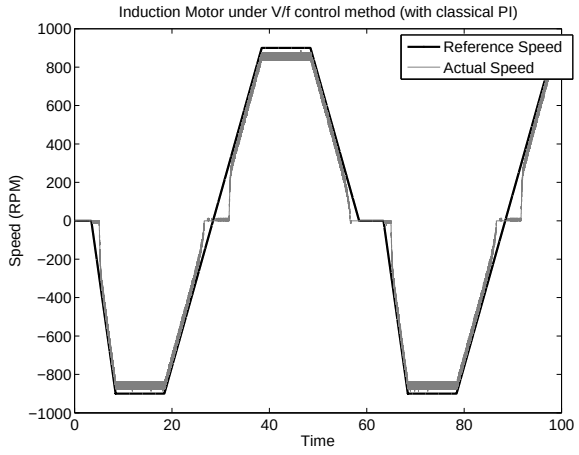

Figure 105. Induction motor speed V/f method using PI controller four quadrant.

CHAPTER 6. CONCLUSION

The thesis constitute of two major techniques to achieve the robustness to the disturbance for better tracking of speed. The first proposed technique produces the robust PI controller parameters while the second approach is tuning robust PI controllers which involves the fractional order integral and hence adding an extra degree of freedom to tune the controller. The techniques proposed are:

- Kharitonov Theorem
- Fractional order controller

6.1. Major Contributions

The major contribution of the thesis towards the development of robust high performance electric drives are:

1. Proposed a method to tune PI controller for indirect field oriented control under parameter uncertainty using Kharitonov theorem. The dynamic simulations shows the excellent dynamic response compared to traditionally tuned PI controller. The improvement of 35% in rise time and 46% decrease in overshoot is obtained in speed response with proposed method.

2. Proposed a fractional order PI controller for indirect field oriented control under parameter uncertainty, the dynamic simulations results are encouraging and indicate that fractional order controllers provide a promising alternative for the design of robust controllers in electric drives applications. Moreover, as the fractional order controller gives the high order controllers at implementation stage, which is compared with high order classical plug-in H_∞ compenstor technique. The improvement of 66% in rise time and 68% decrease in overshoot is attained in speed response with proposed method compared to classical PI controller.

6.2. Significance and Future Work

- The dynamic simulations, with the full nonlinear model considering control saturation, confirm the robustness and superior damping benefits with the controller synthesized using Kharitonov theorem.

- The fractional order controllers for dynamic simulation, with the full nonlinear model considering control saturation, outperforms tracking under parametric uncertainty and load torque variations as an external disturbance than the classical tuned PI controllers.

- The overall improvement is obtained in the drive system, in the form of reduced torque pulsation and shaft vibration.

- The proposed methods provides a systematic approach to robustify control settings that arise in several drive systems subject to similar parametric variations.

- The synthesis of controller using Kharitonov theorem can be improved by using some optimization technique to calculate the best gains of PI controller.

- The proposed method describes only one way to find the PI controller parameters. The process can be reversed by selecting the range of gains and optimize the damping ratio with verification using Kharitonov theorem.

- The laboratory based induction motor can be established by using certain material which can be used as a shield between rotor and stator to control the air gap flux, which in turn can help in controlling the magnetizing inductance L_m of the induction motor.

6.3. Limitations

- The magnetizing inductance L_m variation is temperature dependent and can not be varied to a specific level in lab, which puts the constraints for experimentation to verify the controller designed. Specialized industrial test system is required, typically not in University lab hold those equipment.

BIBLIOGRAPHY

[1] R. Krishnan and A.S. Bharadwaj. A review of parameter sensitivity and adaptation in indirect vector controlled induction motor drive systems. In *21st Annual IEEE Power Electronics Specialists Conference, 1990. PESC '90 Record.*, pages 560–566, 1990.

[2] R. Krishnan and Frank C. Doran. Study of parameter sensitivity in high-performance inverter-fed induction motor drive systems. *IEEE Transactions on Industry Applications.*, IA-23(4):623–635, 1987.

[3] Krishnan R. and Bharadwaj A.S. A review of parameter sensitivity and adaptation in indirect vector controlled induction motor drive systems. *IEEE Transactions on Power Electronics*, 6(4):695–703, 1991.

[4] A. Larabi and M.S. Boucherit. Robust speed-sensorless induction motor with the rotor time constant adaptation. In *Electrical Systems for Aircraft, Railway and Ship Propulsion (ESARS), 2010*, pages 1–6, 2010.

[5] C.P. Bottura and S.A.A. Filho. Robust indirect vector control for the induction machine. In *Proceedings of the IEEE International Symposium on Industrial Electronics, 1999. ISIE '99.*, volume 3, pages 1232–1237 vol.3, 1999.

[6] K. Kubota and K. Matsuse. Speed sensorless field-oriented control of induction motor with rotor resistance adaptation. *IEEE Transactions on Industry Applications*, 30(5):1219–1224, 1994.

[7] N. NAIT-SAID. Rotor resistance estimation of an induction motor to detect broken bars fault using h-h method. *Electric Power Components and Systems*, 32(2):149–161, 2004.

[8] A. Shiri, A. Vahedi, and A. Shoulaie. The effect of parameter variations on the performance of indirect vector controlled induction motor drive. In *IEEE International Symposium on Industrial Electronics, 2006*, volume 3, pages 2377–2381, 2006.

[9] Wai-Chuen Gan and L. Qiu. Design and analysis of a plug-in robust compensator: an application to indirect-field-oriented-control induction machine drives. *IEEE Transactions on Industrial Electronics.*, 50(2):272–282, 2003.

[10] Jie Li and Yanru Zhong. Robust speed control of induction motor drives employing first order auto disturbance rejection controllers. In *IEEE Industry Applications Society Annual Meeting (IAS), 2012*, pages 1–7, Oct 2012.

[11] K. Hasse. Zum dynamischen verhalten der asynchronmachine bei betrieb mit variable standerfrequenz und standerspannung. *ETZ-A*, pages 77–81, 1968.

[12] F. Blaschke. The principle of field orientation applied to the new trans-vector closed-loop control system for rotating field machines. *Siemens-Review*, 39:217–220, 1971.

[13] T.A. Lipo and A.B. Plunkett. A novel approach to induction motor transfer functions. *IEEE Transactions on Power Apparatus and Systems.*, PAS-93(5):1410–1418, 1974.

[14] R.H. Park. Two reaction theory of synchronous machine generalized method of analysis part 1. *AIEE Trans.*, pages 716–727, 1929.

[15] M. Depenbrock. Direct self-control (dsc) of inverter-fed induction machine. *IEEE Transactions on Power Electronics.*, 3(4):420–429, 1988.

[16] I. Takahashi and T. Noguchi. A new quick-response and high-efficiency control strategy of an induction motor. *IEEE Transactions on Industry Applications*, IA-22(5):820–827, 1986.

[17] P. Vas. *Sensorless Vector and Direct Torque Control*. Oxford Univeristy Press, London, UK, 1998.

[18] E.L. Owen, Marvin M. Morack, C. Curtis Herskind, and Arthur S. Grimes. Ac adjustable-speed drives with electronic power converters-the early days. *IEEE Transactions on Industry Applications.*, IA-20(2):298–308, 1984.

[19] W. Leonhard. Microcomputer control of high dynamic performance ac-drivesa survey. *Automatica*, 22(1):1–19, 1986.

[20] H. Huffman. Introduction to solid-state adjustable speed drives. In *Conference Record of the 1989 IEEE Industry Applications Society Annual Meeting, 1989.*, pages 1761–1768 vol.2, 1989.

[21] Susumu Tadakuma and Minoru Ehara. Historical and predicted trends of industrial ac drives. In *Proceedings of the IECON '93., International Conference on Industrial Electronics, Control, and Instrumentation, 1993.*, pages 655–661 vol.2, 1993.

[22] Takahashi I. and Noguchi T. Take a look back upon the past decade of direct torque control [of induction motors]. In *IECON 97. 23rd International Conference on Industrial Electronics, Control and Instrumentation, 1997.*, volume 2, pages 546–551 vol.2, 1997.

[23] T.M. Jahns and E.L. Owen. Ac adjustable-speed drives at the millennium: how did we get here? *IEEE Transactions on Power Electronics.*, 16(1):17–25, 2001.

[24] G.K Singh. Multi-phase induction machine drive researcha survey. *Electric Power Systems Research*, 61(2):139 – 147, 2002.

[25] J. Holtz. Developments in sensorless ac drive technology. In *International Conference on Power Electronics and Drives Systems, 2005. PEDS 2005.*, volume 1, pages 9–16, 2005.

[26] Z.Q. Zhu and D. Howe. Electrical machines and drives for electric, hybrid, and fuel cell vehicles. *Proceedings of the IEEE*, 95(4):746–765, 2007.

[27] J. Bocker and S. Mathapati. State of the art of induction motor control. In *IEEE International Electric Machines Drives Conference, 2007. IEMDC '07.*, volume 2, pages 1459–1464, 2007.

[28] J.W. Finch and D. Giaouris. Controlled ac electrical drives. *IEEE Transactions on Industrial Electronics*, 55(2):481–491, 2008.

[29] I. Boldea. Control issues in adjustable speed drives. *IEEE Industrial Electronics Magazine,*, 2(3):32–50, Sept 2008.

[30] Bose B.K. Power electronics and motor drives recent progress and perspective. *IEEE Transactions on Industrial Electronics,*, 56(2):581–588, 2009.

[31] Hossein Madadi Kojabadi. A comparative analysis of different pulse width modulation methods for low cost induction motor drives. *Energy Conversion and Management*, 52(1):136 – 146, 2011.

[32] Ibrahim M. Alsofyani and N.R.N. Idris. A review on sensorless techniques for sustainable reliablity and efficient variable frequency drives of induction motors. *Renewable and Sustainable Energy Reviews*, 24(0):111 – 121, 2013.

[33] A. Nabae, Kenichi Otsuka, Hiroshi Uchino, and R. Kurosawa. An approach to flux control of induction motors operated with variable-frequency power supply. *IEEE Transactions on Industry Applications*, IA-16(3):342–350, 1980.

[34] J. Holtz and E. Bube. Field-oriented asynchronous pulse-width modulation for high-performance ac machine drives operating at low switching frequency. *IEEE Transactions on Industry Applications.*, 27(3):574–581, 1991.

[35] Sang-Hoon Kim and Seung-Ki Sul. Voltage control strategy for maximum torque operation of an induction machine in the field-weakening region. *IEEE Transactions on Industrial Electronics*, 44(4):512–518, 1997.

[36] H. Abu-Rub, A. Lewicki, A. Iqbal, and J. Guzinski. Medium voltage drives - challenges and requirements. In *IEEE International Symposium on Industrial Electronics (ISIE), 2010*, pages 1372–1377, 2010.

[37] S.H. HosseinNia, I. Tejado, B.M. Vinagre, V. Milanes, and J. Villagra. Low speed control of an autonomous vehicle using a hybrid fractional order controller. In *Control, Instrumentation and Automation (ICCIA), 2011 2nd International Conference on*, pages 116–121, 2011.

[38] Lascu C. Boldea I. and Blaabjerg F. Very-low-speed variable-structure control of sensorless induction machine drives without signal injection. *IEEE Transactions on Industry Applications.*, 41(2):591–598, 2005.

[39] M.-H. Kim and J.C. Hung. Vector control system for induction motor without speed sensor at very low speed. In *Proceedings of the 1995 IEEE IECON 21st International Conference on Industrial Electronics, Control, and Instrumentation, 1995.*, volume 1, pages 524–529 vol.1, 1995.

[40] R. Krishnan. Review of flux-weakening in high performance vector controlled induction motor drives. In *Proceedings of the IEEE International Symposium on Industrial Electronics, 1996. ISIE '96.*, volume 2, pages 917–922 vol.2, 1996.

[41] Oustaloup, Alain, Sabatier, Jocelyn, and Moreau, Xavier. From fractal robustness to the crone approach. *ESAIM: Proc.*, 5:177–192, 1998.

[42] A. Oustaloup, F. Levron, B. Mathieu, and F.M. Nanot. Frequency-band complex noninteger differentiator: characterization and synthesis. *IEEE Transactions on Circuits and Systems I: Fundamental Theory and Applications*, 47(1):25–39, 2000.

[43] B. Singh, S. Jain, and S. Dwivedi. Torque ripple reduction technique with improved flux response for a direct torque control induction motor drive. *Power Electronics, IET*, 6(2):326–342, 2013.

[44] F.F.M. El-Sousy. Adaptive dynamic sliding-mode control system using recurrent rbfn for high-performance induction motor servo drive. *IEEE Transactions on Industrial Informatics.*, 9(4):1922–1936, 2013.

[45] Krishnan R. *Electric Motor Drives: Modeling, Analysis, and Control*. Prentice Hall PTR, 2001.

[46] O. Barambones and P. Alkorta. Position control of the induction motor using an adaptive sliding mode controller and observers. *IEEE Transactions on Industrial Electronics.*, PP(99):1–1, 2014.

[47] H.A. Shah, A.T. Patel, S.K. Shah, and R. Patel. Controller design via sliding mode control approach of induction motor – a survey. In *Fourth International Conference on Advanced Computing Communication Technologies (ACCT), 2014*, pages 541–546, Feb 2014.

[48] F. Alonge, F. DIppolito, and A. Sferlazza. Sensorless control of induction-motor drive based on robust kalman filter and adaptive speed estimation. *IEEE Transactions on Industrial Electronics.*, 61(3):1444–1453, March 2014.

[49] F. Ben Salem and N. Derbel. Vsc-based dtc-svm with adaptive parameter estimation. In *11th International Multi-Conference on Systems, Signals Devices (SSD), 2014*, pages 1–7, Feb 2014.

[50] A. Taheri and M. Mohammadbeigi. Speed sensor-less estimation and predictive control of six-phase induction motor using extended kalman filter. In *5th Power Electronics, Drive Systems and Technologies Conference (PEDSTC), 2014*, pages 13–18, Feb 2014.

[51] A. Raisemche, M. Boukhnifer, C. Larouci, and D. Diallo. Two active fault-tolerant control schemes of induction-motor drive in ev or hev. *IEEE Transactions on Vehicular Technology*, 63(1):19–29, Jan 2014.

[52] Zhong gang Yin, Chang Zhao, Yan-Ru Zhong, and Jing Liu. Research on robust performance of speed-sensorless vector control for the induction motor using an interfacing multiple-model extended kalman filter. *IEEE Transactions on Power Electronics.*, 29(6):3011–3019, June 2014.

[53] Amezquita Brooks L. Liceaga Castro J. and Liceaga Castro E. Speed and position controllers using indirect field-oriented control: A classical control approach. *IEEE Transactions on Industrial Electronics.*, 61(4):1928–1943, April 2014.

[54] M.O. Mustafa, G. Nikolakopoulos, and T. Gustafsson. A robust linear discrimination fault classification scheme for three phase induction motors. In *International Conference on Control, Decision and Information Technologies (CoDIT), 2013*, pages 524–529, May 2013.

[55] G. Rubio-Astorga, J.D. Sanchez-Torres, J. Canedo, and A.G. Loukianov. High-order sliding mode block control of single-phase induction motor. *IEEE Transactions on Control Systems Technology.*, PP(99):1–1, 2013.

[56] A. Ltifi, M. Ghariani, and R. Neji. Pi sliding mode control for the non-linear system. In *10th International Multi-Conference on Systems, Signals Devices (SSD), 2013*, pages 1–8, March 2013.

[57] Sira Ramirez H. Gonzalez Montanez F. CortesRomero J.A. and Luviano Juarez A. A robust linear field-oriented voltage control for the induction motor: Experimental results. *IEEE Transactions on Industrial Electronics.*, 60(8):3025–3033, Aug 2013.

[58] T. Terras, S. Hadjeri, A. Mezouar, and T.M. Chikouche. Robust speed control with rotor resistance estimation. *Canadian Journal of Electrical and Computer Engineering.*, 36(2):43–51, Spring 2013.

[59] Antonio Barbosa de Souza Junior, Eber de Castro Diniz, Dalton de Araujo Honorio, Luiz Henrique Silva Colado Barreto, and Laurinda Lcia Nogueira dos Reis. Hybrid control robust using logic fuzzy applied to the position loop for vector control to induction motors. *Electric Power Components and Systems*, 42(6):533–543, 2014.

[60] S. Drid, M. Tadjine, and M.S. Nait-Said. Robust backstepping vector control for the doubly fed induction motor. *Control Theory Applications, IET*, 1(4):861–868, July 2007.

[61] G. Kenne, T. Ahmed-Ali, H. Nkwawo, and F. Lamnabhi-Lagarrigue. Robust rotor flux and speed control of induction motors using on-line time-varying rotor resistance adaptation. In *44th IEEE Conference on Decision and Control, 2005*

and 2005 European Control Conference. CDC-ECC '05., pages 7768–7774, Dec 2005.

[62] B. Aloliwi, H.K. Khalil, and E.G. Strangas. Robust speed control of induction motors using adaptive observer. In *Proceedings of the 1999 American Control Conference, 1999.*, volume 2, pages 931–935 vol.2, Jun 1999.

[63] H.K. Khalil and E.G. Strangas. Robust speed control of induction motors using position and current measurements. *IEEE Transactions on Automatic Control.*, 41(8):1216–1220, Aug 1996.

[64] Fang-Zheng Peng and T. Fukao. Robust speed identification for speed-sensorless vector control of induction motors. *IEEE Transactions on Industry Applications.*, 30(5):1234–1240, Sep 1994.

[65] C. Lascu, I. Boldea, and F. Blaabjerg. Variable-structure direct torque control - a class of fast and robust controllers for induction machine drives. *IEEE Transactions on Industrial Electronics.*, 51(4):785–792, Aug 2004.

[66] P.A. Egiguren and B.C. Oscar. Robust position control of induction motor drives. In *IEEE International Symposium on Industrial Electronics (ISIE), 2010*, pages 1468–1473, July 2010.

[67] Hung-Wei Lin Yeong-Hwa Chang, Chun-I Wu and Nien-Der Kuo. Robust performance control of vector-controlled induction motors with gain-scheduled estimation and input-output linearization. *International Journal of Innovative Computing, information and control*, 7:269–288, January 2011.

[68] S. Peresada, A. Tilli, and A. Tonielli. Robust output feedback control of a doubly-fed induction machine. In *The 25th Annual Conference of the IEEE Industrial*

Electronics Society, 1999. IECON '99 Proceedings., volume 3, pages 1348–1354 vol.3, 1999.

[69] Z. Peroutka and K. Zeman. Robust field weakening algorithm for vector-controlled induction machine traction drives. In *32nd Annual Conference on IEEE Industrial Electronics, IECON 2006.*, pages 856–861, Nov 2006.

[70] B.N. Singh and K.D. Wanner. Novel and ruggedized power electronics for off-highway vehicles. In *IEEE Vehicle Power and Propulsion Conference, 2009. VPPC '09.*, pages 1043–1048, 2009.

[71] N. Mohan. *Advanced Electric Drives: Analysis, Control and Modeling Using Simulink*. Mnpere, 2001.

[72] M. Menaa, O. Touhami, and R. Ibtiouen. Estimation of the rotor resistance in induction motor by application of the spiral vector theory associate to extended kalman filter. In *Proceedings of the 35th Southeastern Symposium on System Theory, 2003.*, pages 211–216, 2003.

[73] D.J. Atkinson, J.W. Finch, and P.P. Acarnley. Estimation of rotor resistance in induction motors. *IEE Proceedings Electric Power Applications.*, 143(1):87–94, 1996.

[74] Chunting Mi, J. Shen, N. Natarajan, M. Filippa, and R. Ong. Field-oriented control of induction motors with direct rotor current estimation. In *The 4th International Power Electronics and Motion Control Conference, 2004. IPEMC 2004.*, volume 1, pages 389–392 Vol.1, 2004.

[75] M. Ghanes and Gang Zheng. On sensorless induction motor drives: Sliding-mode observer and output feedback controller. *IEEE Transactions on Industrial Electronics.*, 56(9):3404–3413, Sept 2009.

[76] J.W. Umland and M. Safiuddin. Magnitude and symmetric optimum criterion for the design of linear control systems: what is it and how does it compare with the others? *IEEE Transactions on Industry Applications.*, 26(3):489–497, 1990.

[77] V. L. Kharitonov. Asymptotic stability of an equlibrium position of a family of systems of linear differential equations. *Differential Uravnen*, 14:2086–2088, 1978.

[78] M. A. Pai and P.W. Sauer. A framework for application of generalized kharitonov's theorem in the robust stability analysis of power systems. In *Proceedings of the 28th IEEE Conference on Decision and Control, 1989.*, pages 1818–1821 vol.2, 1989.

[79] Po-Yu Kuo, S. Saibua, Guanming Huang, and Dian Zhou. An efficient method for evaluating analog circuit performance bounds under process variations. *IEEE Transactions on Circuits and Systems II: Express Briefs.*, 59(6):351–355, 2012.

[80] H. M. Soliman, A. L. Elshafei, A.A. Shaltout, and M. F. Morsi. Robust power system stabiliser. *IEE Proceedings-Generation, Transmission and Distribution.*, 147(5):285–291, 2000.

[81] Ned Mohan. *ELECTRIC DRIVES An Integrative Approach*. MNPERE, 2003.

[82] P.C. Krause, O. Wasynczuk, S.D. Sudhoff, and S. Pekarek. *Analysis of Electric Machinery and Drive Systems*. IEEE Press Series on Power Engineering. Wiley, 2013.

[83] Ivos Petras. Fractional - order feedback control of dc motor. *Journal of Electrical Engineering*, 60(3):117–128, 2009.

[84] Concepción A. Monje, Blas M. Vinagre, Vicente Feliu, and YangQuan Chen. Tuning and auto-tuning of fractional order controllers for industry applications. *Control Engineering Practice*, 16(7):798 – 812, 2008.

[85] V. Feliu A.J. Calderon, B.M. Vinagre. Fractional order control strategies for power electronic buck converters. *ELSEVIER, Signal Processing, Special Section: Fractional Calculus Applications in Signals and System*, 86(10):28032819, 2006.

[86] Concepcion A. Monje Blas M. Vinagre Vicente Feliu YangQuan Chen. Tuning and auto-tuning of fractional order controllers for industry applications. *ELSEVIER, ScienceDirect, Control Engineering Practices*, 16(7):798812, 2007.

[87] Igor Podlubny. Geometric and physical interpretation of fractional integration and fractional differentiation. *Fractional Calculus and Applied Analysis*, Fractional Calculus and Applied Analysis(4):367–386, 2002.

[88] Alain Oustaloup Francois Levron Benoit Mathieu Florence M. Nanot. Frequency-band complex noninteger differentiator: Characterization and synthesis. *IEEE Transacntion on Circuits and Systems: Fundamenta Theory and Applications*, 47(1):25–39, 2000.

[89] Joceulin Sabatier Alain Oustaloup and Patrick Lanusse. From fractal robustness to crone control. *Fractional Calculus and Applied Analysis*, 5:177–192, 1999.

[90] B M Vinagre I Podlubny L Dorcak V Feliu. On fractional pid controllers: A frequency domain approach. *Proceedings of IFAC Workshop on Digital Control*, pages 273–292, 2000.

[91] M. Shiroei and A.M. Ranjbar. Supervisory predictive control of power system load frequency control. *International Journal of Electrical Power & Energy Systems*, 61(0):70 – 80, 2014.

APPENDIX A. INDUCTION MOTOR MODEL

The dynamic model of induction motor is well established and is discussed in literature rigorously (references). This paper uses dynamic model from (Ned Book reference) in synchronously rotating reference frame. For high performance drives indirect field oriented control technique is used in this paper. The dynamic model represented in d and q axis is given below:

$$v_{sd} = R_s i_{sd} + \frac{d}{dt}\lambda_{sd} - \omega_d \lambda_{sq} \tag{A.1}$$

$$v_{sq} = R_s i_{sq} + \frac{d}{dt}\lambda_{sq} + \omega_d \lambda_{sd} \tag{A.2}$$

$$0 = R_r i_{rd} + \frac{d}{dt}\lambda_{rd} - \omega_{dA} \lambda_{rq} \tag{A.3}$$

$$0 = R_r i_{rq} + \frac{d}{dt}\lambda_{rq} + \omega_{dA} \lambda_{rd} \tag{A.4}$$

$$T_{em} = \frac{p}{2}(\lambda_{rq} i_{rd} - \lambda_{rd} i_{rq}) \tag{A.5}$$

In addition, d-axis (common to stator and rotor) is aligned with the rotor flux linkage space vector, giving the model in *rotor flux orientation*. The assumption of rotor flux orientation works fine even if motor is subjected to line start or used with scalar speed controller techniques. The benefit of aligning d-axis along rotor flux linkage causes the q-axis flux linkage component to be zero, $\lambda_{rq}(t) = 0$ and also its derivative is $\frac{d\lambda_{rq}}{dt} = 0$ The q-axis flux linkage equation becomes

$$\lambda_{rq} = L_r i_{rq} + L_m i_{sq} \tag{A.6}$$

becomes

$$i_{rq} = -\frac{L_m}{L_r} i_{sq} \tag{A.7}$$

In squirrel cage induction motor, the rotor is short circuited from the ends which yields $v_{rq} = 0$ and $v_{rd} = 0$. Since $v_{rq} = 0$ and $\frac{d\lambda_{rq}}{dt} = 0$ the equation A.4 becomes:

$$0 = R_r i_{rq} + \omega_{dA} \lambda_{rd} \tag{A.8}$$

$$\omega_{dA} = -R_r \frac{i_{rq}}{\lambda_{rd}} \tag{A.9}$$

By equations A.7, and A.9 we get the instantaneous speed of dq-winding to rotor A-axis speed:

$$\omega_{dA} = \frac{L_m}{\tau_r \lambda_{rd}} i_{sq} \tag{A.10}$$

where $\tau_r$is defined as rotor time constant and is given as: $\tau_r = \frac{L_r}{R_r}$.

Based on the same above assumption of d-axis alignment with rotor flux linkage space vector, the equation for electromagnetic torque A.5 becomes:

$$T_{em} = -\frac{p}{2} \lambda_{rd} i_{rq} \tag{A.11}$$

From equation A.7, the equation A.11 can be written in terms of i_{sq} as:

$$T_{em} = \frac{p}{2} \lambda_{rd} \frac{L_m}{L_r} i_{sq} \tag{A.12}$$

The simplified block diagram of induction motor under indirect vector control is shown in Figure 5. The i^*_{sd} and i^*_{sq} are the reference values generated from parameter based vector control block. The feedback currents are sensed from the induction motor terminals are transformed into direct and quadrature current components, and compared with the reference currents to generate the reference direct and quadrature axis voltages, v_{ds} and v_{qs}, which are transformed into three phase reference voltages v^*_a, v^*_b and v^*_c, for space vector PWM inverter. The outer speed loop used for variable

speed drives in which the reference speed is compared with measured speed of motor, which fed to PI controller to generate reference torque signal. For speed operations up to rated speed the reference flux is a constant value of the maximum flux, when the torque produced is zero. Over the rated speed operations the field weakening technique is used [45].

APPENDIX B. INDUCTION MOTOR TRANSFER FUNCTION $G(S)$

The Transfer function of the induction motor is obtained numerically solved at the steady state condition and generic form is given as:

$$G(s) = \frac{\omega_m}{V_{qs}} = \frac{b_3 s^3 + b_2 s^2 + b_1 s + b_0}{a_5 s^5 + a_4 s^4 + a_3 s^3 + a_2 s^2 + a_1 s + a_0} \tag{B.1}$$

where a_i and b_i are the numerically obtained coefficients of numerator and denominator of the transfer function.

The inverter transfer function is given by:

$$I(s) = \frac{K_{inv}}{1 + sT_{inv}} \tag{B.2}$$

$$K_{inv} = 0.65\frac{V_{dc}}{V_{cm}} \tag{B.3}$$

$$T_{inv} = \frac{1}{2f_c} \tag{B.4}$$

here, V_{cm} denotes the maximum control voltage and V_{dc}, the DC link voltage. The factor 0.65 is multiplied to obtain maximum fundamental voltage which can be obtained from DC link [45].

The closed loop transfer function of the induction motor with inverter and controller is:

$$G_{cl}(s) = \frac{n_4 s^4 + n_3 s^3 + n_2 s^2 + n_1 s + n_0}{s^7 + d_6 s^6 + d_5 s^5 + d_4 s^4 + d_3 s^3 + d_2 s^2 + d_1 s + d_0} \tag{B.5}$$

where G_{cl} is transfer function between measured speed and reference speed $\frac{\omega_m}{\omega_m^*}$.

$$
\begin{aligned}
n_4 &= K_1(K_P b_3) \\
n_3 &= K_1(K_I b_3 + K_p b_2) \\
n_2 &= K_1(K_I b_2 + K_p b_1) \\
n_1 &= K_1(K_I b_1 + K_p b_0) \\
n_0 &= K_I b_0 \\
d_7 &= 1 \\
d_6 &= (K_2 + a_4) \\
d_5 &= (a_4 K_2 + a_3) \\
d_4 &= (K_2 a_3 + a_2 + K_I K_P b_3) \\
d_3 &= (K_2 a_2 + a_1 + K_I b_3 + K_P b_2) \\
d_2 &= (K_2 a_1 + a_0 + K_I b_2 + K_P b_1) \\
d_1 &= (a_2 K_2 + K_I b_1 + K p b_0) \\
d_0 &= K_I b_0
\end{aligned} \tag{B.6}
$$

The limits on the outer loop speed controller in block diagram shown in Figure (6) are: $T_e^{ref} = \pm T_b$ and the limits for inner loops are:$V_{sd}^{ref} = \pm V_{dc}$, $V_{sq}^{ref} = \pm V_{dc}$ where subscript with zero shows the steady state values at full rated load.

The machine parameters used in all simulations are:

R_s=1.77 Ω, R_r=1.34 Ω, L_s=383 mH

L_r=381 mH, L_m=369 mH, J_{eq}=0.025 $kg.m^2$

p=4, Power= 3HP/2.4kW, Voltage=460 V (L-L,rms)

APPENDIX C. MACHINE PARAMETERS AND CALCULATION OF INITIAL CONDITIONS

```
%*************************************************************************
% Author:       Chaudhry Arshad Mehmood
%
% Description:  Partial Code is obtained from Ned Mohan Book to calculate
%               the initial conditions, flux weakening lookup table and
%               classical PI controller parameter calculations.
%*************************************************************************
%                          FFFFF   IIIII   N     N      A       L
%                          F         I     N N   N     A A      L
%                          FFF       I     N  N  N    AAAAA     L
%                          F         I     N   N N   A     A    L
%                          F       IIIII   N     N  A       A   LLLLL

% DDDD    IIIII      SSS     SSS    EEEE    RRRR    TTTTT       A       TTTTT  IIIII    OOOO    N     N
% D   D     I       S       S       E       R   R     T        A A        T      I     O    O   N N   N
% D   D     I         S       S     EEE     RRRR      T       AAAAA       T      I     O    O   N  N  N
% D   D     I           S       S   E       R  R      T      A     A      T      I     O    O   N   N N
% DDDD    IIIII      SSS     SSS    EEEE    R   R     T     A       A     T    IIIII    OOOO    N     N

%                              CCC    OOOO    DDDD    EEEE
%                             C      O    O   D   D   E
%                             C      O    O   D   D   EEE
%                             C      O    O   D   D   E
%                              CCC    OOOO    DDDD    EEEE

%
% Calculation of Initial Conditions
% Induction Motor Parameters
% Rated Torque is 13.09 N-m
clc;
clear all;
Rs=1.77;
Rr=1.34;
Rrm=1.34;
Xls=5.25;
Xlr=4.57;
Xm=139;
Jeq=0.025;
p=4;


% Steady State Operating Condition
f=60; VLLrms= 460; s=0.0172;                  % phase-a voltage is at its positive peak at t=0
Wsyn=2*pi*f;                                          % synchronous speed in electrical rad/s
Wm=(1-s)*Wsyn;                                        % rotor speed in electrical rad/s

% Phasor Calculations
Va = VLLrms * sqrt(2)/ sqrt(3);                       % Va phasor

% SpaLsce Vectors at time t=0 with stator a-axis as the reference
Vs_0 = (3/2) * Va;                                    % Vs(0) space vector
Theta_Vs_0 = angle(Vs_0);                             % angle of Vs(0) space vector

% We will assume that at t=0, d-axis is aligned to the stator a-axis.  Therefore, Theta_da_0=0
Theta_da_0 = 0;
Vsd_0 = sqrt(2/3) * abs(Vs_0) * cos(Theta_Vs_0 - Theta_da_0);
Vsq_0 = sqrt(2/3) * abs(Vs_0) * sin(Theta_Vs_0 - Theta_da_0);

% Calculation of machine inductances
Ls = (Xls + Xm) / (2*pi*f);
Lm = Xm / (2*pi*f);
Lr = (Xlr + Xm) / (2*pi*f);
tau_r=Lr/Rr;

% Calculations of dq-winding currents
A = [Rs        -Wsyn*Ls       0         -Wsyn*Lm  ;...
     Wsyn*Ls    Rs            Wsyn*Lm    0        ;...
     0         -s*Wsyn*Lm     Rr        -s*Wsyn*Lr;...      % Matrix [A]
     s*Wsyn*Lm  0             s*Wsyn*Lr  Rr];
Ainv = inv(A);
V_dq_0=[Vsd_0; Vsq_0; 0; 0];
I_dq_0=Ainv*V_dq_0;
Isd_0=I_dq_0(1);
Isq_0=I_dq_0(2);
Ird_0=I_dq_0(3);
Irq_0=I_dq_0(4);

% Electromagnetic Torque, which equals Load Torque in Initial Steady State
Tem_0 = (p/2) * Lm * (Isq_0 * Ird_0 - Isd_0 * Irq_0);
TL_0 = Tem_0
```

```
% Wmech = rotor speed in actual rad/s
Wmech_0=(2/p)*Wm;% (2/p)*(1-s)*Wsyn; %(2/p)*Wm      % Eq. 3-34

% Inductance matrix M in Eq. 3-61
M = [Ls 0  Lm 0 ;...
     0  Ls 0  Lm;...
     Lm 0  Lr 0 ;...
     0  Lm 0  Lr];

% dq winding Flux Linkages with the d-axis aligned with the stator a-axis
fl_dq_0 = M * [Isd_0; Isq_0; Ird_0; Irq_0];    % dq-winding fluxes in vector form
fl_sd_0 = fl_dq_0(1);
fl_sq_0 = fl_dq_0(2) ;
fl_rd_0 = fl_dq_0(3);
fl_rq_0 = fl_dq_0(4);
[thetar, fl_r_dq_0]=cart2pol(fl_rd_0, fl_rq_0);
[thetas, fl_s_dq_0]=cart2pol(fl_sd_0, fl_sq_0);
[theta_Is_dq, Is_dq_0]=cart2pol(Isd_0, Isq_0);
[theta_Vs_dq, Vs_dq_0]=cart2pol(Vsd_0, Vsq_0);

% d-axis is now aligned with the rotor flux which results in the following new values:
fl_rd_0=fl_r_dq_0 ;      %fl_rq_0 equals zero
[fl_sd_0, fl_sq_0]=pol2cart(thetas-thetar, fl_s_dq_0);
[Isd_0, Isq_0]=pol2cart(theta_Is_dq-thetar, Is_dq_0);
[Vsd_0, Vsq_0]=pol2cart(theta_Vs_dq-thetar, Vs_dq_0);

% Calculations for the controller.
Wc=25; % crossover freq in rad/s
k=(p/2)*(Lm*Lm/Lr)*Isd_0;
PM=60*pi/180;                           % phase margin in rad/s
Wc_kp_by_ki=tan(PM);
ki=Wc*Wc*Jeq/(k*sqrt(1+(tan(PM)^2)));
kp=ki*Wc_kp_by_ki/Wc;

% check to show that at Wc,  GOLmag=1 and GOLang= (-180 degrees + phase margin of 60 degrees)
GOL=(kp+ki/(j*Wc))*k/(Jeq*j*Wc) ;        % open-loop transfer function
GOLmag=abs(GOL);
GOLang=angle(GOL)*180/pi;

% PI in current loop
sigma=1-Lm*Lm/(Ls*Lr);
Wci=10*Wc ;                  % Current-loop bandwidth is qi times that of the speed loop
PMi=PM;
Wci_kpi_by_kii=tan(PMi-pi/2+atan(Wci*Ls*sigma/Rs));
kii=Wci*sqrt(Rs*Rs+(Wci*Ls*sigma)^2)/sqrt(Wci_kpi_by_kii^2+1);
kpi=Wci_kpi_by_kii*kii/Wci;
% check to show that at Wci,  GOLimag=1 and GOLiang= (-180 degrees + phase margin of 60 degrees)
GOLi=(kpi+kii/(j*Wci))/(Rs+j*Wci*Ls*sigma);
GOLimag=abs(GOLi);
GOLiang=angle(GOLi)*180/pi;

load Lookup_table_data.mat
speed= data(:,1);
Lambda_r=data(:,4);
```

APPENDIX D. FLUX WEAKENING LOOKUP TABLE

```
%**************************************************************************
% Author:       Chaudhry Arshad Mehmood
%
% Description:  Calculate flux weakening lookup table
%
%**************************************************************************
%                           FFFFF   IIIII   N     N      A       L
%                           F         I     N N   N     A A      L
%                           FFF       I     N  N  N    AAAAA     L
%                           F         I     N   N N   A     A    L
%                           F       IIIII   N     N  A       A   LLLLL

% DDDD    IIIII      SSS     SSS    EEEE    RRRR    TTTTT       A       TTTTT  IIIII    OOOO    N     N
% D   D     I       S       S       E       R   R     T        A A        T      I     O    O   N N   N
% D   D     I         S       S     EEE     RRRR      T       AAAAA       T      I     O    O   N  N  N
% D   D     I           S       S   E       R  R      T      A     A      T      I     O    O   N   N N
% DDDD    IIIII      SSS     SSS    EEEE    R   R     T     A       A     T    IIIII    OOOO   N     N

%                               CCC    OOOO    DDDD    EEEE
%                              C      O    O   D   D   E
%                              C      O    O   D   D   EEE
%                              C      O    O   D   D   E
%                               CCC    OOOO    DDDD    EEEE



clc;
clear all;
format compact;
%%%%%%%%%% MAcine Data %%%%%%%%%%
% Induction Motor Parameters
% Rated Torque is 13.09 N-m
Rs=1.77;
Rs=1.77;
Rr=1.34;
Rrm=1.34;
Xls=5.25;
Xlr=4.57;
Xm=139;
Jeq=0.025;
p=4;
f=60; VLLrms= 460; s=0.0172;   % phase-a voltage is at its positive peak at t=0
Ls = (Xls + Xm) / (2*pi*f);
Lm = Xm / (2*pi*f);
Lr = (Xlr + Xm) / (2*pi*f);
% Steady State Operating Condition
ws=2*pi*f;                                          % synchronous speed in electrical rad/s
wm=(1-s)*ws;                                        % rotor speed in electrical rad/s
Vs = VLLrms * sqrt(2)/ sqrt(3);
P_out = 3.25 * 746; % Rated power of motor


%Base Quantities
wb = 2 * pi *f;                     %Base Frequency
Vb = sqrt(2 / 3) * Vs;     %Base Peak Phase Voltage
Ib = P_out / (3 * Vb);          %Base Current
Zb = Vb / Ib;
Lb = Zb / wb;
Rrn = Rr /Zb;
wrn = wm / wb;
Lsn = Ls /Lb;
Lmn = Lm / Lb;
Lrn = Lr /Lb;
%%%%%%%%%% Synchronous Reference Fram %%%%%%%%%%%%

vqs =  Vs * sqrt (2/3);
vds = 0;
vqd = [vqs vds 0 0]';
% The steady state flux linkages are evaluated from the steady state
% current; they in turn, are found by using the synchronous frame
% equations with the substitution of p = 0 and with slip speed being zero.
% because the slip speed is zero, the machine does not produce
% electromagnetic torque; thus the stator currents are utilized to produce
% solely the stator and rotor flux linkages
wsl = 0;
sync_matrix = [Rs         ws * Ls    0          ws * Lm;
               -ws* Ls    Rs         -ws * Lm   0;
               0          wsl * Lm   Rr         wsl * Lr;
               -wsl * Lm  0          -wsl * Lr  Rr];
 i = sync_matrix \ vqd;

 Iqs = i(1,1);
 Ids = i(2,1);
```

```
Iqr = i(3,1);
Idr = i(4,1);

% Electromagnetic Torque is zero because of condition of wsl = 0

Tem = (3 / 4) * p * Lm * (Iqs * Idr - Ids * Iqr);

% Rotor Flux Linkages (in Wb - Turn) are

   lambda_qr = Lm * Iqs + Lr * Iqr;
   lambda_dr = Lm * Ids + Lr * Idr;

% Resultant rotor flux  (in Wb - Turn) is
   lambda_r = sqrt (lambda_qr^2 + lambda_dr^2)

% Stator Flux Linkages (in Wb - Turn) are

   lambda_qs = Ls * Iqs + Lm * Iqr;
   lambda_ds = Ls * Ids + Lr * Idr;

% Resultant rotor flux  (in Wb - Turn) is
   lambda_s = sqrt (lambda_qs^2 + lambda_ds^2);

% Stator Current Magnitude is

   Is1 = sqrt (Ids^2 + Iqs^2);
   If = Is1;     % Peak value not rms value

% If is equal to the flux producing stator current in the machine. This is
% a peak value not the rms value. The friction and windage losses are not
% given, so they can be neglected. Therefore, the electromagnetic torque
% is equal to shaft torque; its rated value os obtained as

   Te = P_out / (wm *(2/p));

%  The torque constant K_te is

   K_te = (3 / 4) * p * (Lm / Lr);

% By using rthe torque constant, the torque producing component of the
% stator current and the cuurent phasor are obtained as

   It = Te / (K_te * lambda_r);
   Isr = sqrt (If^2 + It^2);
   theta_t = atan (It/If);   % angle is in radians
% The slip speed is verified from the above as
   wsl = (Rr * It) / (Lr * If);

% From steady state rotor equations , the rotor currents are found as:

   Iqd_r_matrix = [Rr       wsl* Lr;
                   -wsl*Lr  Rr];
   Iqdr = wsl * Lm * inv(Iqd_r_matrix) * [-If It]';

   Iqr = Iqdr(1,1);
   Idr = Iqdr(2,1);
   Ir1 = sqrt(Iqr ^2 + Idr ^2);
% The stator voltages are computed from the stator steady-state equation
   Vqs = Rs * It + ws * Ls *If + ws * Lm *Idr;
   Vds = Rs * If - ws * Ls *It - ws * Lm *Iqr;
   Vsr = sqrt ( Vqs ^2 + Vds^2);
   V = sqrt(3/2) * Vsr;

%  Base Values
   Ifrn = If /Ib;
   Itrn = It /Ib;
   Vsn = Vsr / Vb;
   Isn = Isr /Ib;
   sigma = (1 - (Lmn^2 /(Lrn * Lsn)));
   an = sigma * Lsn;
   a = sigma;
% an = (1 - (Lmn^2/(Lrn*Lsn)));
wrn =5;
Ks = (Rrn * Itrn) / (wb * Lrn * Ifrn);

d1 = (Lsn * Ifrn)^2 - (an * Ifrn)^2;
d2 = -Vsn^2 + 2*Ks*(Lsn * Ifrn)^2 - 2 * Ks * (an * Ifrn)^2 + (an * wrn * Isn)^2;
d3 = (Lsn * Ifrn *Ks)^2 -(an * Ks * Ifrn)^2 + 2*Ks *(an * Isn * wrn)^2;
d4 = (an* Ks * wrn * Isn)^2;
roots ([d1 0 d2 0 d3 0 d4])
```

APPENDIX E. HURWITZ MATRICES SOLUTION

```
%**************************************************************************
% Author:       Chaudhry Arshad Mehmood
%
% Description:  Hurwitz Matrix solution obtained Through Kharitonov Theorem
%
%**************************************************************************
%                           FFFFF   IIIII   N     N      A       L
%                           F         I     N N   N     A A      L
%                           FFF       I     N  N  N    AAAAA     L
%                           F         I     N   N N   A     A    L
%                           F       IIIII   N     N  A       A   LLLLL

% DDDD    IIIII      SSS     SSS    EEEE    RRRR    TTTTT      A       TTTTT  IIIII    OOOO    N     N
% D   D     I       S       S       E       R   R     T       A A        T      I     O    O   N N   N
% D   D     I         S       S     EEE     RRRR      T      AAAAA       T      I     O    O   N  N  N
% D   D     I           S       S   E       R  R      T     A     A      T      I     O    O   N   N N
% DDDD    IIIII      SSS     SSS    EEEE    R   R     T    A       A     T    IIIII    OOOO    N     N

%                                CCC    OOOO   DDDD    EEEE
%                               C      O    O  D   D   E
%                               C      O    O  D   D   EEE
%                               C      O    O  D   D   E
%                                CCC    OOOO   DDDD    EEEE
% clear all
close all
clc

   %%%%%%%%%%%%%%%%%%%%%%%%%%%%%%%%%%%%%%%%%%%%%%%%%%%%%%%%%%%%%%%
   %%%% Parameters for first Polynomial of Karithonov Theorem%%%%%
   %%%%%%%%%%%%%%%%%%%%%%%%%%%%%%%%%%%%%%%%%%%%%%%%%%%%%%%%%%%%%%%
Ki1 = sym('Ki1');
Kp1 = sym('Kp1');
a0 = 1.232e9 * Ki1;
a1 = 1.328e9 * Kp1 + 7.268e7 * Ki1;
a2 = 1.604e9 + 2.903e8 * Kp1 + 1.893e6 * Ki1;
a3 = 30401000 + 1.893e6 * Kp1 + 3450 * Ki1;
a4 = 153371.25 + 63911.25 * Kp1;
a5 = 228.275;
a6 = 1.08695;
a7 = 0.25e-3;

%%%%%%%%%%%%%%%%%%%%%%%%%%%%%%%%%%%%%%%%%%%%%%%%%%%%%%%%%%%%%%%%%%%%%%%%%%%%%%%%%%
% Leading Principal Minors and their determinants of First Karithonov Polynomial %
%%%%%%%%%%%%%%%%%%%%%%%%%%%%%%%%%%%%%%%%%%%%%%%%%%%%%%%%%%%%%%%%%%%%%%%%%%%%%%%%%%

lp11 = a1; lp11d=det(lp11);

lp12=[a1 a3;a0 a2]; lp12d=det(lp12);

lp13=[a1 a3 a5;a0 a2 a4;0 a1 a3]; lp13d=det(lp13);

lp14=[a1 a3 a5 a7;a0 a2 a4 a6;0 a1 a3 a5;0 a0 a2 a4]; lp14d=det(lp14);

lp15=[a1 a3 a5 a7 0;a0 a2 a4 a6 0;0 a1 a3 a5 a7;0 a0 a2 a4 a6;
    0 0 a1 a3 a5];
    lp15d=det(lp15);

lp16=[a1 a3 a5 a7 0 0;a0 a2 a4 a6 0 0;0 a1 a3 a5 a7 0;0 a0 a2 a4 a6 0;
    0 0 a1 a3 a5 a7;0 0 a0 a2 a4 a6];
    lp16d=det(lp16);

lp17=[a1 a3 a5 a7 0 0 0;a0 a2 a4 a6 0 0 0;0 a1 a3 a5 a7 0 0;0 a0 a2 a4 a6 0 0;
    0 0 a1 a3 a5 a7 0;0 0 a0 a2 a4 a6 0;0 0 0 a1 a3 a5 a7];
    lp17d=det(lp17);
    ss112=solve(lp11d,lp12d, Ki1, Kp1);
    ss123=solve(lp13d,lp12d, Ki1, Kp1);
    ss134=solve(lp13d,lp14d, Ki1, Kp1);
    ss145=solve(lp15d,lp14d, Ki1, Kp1);
    ss156=solve(lp15d,lp16d, Ki1, Kp1);
    ss167=solve(lp16d,lp17d, Ki1, Kp1);
    ss171=solve(lp11d,lp17d, Ki1, Kp1);

    ss1=[ss112.Kp1 ss112.Ki1; ss123.Kp1 ss123.Ki1; ss134.Kp1 ss134.Ki1;
        ss145.Kp1 ss145.Ki1; ss156.Kp1 ss156.Ki1; ss167.Kp1 ss167.Ki1;
        ss171.Kp1 ss171.Ki1];
    format
    ss1re=double(ss1);
% figure(1);
% DrawCircle(0,0,max(ss1re(:,1)/2),100,'k');
% hold on
% figure(2);
% DrawCircle(0,0,max(ss1re(:,2)/2),100,'k');
% hold on
```

```
   %%%%%%%%%%%%%%%%%%%%%%%%%%%%%%%%%%%%%%%%%%%%%%%%%%%%%%%%%%%%%%%%
   %%%% Parameters for second Polynomial of Karithonov Theorem%%%%%
   %%%%%%%%%%%%%%%%%%%%%%%%%%%%%%%%%%%%%%%%%%%%%%%%%%%%%%%%%%%%%%%%
Ki2 = sym('Ki2');
Kp2 = sym('Kp2');
a0 = 1.712e10 * Ki2;
a1 = 1.328e9 * Kp2 + 7.268e7 * Ki2;
a2 = 1.122e8 + 7.268e8 * Kp2 + 1.62e6 * Ki2;
a3 = 30401000 + 1.893e6 * Kp2 + 3450 * Ki2;
a4 = 180900 + 63911.25 * Kp2;
a5 = 228.275;
a6 = 1.0476;
a7 = 0.25e-3;

%%%%%%%%%%%%%%%%%%%%%%%%%%%%%%%%%%%%%%%%%%%%%%%%%%%%%%%%%%%%%%%%%%%%%%%%%%%%%%%%%%%
% Leading Principal Minors and their determinants of Second Karithonov Polynomial %
%%%%%%%%%%%%%%%%%%%%%%%%%%%%%%%%%%%%%%%%%%%%%%%%%%%%%%%%%%%%%%%%%%%%%%%%%%%%%%%%%%%


lp21 = a1; lp21d=det(lp21);

lp22=[a1 a3;a0 a2]; lp22d=det(lp22);

lp23=[a1 a3 a5;a0 a2 a4;0 a1 a3]; lp23d=det(lp23);

lp24=[a1 a3 a5 a7;a0 a2 a4 a6;0 a1 a3 a5;0 a0 a2 a4]; lp24d=det(lp24);

lp25=[a1 a3 a5 a7 0;a0 a2 a4 a6 0;0 a1 a3 a5 a7;0 a0 a2 a4 a6;
    0 0 a1 a3 a5];
    lp25d=det(lp25);

lp26=[a1 a3 a5 a7 0 0;a0 a2 a4 a6 0 0;0 a1 a3 a5 a7 0;0 a0 a2 a4 a6 0;
    0 0 a1 a3 a5 a7;0 0 a0 a2 a4 a6];
    lp26d=det(lp26);

lp27=[a1 a3 a5 a7 0 0 0;a0 a2 a4 a6 0 0 0;0 a1 a3 a5 a7 0 0;0 a0 a2 a4 a6 0 0;
    0 0 a1 a3 a5 a7 0;0 0 a0 a2 a4 a6 0;0 0 0 a1 a3 a5 a7];
    lp27d=det(lp27);

    ss212=solve(lp21d,lp22d, Ki2, Kp2);
    ss223=solve(lp23d,lp22d, Ki2, Kp2);
    ss234=solve(lp23d,lp24d, Ki2, Kp2);
    ss245=solve(lp25d,lp24d, Ki2, Kp2);
    ss256=solve(lp25d,lp26d, Ki2, Kp2);
    ss267=solve(lp26d,lp27d, Ki2, Kp2);
    ss271=solve(lp21d,lp27d, Ki2, Kp2);

   ss2=[ss212.Kp2 ss212.Ki2; ss223.Kp2 ss223.Ki2; ss234.Kp2 ss234.Ki2;
        ss245.Kp2 ss245.Ki2; ss256.Kp2 ss256.Ki2; ss267.Kp2 ss267.Ki2;
        ss271.Kp2 ss271.Ki2];
    format
    ss2re=double(ss2);
% figure(1);
% DrawCircle(0,0,max(ss2re(:,1)/2),100,'g');
% hold on
% figure(2);
% DrawCircle(0,0,max(ss2re(:,2)/2),100,'g');
% hold on

   %%%%%%%%%%%%%%%%%%%%%%%%%%%%%%%%%%%%%%%%%%%%%%%%%%%%%%%%%%%%%%%
   %%%% Parameters for Third Polynomial of Karithonov Theorem%%%%%
   %%%%%%%%%%%%%%%%%%%%%%%%%%%%%%%%%%%%%%%%%%%%%%%%%%%%%%%%%%%%%%%
Ki3 = sym('Ki3');
Kp3 = sym('Kp3');
a0 = 1.712e10 * Ki3;
a1 = 1.712e10 * Kp3 + 2.903e8 * Ki3;
a2 = 1.122e8 + 7.268e8 * Kp3 + 1.62e6 * Ki3;
a3 = 7513050 + 1.62e6 * Kp3 + 3450 * Ki3;
a4 = 180900 + 63911.25 * Kp3;
a5 = 391.15;
a6 = 1.0476;
a7 = 0.25e-3;

%%%%%%%%%%%%%%%%%%%%%%%%%%%%%%%%%%%%%%%%%%%%%%%%%%%%%%%%%%%%%%%%%%%%%%%%%%%%%%%%%%%
% Leading Principal Minors and their determinants of Third Karithonov Polynomial %
%%%%%%%%%%%%%%%%%%%%%%%%%%%%%%%%%%%%%%%%%%%%%%%%%%%%%%%%%%%%%%%%%%%%%%%%%%%%%%%%%%%


lp31 = a1; lp31d=det(lp31);

lp32=[a1 a3;a0 a2]; lp32d=det(lp32);

lp33=[a1 a3 a5;a0 a2 a4;0 a1 a3]; lp33d=det(lp33);

lp34=[a1 a3 a5 a7;a0 a2 a4 a6;0 a1 a3 a5;0 a0 a2 a4]; lp34d=det(lp34);

lp35=[a1 a3 a5 a7 0;a0 a2 a4 a6 0;0 a1 a3 a5 a7;0 a0 a2 a4 a6;
    0 0 a1 a3 a5];
    lp35d=det(lp35);
```

```
lp36=[a1 a3 a5 a7 0 0;a0 a2 a4 a6 0 0;0 a1 a3 a5 a7 0;0 a0 a2 a4 a6 0;
    0 0 a1 a3 a5 a7;0 0 a0 a2 a4 a6];
    lp36d=det(lp36);

lp37=[a1 a3 a5 a7 0 0 0;a0 a2 a4 a6 0 0 0;0 a1 a3 a5 a7 0 0;0 a0 a2 a4 a6 0 0;
    0 0 a1 a3 a5 a7 0;0 0 a0 a2 a4 a6 0;0 0 0 a1 a3 a5 a7];
    lp37d=det(lp37);

    ss312=solve(lp31d,lp32d, Ki3, Kp3);
    ss323=solve(lp33d,lp32d, Ki3, Kp3);
    ss334=solve(lp33d,lp34d, Ki3, Kp3);
    ss345=solve(lp35d,lp34d, Ki3, Kp3);
    ss356=solve(lp35d,lp36d, Ki3, Kp3);
    ss367=solve(lp36d,lp37d, Ki3, Kp3);
    ss371=solve(lp31d,lp37d, Ki3, Kp3);

   ss3=[ss312.Kp3 ss312.Ki3; ss323.Kp3 ss323.Ki3; ss334.Kp3 ss334.Ki3;
        ss345.Kp3 ss345.Ki3; ss356.Kp3 ss356.Ki3; ss367.Kp3 ss367.Ki3;
        ss371.Kp3 ss371.Ki3];
   ss3re=double(ss3);
% figure(1);
% DrawCircle(0,0,max(ss3re(:,1)/2),100,'b');
% hold on
% figure(2);
% DrawCircle(0,0,max(ss3re(:,2)/2),100,'b');
% hold on

   %%%%%%%%%%%%%%%%%%%%%%%%%%%%%%%%%%%%%%%%%%%%%%%%%%%%%%%%%%%%%%%%%%
   %%%% Parameters for Fourth Polynomial of Karithonov Theorem%%%%%
   %%%%%%%%%%%%%%%%%%%%%%%%%%%%%%%%%%%%%%%%%%%%%%%%%%%%%%%%%%%%%%%%%%
Ki4 = sym('Ki4');
Kp4 = sym('Kp4');
a0 = 1.328e9 * Ki4;
a1 = 1.712e10 * Kp4 + 2.903e8 * Ki4;
a2 = 1.604e9 + 2.903e8 * Kp4 + 1.893e6 * Ki4;
a3 = 7513050 + 1.62e6 * Kp4 + 3450 * Ki4;
a4 = 153371.25 + 63911.25 * Kp4;
a5 = 391.15;
a6 = 1.08695;
a7 = 0.25e-3;

%%%%%%%%%%%%%%%%%%%%%%%%%%%%%%%%%%%%%%%%%%%%%%%%%%%%%%%%%%%%%%%%%%%%%%%%%%%%%%%%%%
% Leading Principal Minors and their determinants of Fourth Karithonov Polynomial %
%%%%%%%%%%%%%%%%%%%%%%%%%%%%%%%%%%%%%%%%%%%%%%%%%%%%%%%%%%%%%%%%%%%%%%%%%%%%%%%%%%


lp41 = a1; lp41d=det(lp41);

lp42=[a1 a3;a0 a2]; lp42d=det(lp42);

lp43=[a1 a3 a5;a0 a2 a4;0 a1 a3]; lp43d=det(lp43);

lp44=[a1 a3 a5 a7;a0 a2 a4 a6;0 a1 a3 a5;0 a0 a2 a4]; lp44d=det(lp44);

lp45=[a1 a3 a5 a7 0;a0 a2 a4 a6 0;0 a1 a3 a5 a7;0 a0 a2 a4 a6;
    0 0 a1 a3 a5];
    lp45d=det(lp45);

lp46=[a1 a3 a5 a7 0 0;a0 a2 a4 a6 0 0;0 a1 a3 a5 a7 0;0 a0 a2 a4 a6 0;
    0 0 a1 a3 a5 a7;0 0 a0 a2 a4 a6];
    lp46d=det(lp46);

lp47=[a1 a3 a5 a7 0 0 0;a0 a2 a4 a6 0 0 0;0 a1 a3 a5 a7 0 0;0 a0 a2 a4 a6 0 0;
    0 0 a1 a3 a5 a7 0;0 0 a0 a2 a4 a6 0;0 0 0 a1 a3 a5 a7];
    lp47d=det(lp47);

    ss412=solve(lp41d,lp42d, Ki4, Kp4);
    ss423=solve(lp43d,lp42d, Ki4, Kp4);
    ss434=solve(lp43d,lp44d, Ki4, Kp4);
    ss445=solve(lp45d,lp44d, Ki4, Kp4);
    ss456=solve(lp45d,lp46d, Ki4, Kp4);
    ss467=solve(lp46d,lp47d, Ki4, Kp4);
    ss471=solve(lp41d,lp47d, Ki4, Kp4);


    ss4=[ss412.Kp4 ss412.Ki4; ss423.Kp4 ss423.Ki4; ss434.Kp4 ss434.Ki4;
         ss445.Kp4 ss445.Ki4; ss456.Kp4 ss456.Ki4; ss467.Kp4 ss467.Ki4;
         ss471.Kp4 ss471.Ki4];
    ss4re=double(ss4);
%  figure(1);
% DrawCircle(0,0,max(ss4re(:,1)/2),100,'r');
% title('Proportional Gain');
% hold on
% figure(2);
% DrawCircle(0,0,max(ss4re(:,2)/2),100,'r');
% title('Integral Gain');
% hold on
```

```
[Kp11min Kp11max]= minmax(ss1re(:,1));
[Kp12min Kp12max]= minmax(ss2re(:,1));
[Kp13min Kp13max]= minmax(ss3re(:,1));
[Kp14min Kp14max]= minmax(ss4re(:,1));

[Ki11min Ki11max]= minmax(ss1re(:,1));
[Ki12min Ki12max]= minmax(ss2re(:,1));
[Ki13min Ki13max]= minmax(ss3re(:,1));
[Ki14min Ki14max]= minmax(ss4re(:,1));
format compact;
Kp1min =[Kp11min Kp12min Kp13min Kp14min]
Kp1max =[Kp11max Kp12max Kp13max Kp14max]

Ki1min =[Ki11min Ki12min Ki13min Ki14min]
Ki1max =[Ki11max Ki12max Ki13max Ki14max]
```

APPENDIX F. LINEARIZED TRANSFER FUNCTIONS

```
%************************************************************************
% Author:       Chaudhry Arshad Mehmood
%
% Description:  Transfer Functions Numerically Obtained From Matlab
%
%************************************************************************
Rr at 50%

     3450 s^3 + 1.621e006 s^2 + 7.268e007 s + 1.328e009
-----------------------------------------------------------
s^5 + 190.4 s^4 + 1.515e005 s^3 + 7.485e006 s^2 + 1.122e008 s

Rr at 200%

  3450 s^3 + 1.893e006 s^2 + 2.903e008 s + 1.712e010
-------------------------------------------------------
s^5 + 347.8 s^4 + 1.734e005 s^3 + 3e007 s^2 + 1.604e009 s


Lm at 50 %
     150.9 s^3 + 5.849e004 s^2 + 5.486e005 s + 4.542e006
-----------------------------------------------------------
s^5 + 21.24 s^4 + 1.423e005 s^3 + 1.305e006 s^2 + 9.002e006 s

Lm rated

     3450 s^3 + 1.712e006 s^2 + 1.452e008 s + 4.593e009
-----------------------------------------------------------
s^5 + 242.9 s^4 + 1.574e005 s^3 + 1.498e007 s^2 + 4.139e008 s

Rated
      3450 s^3 + 4.189e005 s^2 + 9.56e006 s + 9.049e008
-----------------------------------------------------------
s^5 + 242.9 s^4 + 1.574e005 s^3 + 1.498e007 s^2 + 4.139e008 s


Lm= 80 and Rr 200
     459.3 s^3 + 1.49e004 s^2 + 4.07e005 s + 2.132e007
-----------------------------------------------------------
s^5 + 57.89 s^4 + 1.432e005 s^3 + 4.97e006 s^2 + 4.992e007 s
```

APPENDIX G. SYMMETRIC OPTIMUM PI CONTROLLER DESIGN

```
%*************************************************************************
% Author:       Chaudhry Arshad Mehmood
%
% Description:  Calculate Controller parameter for Symmetric Optimum Technique
%
%*************************************************************************
clear all
close all
clc;
If = 48;
fc = 2000;
Bt = 0.05;
Hw = .050;   % Speed filter Parameter
Tw = 0.002;  % Speed Filter Parameter
Vcm = 10;
J = 0.025;
Vdc = 200;
Hc = 1;%0.333;
Rs = 1.77;
Rr = 1.34;
Lm = 139/(2*pi*60);
Lr1 = 4.57/(2*pi*60);
Ls1 = 5.25/(2*pi*60);
Ls = Lm+Ls1;
Lr = Lm+Lr1;
p = 4;
% Rs1=Rs
% J1 = J
% for J=.2 * J1: .004: 3.5 *J1

Ra = Rs + Rr*Ls/Lr;
Ka = 1/Ra;
La = Ls - (Lm^2)/Lr;
% La = 0.0037;
Ta = La/Ra;
Tm = J/Bt;
Kt = (3/2)*(p/2)*((Lm^2)*If/Lr);
Km = (p/2)*(Kt/Bt);
Kb = (p/2)*(Kt/Bt)*Ls*If;
Tin = 1/(2*fc);
Kin = 0.65*Vdc/Vcm;
Tar = Ta + Tin;
T1 = 0.00074;
T2 = 0.1173;

%approximate current loop
% Ki = Kin/Ra;
Ki = 2.8708;
Ti = T1;

%speed controller
Kg = (Ki*Km*Hw)/Tm;
% Kg = 104.1;
Twi = Tw + Ti;
Ts = 6*Twi;
Ks =  4/(9*Kg*Twi); %.5606
Kps = Ks %proportional gain
Kis = Ks/Ts %integral gain
s = tf('s');
Gin = Kin/(1 + s*Tin);
G1 = Ka/(1 + s*Ta);
G2 = Kb/(1 + s*Tm);
G12 = feedback(G1,G2);

%exact current loop transfer function
% Gi = Gin*G12 /(1 + Hc*Gin*G12);
Gi1 = series(Gin, G12);
Gi = feedback(Gi1, Hc);

%simplified current loop transfer function
Gis = Ki/(1 + s*Ti);
figure(1)
bodemag(Gi,Gis)
title('Simplified and exact current loop frequency response') ;
% axis([100 100000 -5 10]);
grid;
%%%%%%%%%%%%%%%%%%%%%%%%%%%%%%%%%%%%%%%%%%%%%%%%%%%%%Exact Speed Loop%%%%%%%%%%%%%%%%
%exact speed loop tf
Gwf = (Km/(1 + s*Tm)) * (Ks*(1 + s*Ts)/(s*Ts))*Gi;
Gw = Hw / (1 + s*Tw);
```

```
% Gwe = Gwf / (1 + Gwf*Gw);
Gwe = feedback(Gwf,Gw);
% title('Results with Symmetric Optimum')
%simplified speed loop transfer function
Gf = (Km/(1 + s*Tm)) * (Ks*(1 + s*Ts)/(s*Ts)) * (Ki/(1 + s*Ti));
% Gws = Gf/(1 + Gf*Gw);
Gws = feedback(Gf,Gw);

%%%%smoothed speed loop tf for exact by introducing a pole of -1/Ts
Gswe = Gwe/(1 + s*Ts);
%%%smoothed speed loop tf for approximate by introducing a pole of -1/Ts
Gsws = Gws/(1 + s*Ts);
figure(2);
bodemag(Gwe,Gws,Gswe,Gsws)
title('Smoothed simplified speed loop frequency response') ;
axis([10 1000 -20 100])
grid;
```

APPENDIX H. LINEARIZED TRANSFER FUNCTIONS

```
%*************************************************************************
% Author:       Chaudhry Arshad Mehmood
%
% Description:  Plug-in H-infinity compensator for speed control Matlab Code
% The code requires the mu-Analysis and Synthesis Toolbox
%
%*************************************************************************

clc;
% The parameters from the reference paper (ref number is given in chapter)
% Kp=1.5307;
% Ki=50;
% J = 0.01111;

% Classical PI tuning already tuned in the thesis
Kp=0.24;
Ki=3.53;
J = 0.025;
Bm = 7.355e-4;
W2=1;
W1=8*(tf([Kp Ki],[1 0]));
P=tf([1/J],[1 Bm/J]);
% Finding K3 the optimal H-infinity controller
[K,CL,GAM,INFO]=ncfsyn(P,-W1,W2);
[b, a]=ss2tf(INFO.Ks.a, INFO.Ks.b, INFO.Ks.c, INFO.Ks.d);
K3=tf(b,a);
sys1=zpk(K3)
% Finding Q Plug in robust compensator
X2=1;
K2=W1*K3*W2;
M=1;
N=P;
Y0=tf([1 0],[Kp Ki]);
Q=((K2*Y0)-X2)/(M+(K2*N));
sys=zpk(Q);
```

APPENDIX I. LIST OF PUBLICATION

1. Chaudhry Arshad Mehmood, Muhammad Ali, Rahat Naseem and et al., *Robust Speed Control of Interior Permanent Magnet Synchronous Machine "Fractional Order Control"*, Electro/Information Technology (EIT), 2014 IEEE International Conference on, 5-7 June 2014.

2. Chaudhry Arshad Mehmood and Rajesh G. Kavasseri, *Letter to the Editor: On the use of Fractional Order Controllers (FrOC) for performance improvements in AC Drives*, Taylor and Francis, Electric Power Components and Systems (Submitted: 16 February 2014, Revised: 19 May 2014).

3. Chaudhry Arshad Mehmood and Rajesh G. Kavasseri, *Fractional Order Controller for Electric Drives Under Parameter Uncertainty: A Controller Performance Analysis*, Journal of Electrical Systems (Submitted).

4. Chaudhry Arshad Mehmood and Rajesh G. Kavasseri, *Robust Controller Design for Induction Motor Drives based on Kharitonov's Theorem*, WSEAS Transactions on Systems (Submitted).